ENCAPSULATION OF FOOD ADDITIVES AND DRUGS BY CYCLODEXTRIN FUNCTIONALIZED ELECTROSPUN NANOFIBERS

A DISSERTATION SUBMITTED TO

THE GRADUATE SCHOOL OF ENGINEERING AND SCIENCE

OF BİLKENT UNIVERSITY

IN PARTIAL FULFILLMENT OF THE REQUIREMENTS FOR

THE DEGREE OF

DOCTOR OF PHILOSOPHY

IN

MATERIALS SCIENCE AND NANOTECHNOLOGY

By

ZEHRA IREM YILDIZ

June 2020

ENCAPSULATION OF FOOD ADDITIVES AND DRUGS BY CYCLODEXTRIN FUNCTIONALIZED ELECTROSPUN NANOFIBERS

By Zehra Irem Yildiz

April 2020

We certify that we have read this dissertation and that in our opinion it is fully adequate, in scope and in quality, as a thesis for the degree of Doctor of Philosophy.

_____

Engin Durgun

_____

Tamer Uyar

_____

Servet Gülüm Şumnu

_____

Çağlar Elbüken

_____

Pınar Huri

_____

Fatih İnci

Approved for the Graduate School of Engineering and Science:

_____

Ezhan Karaşan

Director of the Graduate School

ABSTRACT

ENCAPSULATION OF FOOD ADDITIVES AND DRUGS BY CYCLODEXTRIN FUNCTIONALIZED ELECTROSPUN NANOFIBERS

Zehra İrem Yıldız

Ph.D. in Materials Science and Nanotechnology

Advisor: Engin Durgun

Co-Advisor: Tamer Uyar

June 2020

Electrospun nanofibers attract attention of many areas including food and pharmaceutical industries thanks to their unique physical/mechanical properties like large surface area-to-volume ratio, nanoporous structure, design flexibility and lightweight. Although, in general polymers are used for fabrication of electrospun nanofibers, it is also possible to obtain electrospun nanofibers purely from cyclodextrins (CDs). CDs with truncated cone shape structure are attractive host molecules for the formation of host-guest type inclusion complexes (ICs) with variety of appropriate guest molecules. Creating ICs with CDs causes remarkable enhancement at the properties of the guest molecule, and so CDs have wide range of applications in many areas including food and pharmaceutical industries.

In this thesis, polymer-free electrospun nanofibers from CD-ICs of some food additives and drugs were produced. Firstly, four food additives, menthol, carvacrol, cinnamaldehyde and beta-carotene were encapsulated by electrospun CD nanofibers. Afterwards, the solubility, heat/light stability, antibacterial/antioxidant

activity of the materials were investigated to observe the effects of encapsulation by CD nanofibers on the food additives. Secondly, electrospun CD-IC nanofibers of three types of drugs, sulfisoxazole, paracetamol and catechin were produced. Since one of the most critical point for drug bioavailability is its solubility in water, the obtained electrospun drug/CD-IC nanofibers were mainly investigated in terms of change in their solubility. In the light of analyses, it can be concluded that, main drawbacks of food additives and drugs like high volatility, low solubility and low stability were reduced or removed; besides, their properties such as antioxidant and antibacterial activities were enhanced or preserved.

Keywords: electrospinning, nanofibers, modified cyclodextrins, inclusion complexes, food additives, drugs

ÖZET

GIDA KATKI MADDELERİ VE İLAÇLARIN ELEKTROEĞİRME YÖNTEMİ KULLANILARAK ÜRETİLEN VE SİKLODEKSTRİN MOLEKÜLÜ İLE FONKSİYONLAŞTIRILMIŞ NANOLİFLER İLE ENKAPSÜLASYONU

Zehra İrem Yıldız

Malzeme Bilimi ve Nanoteknoloji, Doktora

Tez Danışmanı: Engin Durgun

Tez Eş Danışmanı: Tamer Uyar

Haziran 2020

Elektroeğirme yöntemi ile elde edilen nanolifler, geniş yüzey alan/hacim oranı, nanogözenekli yapı, tasarım esnekliği ve hafiflik gibi benzersiz fiziksel/mekanik özellikleri sayesinde gıda ve ilaç endüstrileri de dahil olmak üzere birçok alanın dikkatini çekmektedir. Genelde elektroeğirme yöntemi ile nanolif üretiminde polimerler kullanılmasına rağmen, nanoliflerin sadece siklodekstrinlerden (CD'ler) elde edilmesi de mümkündür. Kesik koni biçiminde olan CD'ler, uygun misafir molekülleri ile ev sahibi-misafir tipi inklüzyon kompleksler (IC'ler) yapabilmektedirler. CD'lerle IC'lerin oluşturulması misafir molekülün özelliklerinde kayda değer bir gelişmeye neden olur ve bu yüzden CD'ler gıda ve ilaç endüstrileri de dahil olmak üzere birçok alanda geniş bir uygulama yelpazesine sahiptir.

Bu tezde, bazı gıda katkı maddelerinin ve ilaçların CD-IC'lerinden polimer içermeyen elektroeğirilmiş nanolifler üretilmiştir. İlk bölümde, gıda katkı maddelerinden mentol, karvakrol, sinnamaldehit ve beta-karoten molekülleri elektroeğirilmiş modifiye CD nanolifleri ile enkapsüle edilmiştir. Daha sonra CD nanolifleri ile enkapsülasyonun gıda katkı maddeleri üzerindeki etkilerini gözlemlemek için malzemelerin çözünürlüğü, ısı ve ışık stabilitesi, antibakteriyel ve antioksidan aktivitesi incelenmiştir. İkinci bölümde, ilaç olarak kullanılan sülfisoksazol, parasetamol ve kateşin moleküllerinin elektroeğirilmiş CD-IC nanolifleri modifiye CD'ler kullanılarak üretilmiştir. İlaç biyoyararlanımında en kritik noktalardan biri ilacın sudaki çözünürlüğü olduğu için, elde edilen elektroeğirilmiş ilaç/CD-IC nanolifleri ilaç çözünürlüklerindeki değişim açısından incelenmiştir. Analizler ışığında, gıda katkı maddelerinin ve ilaçların, yüksek uçuculuk, düşük çözünürlük ve düşük stabilite gibi temel dezavantajlarının azaldığı veya ortadan kaldırıldığı sonucuna varılabilirken, antioksidan ve antibakteriyel aktiviteler gibi özelliklerin geliştirildiği veya korunduğu görülmüştür.

Anahtar kelimeler: elektroeğirme, nanolifler, modifiye siklodekstrinler, inklüzyon kompleksleri, gıda katkı maddeleri, ilaçlar

Kızıma…

Acknowledgements

I would like to thank my advisor Dr. Engin Durgun for his support, guidance and efforts. I am also grateful to him for his patience and understanding of me in the last year of my thesis period. I would like to express my sincere gratitude to my co-advisor and my previous advisor Prof. Tamer Uyar for his valuable guidance, encouragement and understanding throughout my PhD studies. I am proud of being a member of his group; since he guided me to become a good scientist with his virtue, compassion and diligence.

I would like to thank my thesis tracking committee members Prof. Gülüm Şumnu and Dr. Çağlar Elbüken for their advices and encouragements. I would also acknowledge my jury members Dr. Pınar Yılgör Huri and Dr. Fatih İnci for their contribution to my thesis.

I owe a special thanks to Dr. Asli Çelebioğlu, who is like my sister, not only deep scientific support but also her invaluable friendship, understanding and virtuous personality. I would like to give special thanks to my dearest lab mates and sisters Dr. Yelda Ertaş Doğan and Dr. Zeynep Aytaç for creating such a good working ambiance in the laboratory and also for their help and support in all fields of my life. I would like to acknowledge to former members of Uyar Research Group Dr. Amaresh Chandra Pradhan, Dr. Ali Demirci, Dr. Anitha Senthamizhan, Dr. M. Aref Khalily, Dr. Bekir Satılmış, Dr. Bhushan Patil, Dr. Brabu Balusamy, Dr. Fatma Kayacı-Şenırmak, Dr. Fuat Topuz, Dr. Kugalur Shanmugam Ranjith, Dr. Nalan Oya San-Keskin, Dr. Nuray Gündüz, Dr. Osman Arslan, Dr. Ömer Faruk Sarıoğlu,

Dr. Şefika Özcan. I would like to give special thanks to Dr. Mehmet Emin Kılıç for his fruitful collaboration.

I want to thank my friends at UNAM and especially at office for their friendship, help, support and understanding during my PhD. I am very grateful for having the opportunity to work with UNAM facilities. I am especially thankful to Zeynep Erdoğan, Seda Kutkan and Dr. Gökçe Çelik for their contribution to my thesis and to my life.

I would like to acknowledge TUBITAK (The Scientific and Technological Research Council of Turkey) for funding my research and its scholarship, BIDEB 2211-A and TUBITAK projects #213M185, #114Y264 and #115Z488.

Finally, I would like to express my special gratitude to my family. I am grateful to my dear daughter Betül Yıldız for the deep peace and happiness she gave me. The most difficult part of my acknowledgement is to thank my husband Dr. Yakup Yıldız, since words are not enough to explain what his presence has brought me. I would like to thank him for his support, understanding and being always with me in any case. Deepest thanks go to my mom Emine Gürbüz and father Ahmet Gürbüz for their endless support, prayers and beliefs to me. I would like to thank my mother in law Kadriye Yıldız and my father in law Nizamettin Yıldız for their support during thesis period and their prayers. I owe my mothers and fathers special thanks since during thesis writing period, they are like a babysitter and cook without any complaining. I would also like to thank my brother Dr. Okan Gürbüz who has made great contributions to my life and his precious wife Tuğba Gürbüz, who always supports me with her ideas. I send my love to my niece Ela Nas Gürbüz who gives

me positive energy with her loveliness. I would also like to thank my aunt Emriye Cengiz and her family members and my dear cousins Esin Cengiz, Kübra-Abdülkadir-Gülayşe Yüzbaşıoğlu, and Berra-Aytül-Turgut Cengiz who were always with me during my happy and troubled times.

Table of Contents

LIST OF ABBREVIATION

AFD	Average fiber diameter
CD	Cyclodextrin
α-CD	α-cyclodextrin
β-CD	β-cyclodextrin
γ-CD	γ -cyclodextrin
d6-DMSO	Deuterated dimethylsulfoxide
DSC	Differential scanning calorimeter
DMF	N,N Dimethylformamide
DPPH	2,2-diphenyl-1-picrylhydrazyl
E. coli	*Escherichia coli*
EOs	Essential oils
$\mathbf{E_{comp}}$	Complexation energy
$\mathbf{E_{solv}}$	Solvation energy
FTIR	Fourier transform infrared spectrometer
HS GC-MS	Headspace gas chromatography-mass spectrometry
HPβCD	Hydroxypropyl-β-cyclodextrin
HPγCD	Hydroxypropyl-γ-cyclodextrin
IC	Inclusion complex
IZ	Inhibition zone
$\mathbf{K_s}$	Stability constant
NFs	Nanofibers
PVA	Polyvinyl alcohol
$\mathbf{^1H}$ **NMR**	Proton nuclear magnetic resonance
SBE-β-CD	Sulfobutlyether-β-cyclodextrin
SEM	Scanning electron microscope
TGA	Thermogravimetric analyzer
XRD	X-ray diffraction

LIST OF FIGURES

LIST OF TABLES

CHAPTER 1

INTRODUCTION

1.1 Electrospinning

Electrospinning is an efficient method to produce fibrous mats composed of continuous fibers diameter ranging from several microns to few nanometers. Although there are some other methods for the production of nanofibers (melt fibrillation, gas spinning, island-in-sea, self-assembly, phase separation, melt drawing), electrospinning is preferred due to its relatively low cost, relatively high production rate, simplicity of setup [1, 2]. Another superior feature of electrospinning to other methods is capability of fiber production from a variety of materials including synthetic and natural polymers, polymer blends, inorganic materials, sol-gels, ceramics and composite materials [3, 4].

Electrospinning set-up is mainly composed of three parts: high voltage power supply, syringe pump and collector. Electrospinning set-up found in our laboratory at UNAM is shown in Figure 1a with representative schematic view of its components (Figure 1b). In this system, polymer solution or melt is hosted by a syringe connected to a needle. Syringe pump provides pumping of a solution through the needle at a constant and controllable rate. The application of a high voltage to a polymer solution induces charges within the fluid. Then, charges within the highly electrified fluid are distributed over the surface of the drop at the tip of the needle and electrostatic forces and interactions cause deformation in the drop at

the cone-shaped known as Taylor-cone. When electric field reached a critical amount, electrostatic forces overcome the surface tension of polymer solution and a liquid jet from the tip of needle is ejected. While jet goes towards the grounded collector, solvent evaporates and stretching and whipping process leading to formation of thin and long fibers occur. As a result, fibers are deposited on the collector as a nanofibrous webs [5, 6].

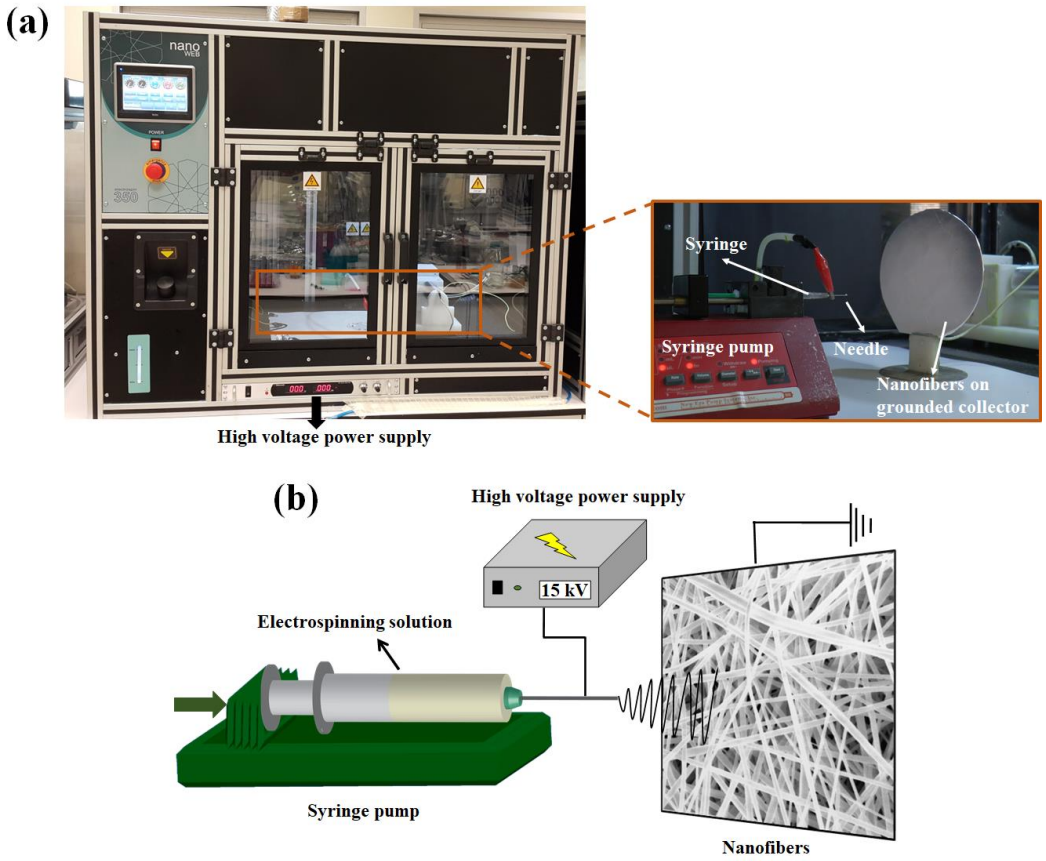

Figure 1. (a) Electrospinning set-up at UNAM and (b) representative schematic view of electrospinning components.

Resultant electrospun nanofibers can have different thickness and different morphologies from beaded to porous structures. There are some parameters of electrospinning process effective on these differences in fibrous structure. These

parameters can be classified mainly under three titles; polymer solution parameters, processing conditions and ambient conditions [6]. Polymer solution parameters categorized as type and molecular weight of polymer, solution viscosity, solution conductivity and surface tension are highly effective on structure of resultant nanofibers [7-12]. In order to maintain continuity of electrospinning jet during electrospinning, chain entanglement of polymer is required and amount of chain entanglement is determined by molecular weight of polymer, solution viscosity and solution concentration. Since stretching of the solution in electrospinning is due to repulsion of charges, conductivity of the solution is critical parameter [6]. Applied voltage, feed rate of solution, distance between syringe and collector, collector type, diameter of needle called as processing conditions are other factors effective on nanofiber structure [7, 9]. Application of high voltage is required to initiate the electrospinning process. A higher voltage results in greater stretching due to greater columbic forces in the jet which cause formation of thinner fibers. On the other hand, finer fibers may be obtained when a lower voltage is applied. Therefore, the optimum voltage for electrospinning should be adjusted. Solvent evaporation is directly related with the feed rate, and distance between collector and needle tip. Distance between collector and the tip of needle also critical for the strength of the electric field. If the distance is too low, solvent does not have enough time to evaporate and fibers merge; however, if the distance is too large, there is no enough electric field to obtain stretching of solution [6]. Temperature and humidity in other words ambient conditions are other parameters affecting structure of resultant nanofibers [6, 10, 13]. Ambient conditions are known to affect solution viscosity and solvent evaporation which are critical for electrospinning.

It is also possible to obtain nanofibers having different morphology like aligned, porous, core-shell and hollow by varying the electrospinning parameters. In case of fixed collector, nanofibers are collected randomly on collector: however, nanofibers can be aligned by using cylindrical rotating collector [14]. Nanofibrous webs already have porous structure; however, porous structure on single fiber can also be obtained by using different approaches [15, 16]. Core-shell nanofibers that have different materials in core and shell part can be obtained by using nozzle specified for this system [17]. Hollow nanofibers are produced by removing core part of core-shell nanofibers [18].

Electrospun nanofibers can be applicable in many areas thanks to their high surface area, light-weight, nano-porous structure and distinctive physical and mechanical properties. Besides, the application of nanofibers can be expanded by fucntionalizing nanofibrous webs with nanoparticles [19-21], drugs [22, 23], food additives [24, 25], inorganic materials [26, 27], etc. As a result, thanks to its unique properties, electrospun nanofibers have potentials to apply in many areas such as food and agriculture [25, 28-41], filtration [42-45], sensors [46-48], energy and electronics [49-51], biomedical [17, 22, 23, 52-55], and enzyme [56] and catalyst [57-60].

1.2 Cyclodextrin

Cyclodextrins (CDs) are cyclic oligosaccharides composed of glucopyranose units linked by α-(1,4)-glycosidic bonds. CDs are produced by enzymatic degradation of starch. Glucosyl transferase (CGTase) is used as an enzyme to hydrolyze off one or several turn of the amylose helix of starch and then the ends are joined together

which results in truncated cone torus-like structure (Figure 2) [56, 61]. As a result of this enzymatic degradation, cyclic oligosaccharides mostly having six, seven and eight glucopyranose units called as α-CD, β-CD and γ-CD are obtained, respectively (Figure 2) [61]. These three CD types are generally named as "native CD" which are considered as first generation, parent or major CDs [56, 62]. The main characteristics of these native CDs are given in Table 1. The solubility of CDs in water are determined by H-bonding in CD ring between C-2-OH group of one glucopyranose unit and C-3-OH group of the adjacent glucopyranose unit [56, 61]. β-CD has a rigid structure thanks to complete secondary belt formation by these H-bonds which is probably reason for the lowest water solubility of β-CD among all CDs [56]. For α-CD, there is an incomplete H-bond belt due to distorted position of one glucopyranose unit which results in formation of four H-bond instead of six. On the other hand, noncoplanar structure of γ-CD makes it more flexible and so γ-CD has the highest water solubility of three native CDs (Table 1) [56].

Table 1. General properties of native CDs.

Properties	**α-CD**	**β-CD**	**γ-CD**
Number of glucopyranose units	6	7	8
Molecular weight(g/mol)	972	1135	1297
Outer diameter (Å)	14.6	15.4	17.5
Cavity diameter (Å)	4.7-5.3	6.0-6.5	7.5-8.3
Height of torus (Å)	7.6	7.6	7.6
Approximate cavity volume ($Å^3$)	174	262	427
Solubility in water at 25 °C (g/100mL)	14.5	1.85	23.2

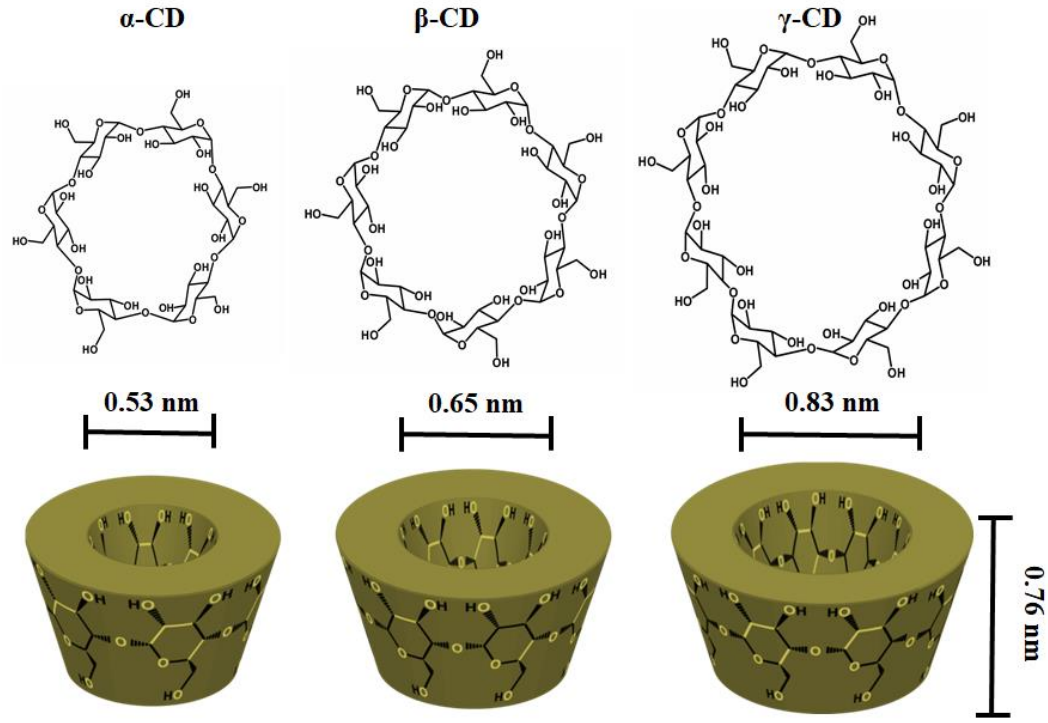

Figure 2. Chemical structure and schematic view of α-CD, β-CD and γ-CD.

Besides these naturally occurring CD types, many CD derivatives are synthesized by chemical modifications. CD molecules are generally modified in which either primary or secondary hydroxyl groups of CDs (Figure 3b) are substituted with different groups like alkly, hyroxyalkyl, carboxyalkyl, amino, thio, tosyl, ether, ester, etc. [62, 63]. There are different aims for such modifications like; to increase solubility of CDs and its complexes; to increase association between CD and its guest; or to obtain insoluble CDs [63]. Industrial production and marketing of CD derivatives require simple production reactions, being nontoxic, having acceptable price, keeping its complex forming ability [56]. Therefore, although there are too many possible CD derivatives, many of them have no production and utilization. On the other hand, highly water soluble hydroxyalkylated CDs, hydroxypropyl-β-

CD (HPβCD) and hydroxypropyl-γ-CD (HPγCD), and sulfobutylether-β-CD (SBE-β-CD) are industrially produced in high amounts (Figure 3a) [56].

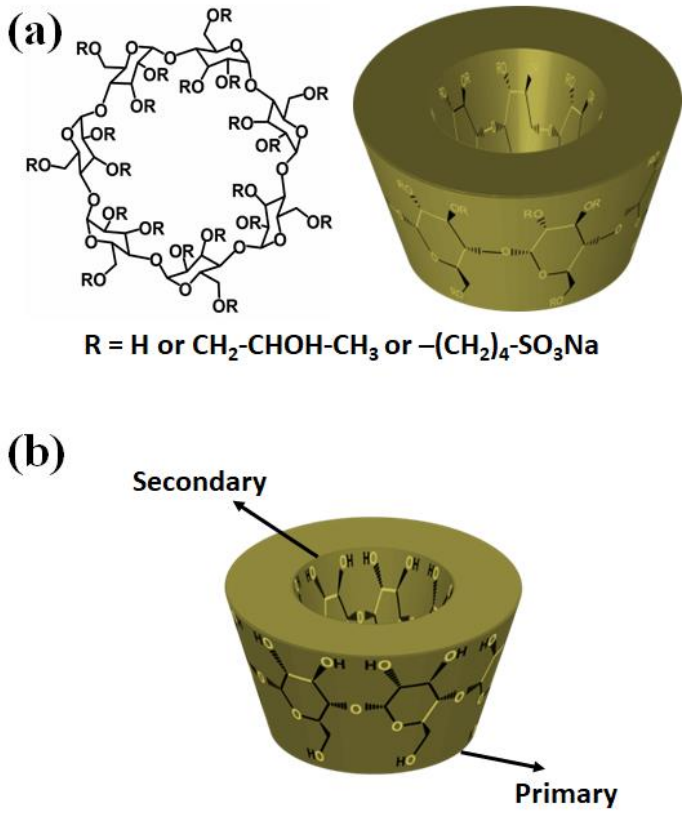

Figure 3. (a) Chemical structure and the schematic view of the modified HPβCD or SBE-β-CD, (b) schematic representation of the primary and secondary side of CD molecules.

In CD molecule structure, glucopyranose units are aligned in register such that all secondary hydroxyl groups (C2 and C3) are located on one side and primary hydroxyls (C6) are located on the other side [61]. Since primary hydroxyls have freedom for rotation, the diameter of two sides are different from each other; narrower (primary hydroxyls) and wider (secondary hydroxyls) (Figure 3b) [56, 61]. The internal cavity of CDs is occupied by C3 and C5 hydrogens, and

glycosidic oxygen bridges which results in relatively hydrophobic cavity [61, 62]. Thanks to this unique molecular structure of CDs, they can form non-covalent host-guest inclusion complexes with guest molecules having appropriate dimension and polarity (Figure 4) [61, 62]. Weak bonds are formed or broken during formation of inclusion complexes in aqueous solution of CD and guest molecule. In an aqueous solution, relatively apolar cavity of CD is filled by water molecules which is unfavorable due to polar-apolar interaction. Therefore, water molecules can be substituted by suitable guest molecule which is less polar than water [56, 63]. In other words, substitution of the enthalpy rich water molecules by appropriate guest molecules is the main driving force for the formation of inclusion complexes [62, 63]. There are several methods to form CD inclusion complexes (CD-IC) which are coprecipitation, slurry, paste, dry mixing, etc. [64]. Coprecipitation method is the most suitable one for laboratory scale preparation of CD-IC. In this method, solution of CD in water was prepared and guest molecule is added to the solution which provides favorable condition for formation of CD-IC [64].

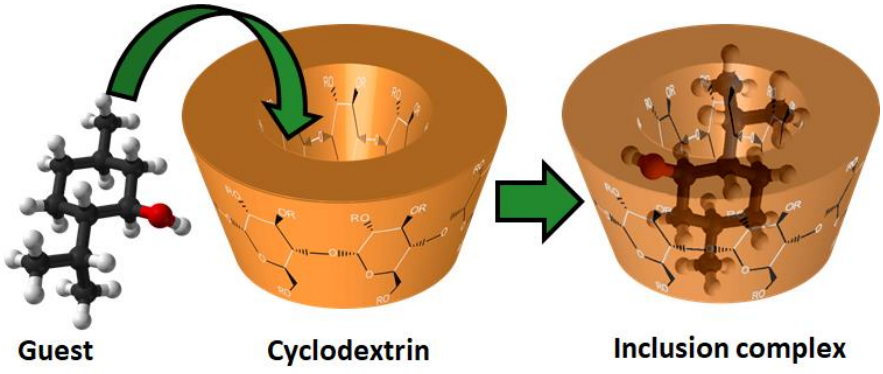

Figure 4. Schematic view of IC formation between CD and guest molecule.

Formation of CD-IC offers profound effects on the properties of guest molecules such as solubility enhancement, stabilization of labile molecules against light, heat

and oxidation, control of volatility, controlled release of guests, and taste modification [62, 64]. Therefore, CDs has wide range of application area in pharmaceuticals [65-67], functional foods [68, 69], cosmetics [70, 71], home/personal care [72] and filtration/membrane[45, 73].

1.3 Electrospinning of cyclodextrin inclusion complexes

Drugs and food additives have some restrictions including low aqueous solubility, low stability against external factors such as light, heat, oxygen, high volatility, and unpleasant taste and odor. Thus, encapsulation of drugs and food additives by using different methods has attracted attention of food and pharmaceutical industries. Formation of CD-ICs are one of the most common encapsulating methods. Besides being very attractive host material due to their structure and properties, non-toxic nature of CDs makes them quite useful for food and pharmaceutical applications. CD-encapsulated molecules can be protected from external factors while increasing their solubility and so their stability, bioavailability and shelf-life are enhanced [74-76]. There are many studies on CD encapsulation in literature to enhance properties of drugs and food additives while removing their drawbacks [75-80]. On the other hand, unique properties of electrospun nanofibrous materials such as nanoporous structure, large surface area, lightweight and design flexibility make them attractive material to encapsulate food additives and drugs [81, 82].

It is also possible to combine the properties of CD-ICs and electrospun nanofibers by integrating CD-ICs of active agents into electrospun nanofibrous mats. CD-ICs of some drugs and food additives were formed and incorporated into polymeric electrospun nanofibers by our group [23, 30, 37-39, 53, 83-87]. In general,

electrospun fibrous materials are obtained by using polymer since long polymer chains provide chain entanglements and overlapping for the fiber formation during the electrospinning process [6, 88, 89]. Therefore, use of small molecules to obtain electrospun nanofibers presents a real challenge. Nonetheless, Celebioglu and Uyar successfully produced uniform nanofibers from CDs without any polymeric matrices, since CD molecules in their highly concentrated solutions can form aggregates via hydrogen bonding [90, 91]. In the light of this, IC nanofibrous webs of CDs with different guest molecules were produced to enhance properties of these guests [22, 25, 32-36, 40, 41, 92-94]. Higher guest content compared to polymer based CD-IC nanofibrous webs is one of the main advantages of polymer-free systems. Besides, production of polymer-free CD-IC nanofibers eliminates the necessity of using organic solvents to dissolve polymer which is unfavorable for food and pharmaceutical industries.

Contribution of this thesis to "Electrospinning of CD-IC nanofibers" research is the application of these concept to some food additives (Chapter 2) and drugs (Chapter 3) and investigating the changes occurred in these guest molecules.

CHAPTER 2

ENCAPSULATION OF FOOD ADDITIVES BY CYCLODEXTRIN FUNCTIONALIZED ELECTROSPUN NANOFIBERS

2.1 Menthol/cyclodextrin inclusion complex nanofibers: Enhanced water solubility and high-temperature stability of menthol

This part of thesis was reprinted (adapted) by permission from Elsevier [95], ("Menthol/cyclodextrin inclusion complex nanofibers: Enhanced water solubility and high-temperature stability of menthol", Z. I. Yildiz, A. Celebioglu, M. E. Kilic, E. Durgun, and T. Uyar, *Journal of Food Engineering*, 224, 27-36, 2018), Copyright (2018) Elsevier.

2.1.1 Introduction

Menthol ((1R,2S,5R)-2-isopropyl-5-methylcyclohexanol) is a flavor/fragrance compound which is naturally occurring, volatile, cyclic terpene alcohol [96]. It is found in plants of Mentha species and gives them the typical minty smell and flavor.

It has used in many fields like pharmacy, food, cosmetics, pesticides etc. [96, 97]. Menthol is a highly volatile compound and it has a very low soluble in water, so, these drawbacks sometimes limit the use of menthol in certain applications [98, 99]. Formation of cyclodextrin inclusion complex (CD-IC) with menthol prevents the loss of menthol during storage and processing [100], and this will also provide higher water solubility for menthol [70]. There are recent studies including encapsulation of menthol by CDs to improve properties of menthol. In one of those studies, inclusion complex of menthol with hydroxypropyl-β-cyclodextrin (HPβCD) in powder form was produced [101] and the thermal stability enhancement of menthol was shown. In another recent study, β-CD grafted chitosan was used for entrapment of menthol molecules to analyse release profile of menthol [99].

In this study, highly concentrated aqueous solutions (160%, w/v) of menthol/CD-IC were prepared with two different CDs; hydroxypropyl-β-cyclodextrin (HPβCD) and hydroxypropyl-γ-cyclodextrin (HPγCD), with 1:1 M ratio (menthol:CD). Then, electrospinning of nanofibers (NFs) these two menthol/CD-IC systems (menthol/HPβCD-IC NFs and menthol/HPγCD-IC NFs) was successfully performed in order to obtain self-standing nanofibrous webs (Figure 5). The water-solubility, thermal stability and the release of menthol from menthol/CD-IC NFs was investigated.

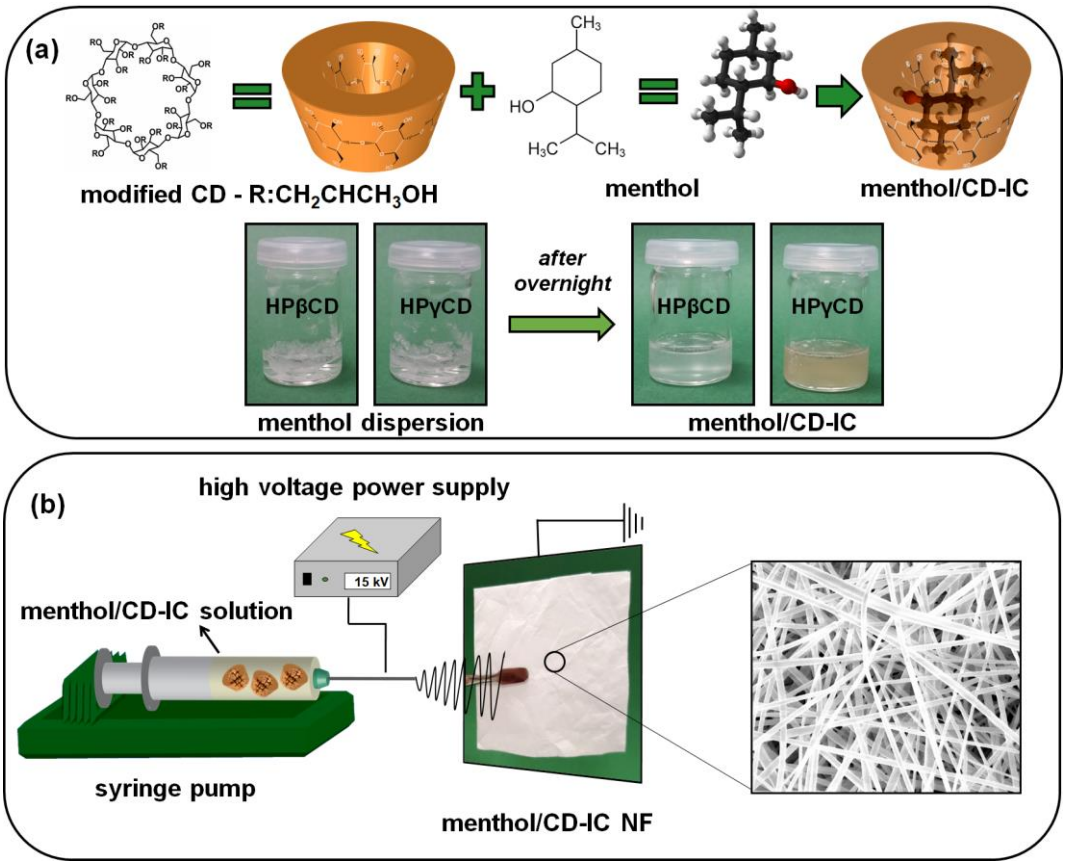

Figure 5. (a) The chemical structure of HPβCD; the schematic representation of menthol/CD-IC formation, menthol/CD-IC aqueous solutions and (b) electrospinning of nanofibers.

2.1.2 Experimental

2.1.2.1 Materials

The hydroxypropyl-β-cyclodextrin (HPβCD, Cavasol®W7 HP Pharma) and hydroxypropyl-γ-cyclodextrin (HPγCD, Cavasol®W8 HP) were given as free-samples for research purpose by Wacker Chemie AG (Germany). Menthol (>99%, Sigma-Aldrich), deuterated dimethylsulfoxide (DMSO-d6, Merck) potassium bromide (KBr, FTIR grade, Sigma-Aldrich) were purchased. All the materials were

used as-received without any further purification process. The deionized water used in this study was obtained from Millipore Milli-Q ultrapure water system.

2.1.2.2 Preparation of electrospinning solutions

CDs can form aggregates via intermolecular hydrogen bonding in their highly concentrated solutions and therefore, electrospinning of nanofibers is possible from such highly concentrated CD solutions without the need of any fiber forming polymeric matrix [91]. In the study of Celebioglu and Uyar [91], bead-free and uniform CD nanofibers were electrospun from the optimized concentration (160% (w/v) of CD with respect to solution) of modified CDs (HPβCD and HPγCD) in water. Therefore, in this study, the same optimized concentration of CD was used to form menthol/CD-IC solutions for the electrospinning. For the preparation of menthol/CD-IC aqueous solutions, firstly, menthol was dispersed in water, then, HPβCD (160%, w/v) and HPγCD (160%, w/v) were separately added to these aqueous menthol dispersion systems. The amount of CD and menthol was adjusted in order to get 1:1 M ratio of menthol/HPβCD-IC and menthol/HPγCD-IC. These suspensions were stirred overnight at room temperature. To minimize the loss of menthol during stirring, the glass vial (5 mL) was sealed tightly. At the end, the aqueous solutions of menthol/HPβCD-IC and menthol/HPγCD-IC were obtained for the electrospinning (Figure 5a). For comparison, pure CD solutions (HPβCD and HPγCD) at a concentration of 160% (w/v) were prepared in water for the electrospinning.

2.1.2.3 Electrospinning of nanofibers

Each solution of CD (HPβCD and HPγCD) and menthol/CD-ICs (menthol/HPβCD-IC and menthol/HPγCD-IC) was loaded into 1 mL syringe having a metallic needle (inner diameter = 0.4 mm) separately. The syringe was placed horizontally on the syringe pump (KD Scientific, KDS 101). High voltage at 10-15 kV was applied between tip of needle and the collector by the high voltage power supply (Spellman, SL Series). The distance between tip and collector was kept at 10-15 cm. The feed rate of the solutions was varied between 0,5 and 1 mL/h. Electrospun nanofibrous webs were collected on the metal collector which was covered by aluminum foil. Electrospinning was performed at 25 C and 35% relative humidity. Pure CD nanofibers (HPβCD NFs and HPγCD NFs) were electrospun for comparative studies with menthol/CD-IC NFs (menthol/HPβCD-IC NFs and menthol/HPγCD-IC NFs).

2.1.2.4 Measurements and characterizations

Phase solubility diagram was obtained according to the method reported by Higuchi and Connors (1965) [102]. An excess amount of menthol was added to aqueous solutions of HPβCD and HPγCD in capped vials which were shaken at room temperature in the dark for 48 h. After 48 h, solutions were filtered through a 0.45-μm membrane filter to remove undissolved part and the dissolved concentration of menthol was spectrophotometrically (Varian, Cary 100) determined. The experiment was carried out in triplicate and average of three measurements was taken. The apparent stability constant (K_s) of menthol/CD-IC was calculated from the phase solubility diagram according to the following equation: K_s = slope/ S_0 (1-slope)

where S_0 is the intrinsic solubility of menthol.

Computational method was also used to study the inclusion complexation between menthol and two types of CD (HPβCD and HPγCD). The first-principles analysis depending on density functional theory (DFT) was performed [103-105]. The exchange-correlation functional was expressed by generalized gradient approximation [106] including van der Waals correction [107]. All the elements were described by pseudopotentials generated by projector augmented-wave method [108]. The energy cutoff for plane wave basis set was chosen as 520 eV. The initial structures of host cyclodextrin, guest molecule (menthol) and their inclusion complexes were relaxed by minimizing the total energy and reducing the forces on atoms below 0.01 eV/A. The Brillouin zone was sampled by single k-point at Gamma-point and supercell was generated such that there is at least 10 Å between periodic images to avoid spurious interactions. The solvent effect was examined by implementing implicit solvent method which uses continuum dielectric description to describe the solvent [109]. Complexation energy (E_{comp}) of the resulting complexes can be computed by using the following formula:

$$E_{comp} = E_{CD} + E_{menthol} - E_{IC}$$

where E_{CD}, $E_{menthol}$ and E_{IC} is the total energy of host CD molecule (HPβCD or HPγCD), the guest molecule (menthol), and their IC, respectively. The energies were calculated in vacuum and water separately considering 1:1 menthol:CD stoichiometry. The solvation energy (E_{solv}) of the considered structures and their IC can be obtained by using calculated energies in vacuum and water by considering the formula below:

$E_{solv} = E_{water} - E_{vacuum}$

E_{water} and E_{vacuum} is the total energy of menthol, CD, or menthol/ CD-IC in water and vacuum, respectively.

A rheometer (Anton Paar, Physica CR 301) equipped with a cone/ plate accessory (spindle type CP 20-4) was used to measure the rheological behavior of menthol/HPβCD-IC and menthol/HPγCD-IC solutions at a constant shear rate of 100 s^{-1} at 25 °C. The conductivity of the solutions was measured by a Multiparameter InoLab® Multi 720-WTW at room temperature.

The morphological analyses of the electrospun nanofibers were performed by using scanning electron microscope (SEM) (FEI Quanta 200 FEG) [41]. Samples were sputtered with 5 nm Au/Pd prior to SEM imaging by PECS-682 to minimize charging problem. The average fiber diameter (AFD) was determined from the SEM images, and around 100 fibers were analysed for each sample.

The infrared spectra for pure menthol, pure CD NFs, and menthol/CD-IC NFs were obtained by using a Fourier transform infrared spectrometer (FTIR) (Bruker-VERTEX 70). For measurement, the samples were blended with KBr and pressed as pellets. The 64 scans were recorded between 4000 cm^{-1} and 400 cm^{-1} at resolution of 4 cm^{-1} [93]. The X-ray diffraction (XRD) (PANalytical X'Pert powder diffractometer) data of the pure menthol, pure CD NFs and menthol/CD-IC NFs were recorded by using Cu Kα radiation in a range of 2θ = 5°-30° [93]. The molar ratio of menthol to CD in menthol/CD-IC NFs was determined by using proton nuclear magnetic resonance (^{1}H NMR, Bruker D PX-400) system. The menthol/CD-IC NFs were dissolved in d6-DMSO at the 30 g L^{-1}

concentration. The spectra were recorded at 400 MHz and at 16 total scan [92]. Thermogravimetric analyses (TGA, TA Q500, USA) were performed for pure menthol, pure CD NFs, and menthol/CD-IC NFs. The TGA were conducted under nitrogen atmosphere by heating the samples from 30 °C to 600 °C at the heating rate of 20 °C/min.

Headspace gas chromatography-mass spectrometry (HS GC-MS, Agilent Technologies 7890A gas chromatograph equipped with 5975C mass spectrometer) was used to determine the amount of menthol released from menthol/HPβCD-IC NF and menthol/HPγCD-IC NF for 150 min. The release experiments were carried out in triplicate and the results were reported as average ± standard deviation. The capillary column was HP-5MS (Hewlett-Packard, Avondale, PA) (30 m X 0.25 mm i.d., 0.25 m film thickness). A 10 mg of menthol/HPβCD-IC NF and menthol/HPγCD-IC NF was separately placed in 20 mL headspace glass vials which was agitated by 500 rpm at 37 °C and 75 °C [41]. The syringe temperature was kept the same as the incubation temperature. The oven temperature was held at 60 °C for 1 min and increased to 165 °C at the rate of 10 °C/min and equilibrated at this temperature for 1 min. Helium was used as a carrier gas at a flow rate of 1.2 mL/ min. The menthol peak was identified by comparing its mass spectrum with that of menthol in the Search 2.0 and NIST MS libraries.

The fast-dissolving character and water-solubility enhancement were studied visually by the addition of water directly to the pure menthol and menthol/CD-IC NFs samples. The photos were taken in which, menthol powder (approximately the same amount found in menthol/CD-IC NFs) and the menthol/CD-IC NFs samples

were placed into petri dishes separately and then, 5 mL of water was added to these petri dishes.

2.1.3 Results and Discussion

2.1.3.1 Phase solubility studies

Phase solubility profiles of menthol/HPβCD-IC and menthol/ HPγCD-IC are given in Figure 6. The diagram of profiles corresponds to the A_L type in which the menthol concentration increased linearly by increasing CD concentration which confirmed the increment in solubility by inclusion complexation. Moreover, this linear trend was the indication of 1:1 M ratio inclusion complex formation tendency between menthol and CD molecules. Stability constant (K_s) values for menthol/HPβCD-IC and menthol/HPγCD-IC were calculated to represent the binding strength between menthol and CDs. K_s values were calculated as 716 M^{-1} and 894 M^{-1} ($R^2 > 0.99$) for menthol/HPβCD-IC and for menthol/HPγCD-IC, respectively, which demonstrated that menthol forms stable complexes with both CD types (HPβCD and HPγCD) with similar stabilities.

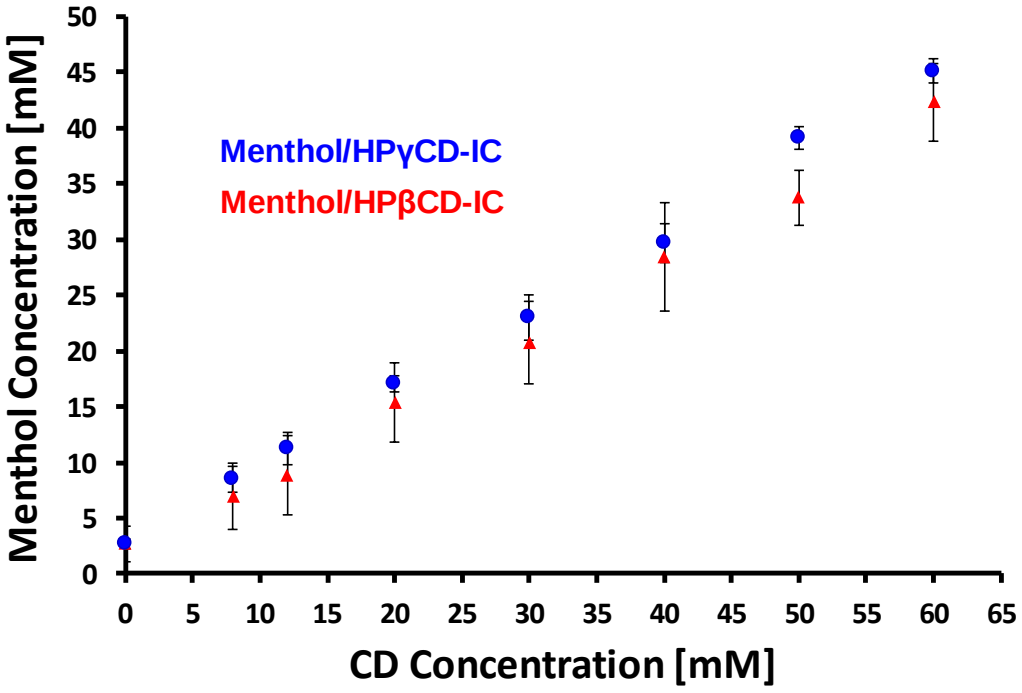

Figure 6. Phase solubility diagrams of menthol/HPβCD-IC and menthol/HPγCD-IC, (n = 3).

2.1.3.2 Computational modeling

The interaction of menthol and CD was examined at various sites for 1:1 stoichiometry and the lowest energy configurations for two vertical orientations of menthol (tail: the methyl group on the front, head: two methyl groups on the front) are illustrated in Figure 7. Our calculations suggested that menthol prefers head and tail orientation for HPβCD and HPγCD, respectively. In both cases, polar hydroxyl group of menthol remained inside the cavity and menthol was shifted towards the sides to enhance the interaction. Cavity of HPβCD and HPγCD is large enough to accommodate menthol in lateral orientation; however, the structure was deformed for HPβCD whereas lateral orientation was possible for HPγCD without deformation. The calculations were repeated in water for the most favourable

geometries and similar structural pattern was obtained, only the complexation energies (E_{comp}) changed. The results are summarized in Table 2.

Positive and high E_{comp} for all cases indicates stable IC formation between menthol and both CD types which was also confirmed by our phase solubility studies. For menthol/HPβCD-IC, the highest E_{comp} was obtained with head orientation in parallel with size matching while for menthol/HPγCD-IC, the highest Ecomp was obtained with tail orientation (Table 2). On the other hand, for both of the CDs, E_{comp} decreased in water. Being menthol a polar molecule, the decrease in E_{comp} can be attributed to polar-polar interaction of guest molecule and the solvent. As discussed above, menthol can also laterally fit into cavity of CD and E_{comp} was calculated as 21.25 and 23.19 kcal/mol in vacuum for HPβCD and HPγCD, respectively. This indicated that interaction of menthol was stronger in lateral orientation for HPγCD when compared to HPβCD. The energy for HPβCD-IC in lateral orientation was comparable with the energy in vertical orientation, suggesting the possibility of complexation in lateral orientation, as well.

The results for E_{solv} of menthol, CDs and their IC are given in Table 2. E_{solv} of menthol was calculated as 2.89 kcal/mol indicating a low solubility in water which is in agreement with the literature [99]. However, E_{solv} values were high for both inclusion complexes, suggesting a substantial increase in solubility upon complexation and the higher E_{solv} was obtained for menthol/HPγCD-IC (79.23 kcal/mol) when compared to menthol/HPβCD-IC (68.93 kcal/mol).

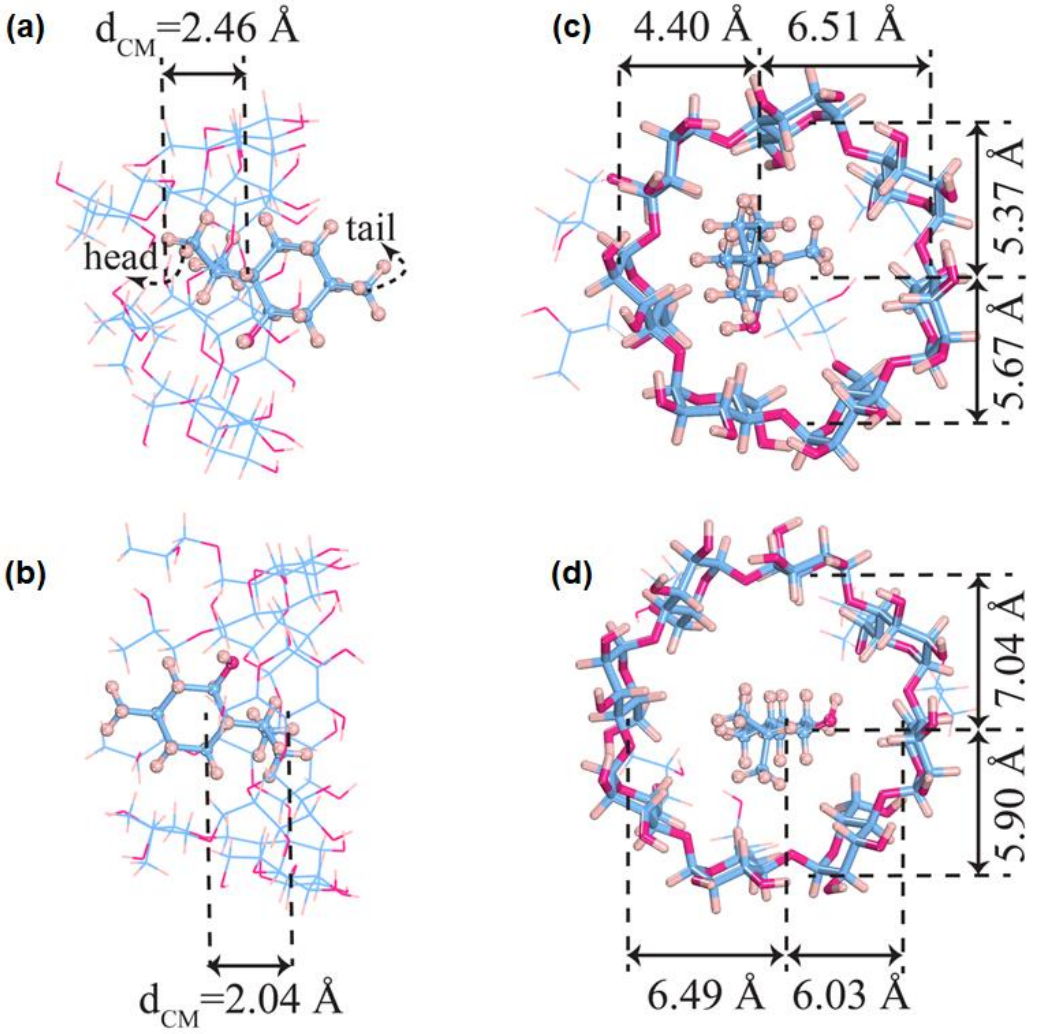

Figure 7. The optimized, lowest energy configurations of side views of ICs of (a) HPβCD and (b) HPγCD; and top view of ICs of (c) HPβCD and (d) HPγCD with menthol. The tail and head vertical orientation of menthol is shown by arrows. (Blue, pink, and light brown balls represent carbon, oxygen, and hydrogen atoms, respectively).

Table 2. Complexation and solvation energies of the menthol, CDs (HPβCD and HPγCD) and menthol within CDs at different orientations.

Host	Guest	Orientation	E_{comp} (vacuum) kcal/mol	E_{comp} (water) kcal/mol	E_{solv} kcal/mol
HPβCD	-	-	-	-	-71.17
HPβCD	Menhtol	Head	26.62	21.50	-68.93
HPβCD	Menhtol	Tail	23.24	-	-
HPβCD	Menhtol	Lateral	21.25	-	-
HPγCD	-	-	-	-	-83.34
HPγCD	Menthol	Head	19.23	-	-
HPγCD	Menthol	Tail	23.71	16.72	-79.23
HPγCD	Menthol	Lateral	23.20	-	-
-	Menthol	-	-	-	-2.89

2.1.3.3 Morphological analyses

The parameters of electrospinning process were optimized for the formation of the bead-free and uniform nanofibers. Highly concentrated (160% CD, w/v) menthol/HPβCD-IC and menthol/HPγCD-IC solutions were used for the electrospinning of nanofibers. The pictures of obtained electrospun nanofibrous webs are shown in Figure 8a-b with their representative SEM images (Figure 8c-d). The average fiber diameter (AFD) was 590 ± 230 nm for menthol/HPβCD-IC NFs and 1005 ± 285 nm for menthol/HPγCD-IC NFs (Table 3). The viscosity of menthol/HPγCD-IC solution was higher than menthol/HPβCD-IC solution and the solution conductivity of menthol/HPγCD-IC was lower than menthol/HPβCD-IC. Hence, the higher AFD of menthol/HPγCD-IC NF was due to its higher solution

viscosity and lower solution conductivity (Table 3) since it is well-known that higher solution viscosity and lower solution conductivity results in less stretching of the electrified jet that forms thicker fibers during electrospinning process [6, 12].

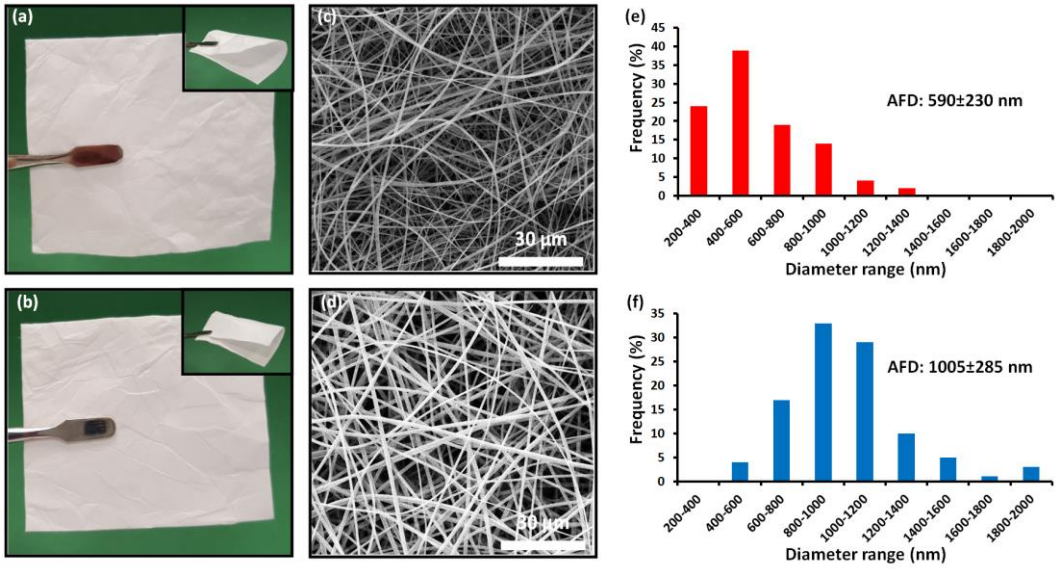

Figure 8. The photographs of (a) menthol/HPβCD-IC NFs and (b) menthol/HPγCD-IC NFs; SEM images of (c) menthol/HPβCD-IC NFs and (d) menthol/HPγCD-IC NFs; the fiber diameter distribution with average fiber diameter (AFD) of (e) menthol/HPβCD-IC NFs and (f) menthol/HPγCD-IC NFs.

Table 3. The properties of the solutions used for electrospinning and morphological characteristics of the resulting menthol/CD-IC NFs.

Solutions	Average fiber diameter (nm)	Fiber diameter range (nm)	Viscosity (Pa·s)	Conductivity (μS/cm)	Morphology
Menthol/HPβCD-IC (1:1)	590±230	210-1375	0.200±0.017	14.63±1.42	Bead free nanofibers
Menthol/HPγCD-IC (1:1)	1005±285	470-1905	0.300±0.015	5.42±0.10	Bead free nanofibers

2.1.3.4 Structural characterizations

The detailed characterizations of menthol/CD-IC NFs were done by using FTIR and XRD. These characterizations were also performed for pure menthol and pure CD NFs for comparison. The FTIR spectra of pure menthol, pure CD nanofibers, and menthol/CD-IC NFs are shown in Figure 9. The characteristic absorption bands of modified CDs are observed at around 3400 cm^{-1} (O-H stretching vibrations), 2932 cm^{-1} (C-H stretching vibrations), 1649 cm^{-1} (HO-H bending vibrations) [110], 1155 cm^{-1} (asymmetric stretching vibration of C-O-C glycosidic bridge) 1032 and 1083 cm^{-1} (C-C, C-O stretching vibrations) [111]. The pure menthol spectrum showed the signature peaks at 3315 cm^{-1} (O-H stretching vibrations), 2850-2957 cm^{-1} (C-H stretching vibrations), 1025-1045 cm1 (C-O stretching vibrations) [99] and 1367 cm^{-1} corresponding to isopropyl group [112]. The overlapping of absorption peaks for menthol and CD molecules made the identification of each compounds complicated for menthol/CD-IC NFs samples. Yet, the sharpest absorption peak of menthol at about 1367 cm^{-1} was present at the FTIR spectra of menthol/CD-IC NFs samples whereas this peak was absent for the pure CD NFs samples (Figure 9). This suggested the presence of menthol in menthol/HPβCD-IC NF and menthol/HPγCD-IC NF samples.

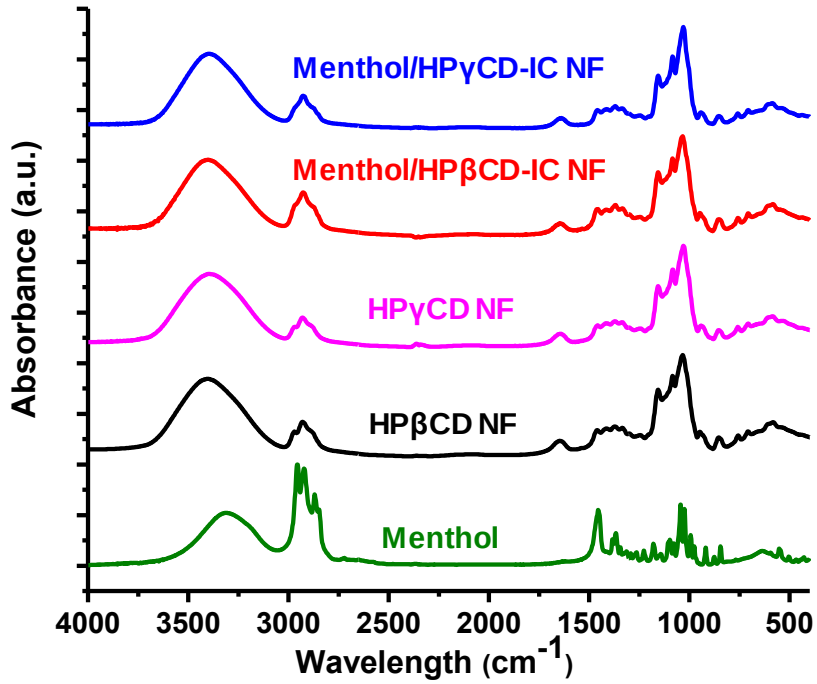

Figure 9. FTIR spectra of pure menthol, pure CD NFs and menthol/CD-IC NFs.

The crystalline structures of menthol, pure CD NFs and menthol/ CD-IC NFs were investigated by XRD. The XRD patterns of menthol/CD-IC NFs webs were very similar to those of pure CD NFs webs having amorphous structure (Figure 10). Besides, they did not show any diffraction peaks of menthol suggesting that menthol molecules were possibly isolated from each other by entering into CD cavities and cannot form any crystalline aggregates [83, 90, 91, 93, 111]. In other words, XRD results suggested the IC formation between CD and menthol molecules in menthol/HPβCD-IC NFs and menthol/HPγCD-IC NFs samples.

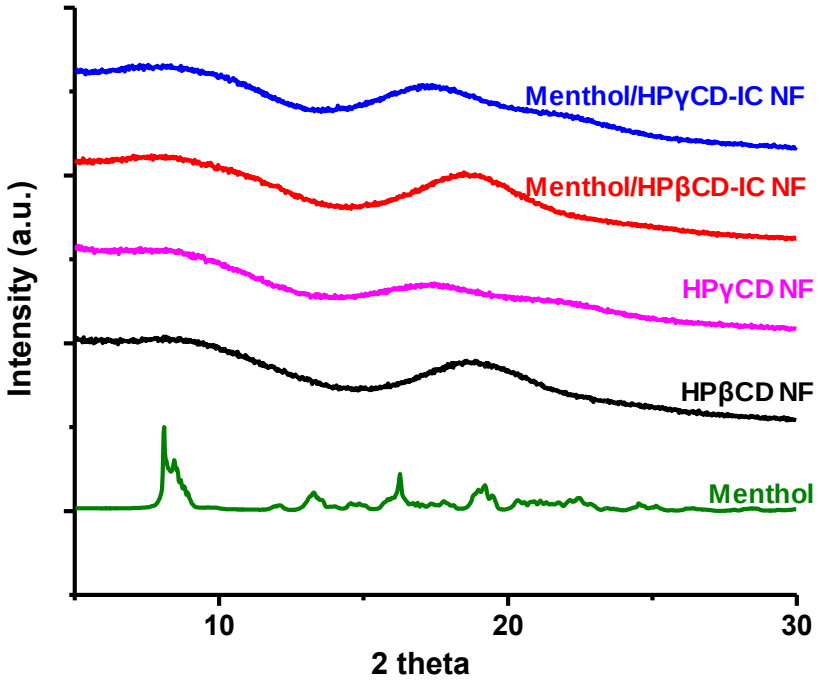

Figure 10. XRD patterns of pure menthol, pure CD NFs and menthol/CD-IC NFs.

2.1.3.5 The molar ratio of menthol in menthol/CD-IC NFs

^{1}H NMR study was performed to validate the presence of menthol and to determine the molar ratio between menthol and CD in menthol/CD-IC NFs by dissolving the samples in d6-DMSO. Initially, a ^{1}H NMR study was performed to detect the characteristic peaks corresponding to protons of CD NFs and pure menthol. The characteristic peaks of menthol were observed in the ^{1}H NMR spectra of menthol/CD-IC NFs which confirmed the presence of menthol in the menthol/CD-IC NFs samples. The molar ratios were calculated by taking integration of menthol peak at around 1.85 ppm (H-e) and the CD peak at around 5.8 ppm (H-1) (Figure 11). It was calculated that the molar ratio of menthol to HPβCD and HPγCD was ~0.75:1.00 and ~0.70:1.00 in menthol/HPβCD-IC NFs and menthol/HPγCD-IC

NFs samples, respectively. The molar ratio found for menthol/CD-IC NFs samples was lower than the initial ratio (1.00:1.00) and this is probably because of some uncomplexed menthol in menthol/CD-IC systems; however, menthol was mostly preserved during electrospinning process and/or during storage. ^{1}H NMR results revealed that menthol/HPβCD-IC NFs shows a slightly higher molar ratio which means higher complexation efficiency than menthol/HPγCD-IC NFs. Encapsulation efficiency (EE%) of menthol for menthol/CD-IC NFs was also calculated from the results of ^{1}H NMR. EE% was found as ~75% for menthol/HPβCD-IC and ~70% for menthol/HPγCD-IC NFs.

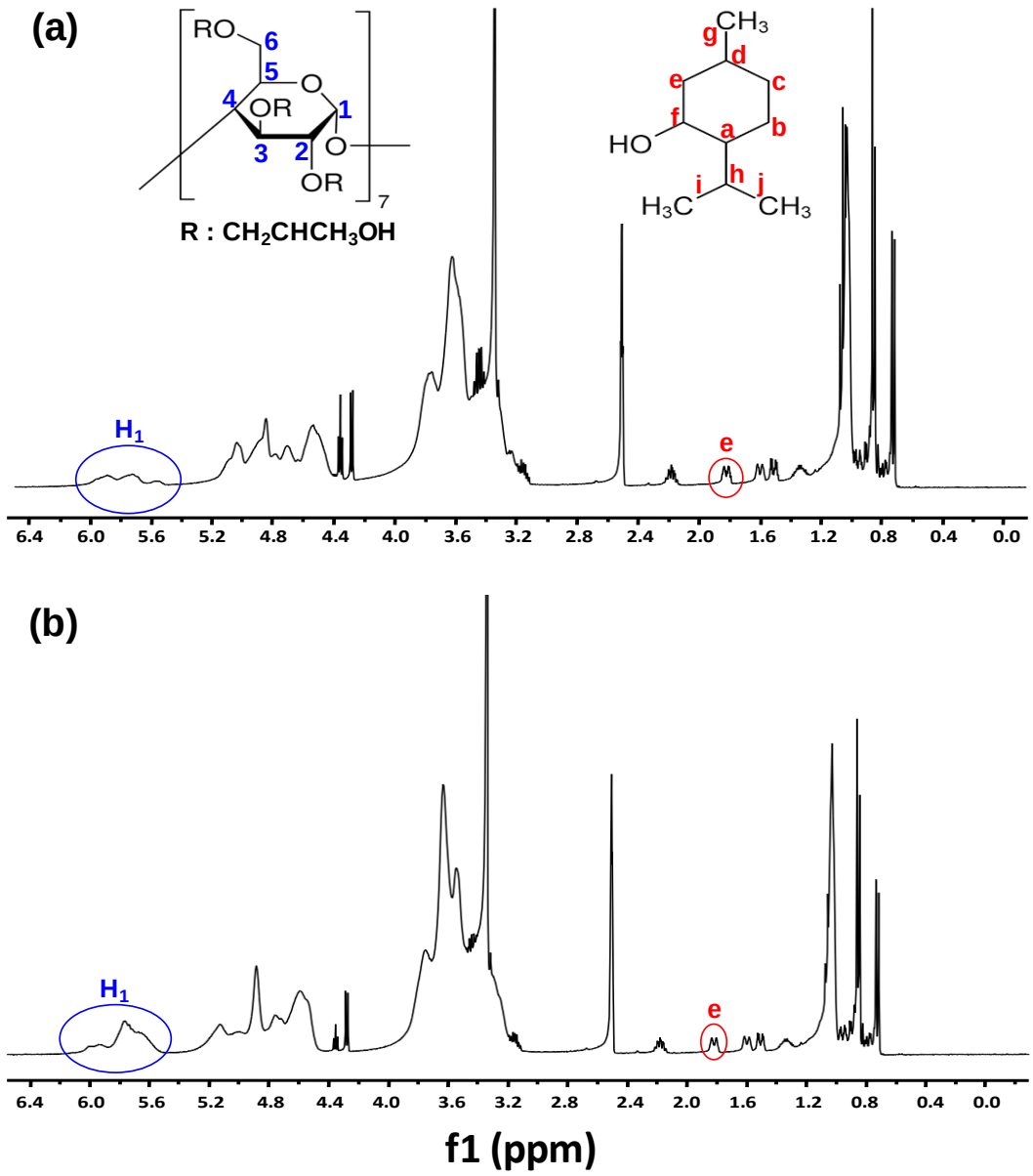

Figure 11. ^{1}H NMR spectra of (a) menthol/HPβCD-IC NFs and (b) menthol/HPγCD-IC NFs dissolved in d6-DMSO.

2.1.3.6 Thermal characterization

The thermal properties and thermal stability of menthol in menthol/CD-IC NFs were investigated by TGA. The TGA studies of pure CD NFs and pure menthol were also performed for comparison. The TGA thermograms of pure CD NFs have

two weight losses (Figure 12). The first one is below 100 °C corresponding to water losses and the second one is above 300 °C corresponding to main degradation of CD molecules. The TGA thermogram of pure menthol has one major weight loss due to its evaporation in the range of 50-130 °C indicating its highly volatile nature. For menthol/CD-IC NFs, the water loss below 100 °C and the CD degradation above 300 °C were also observed. Beside these losses, there was weight loss between 110-220 °C and 150-275 °C for menthol/HPβCD-IC NFs and menthol/HPγCD-IC NFs, respectively, which belong to evaporation of menthol. The evaporation of menthol was shifted from 50 to 130 °C to much higher temperature (110-220 °C and 150-275 °C) for menthol/CD-IC NFs which proved the presence of inclusion complexation between CD and menthol for both menthol/CD-IC NFs samples. TGA data clearly showed that thermal stability of menthol was enhanced significantly for menthol/CD-IC NFs due to IC formation [92]. From TGA thermogram, the amount of menthol in the menthol/HPβCD-IC NFs was calculated as 9.3% (w/w, with respect to HPβCD) that refers to the ~0.90:1.00 M ratio complexation. On the other hand, menthol amount in the menthol/HPγCD-IC NFs was calculated as 7.0% (w/w, with respect to HPγCD) that refers to ~0.75:1.00 M ratio complexation. TGA data indicated that significant amount of menthol was preserved and protected against evaporation during electrospinning process and storage for menthol/CD-IC NFs samples. Although the calculated amount of menthol from TGA in menthol/CD-IC NFs was not exactly same with the menthol amount calculated from ^{1}H NMR analyses, both results were comparable and consistent with each other suggesting that highly volatile menthol

was successfully preserved in menthol/CD-IC NFs samples due to inclusion complexation.

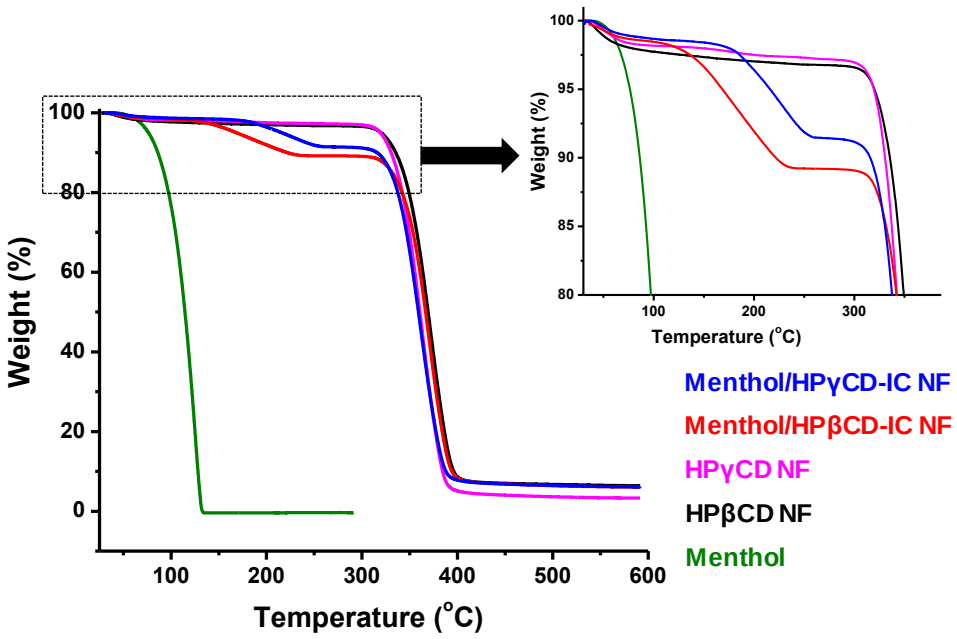

Figure 12. TGA thermogram of pure menthol, pure CD NFs and menthol/CD-IC NFs.

2.1.3.7 Release studies

The high volatility of menthol is very important problem for its shelf-life and applications, therefore; temperature stability and slow release of menthol is very crucial. The release profile of menthol/CD-IC NFs obtained from HS GC-MS are given in Figure 13. The higher amount of menthol released at higher temperature due to uncomplexation of menthol from the CD cavity [113]. The TGA and ^{1}H NMR results showed that menthol/HPβCD-IC NFs has higher amount of menthol and therefore higher amount of menthol released from menthol/HPβCD-IC NFs at both applied temperatures (at 37 °C and at 75 °C) as compared to menthol/HPγCD-

IC NFs. Moreover, after certain time, the release of menthol has become slower for both menthol/CD-IC NFs samples. In other words, the slow-release of menthol was achieved thanks to inclusion complex formation which could lead to shelf-life improvement of menthol for menthol/CD-IC NF samples.

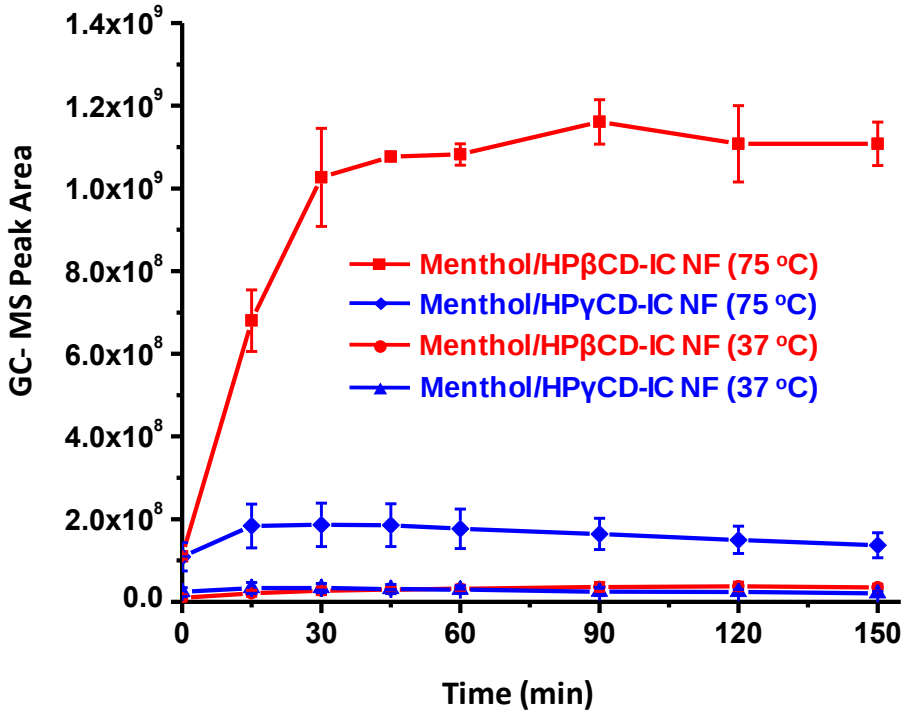

Figure 13. The cumulative release of menthol from menthol/HPβCD-IC NFs and menthol/HPγCD-IC NFs at 37 °C and 75 °C, (n = 3).

2.1.3.8 Dissolution behaviour

The fast-dissolving property and water-solubility enhancement of the menthol for menthol/CD-IC NFs was visually studied (Figure 14). The addition of water to petri dishes dissolved both menthol/CD-IC NFs within 1 s while pure menthol remained undissolved. This proved that menthol/CD-IC NFs has fast-dissolving character and provides water-solubility enhancement of menthol.

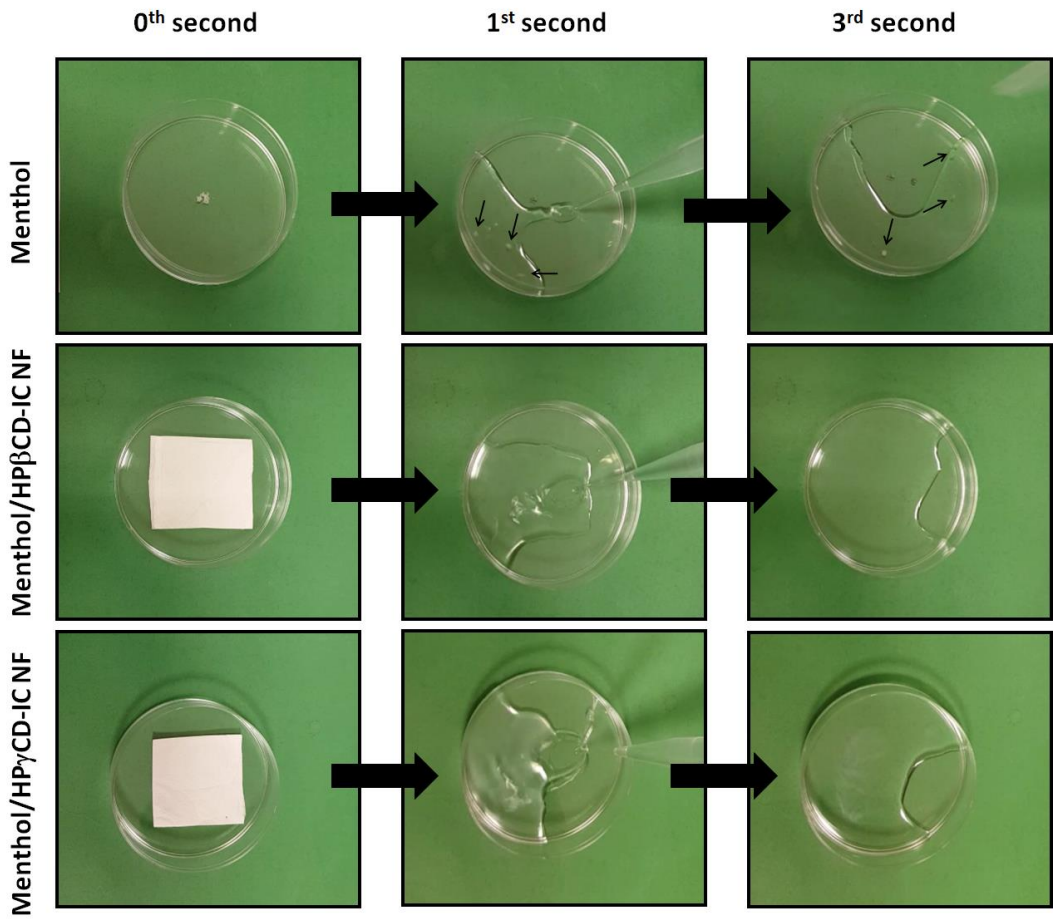

Figure 14. Presentation of the solubility behavior of menthol, menthol/HPβCD-IC NFs and menthol/HPγCD-IC NFs for a few seconds of water exposure (the arrows show the undissolved menthol crystals).

2.1.4 Conclusion

In this study, the fabrication of free-standing nanofibrous webs from menthol/cyclodextrin-inclusion complex (menthol/CD-IC) by using the electrospinning technique without using a carrier polymer matrix was presented. Two modified CDs (HPβCD and HPγCD) were used and the menthol/CD-IC NFs were electrospun from highly concentrated aqueous solutions of menthol/CD-IC. The fast-dissolving menthol/CD-IC NFs have combined advantages of cyclodextrin

inclusion complexation and high surface area of electrospun nanofibers. The menthol/CD-IC NFs have shown improvement for menthol such as enhancement in water-solubility, increase in thermal stability, and slow release of menthol. In brief, encapsulation of menthol in electrospun polymer-free CD-IC NF matrix may have potentials for food, oral-care and pharmaceuticals applications.

2.2 Fast-dissolving carvacrol/cyclodextrin inclusion complex electrospun fibers with enhanced thermal stability, water solubility, and antioxidant activity

This part of thesis was reprinted (adapted) by permission from Springer Nature [114], ("Fast-dissolving carvacrol/cyclodextrin inclusion complex electrospun fibers with enhanced thermal stability, water solubility, and antioxidant activity", Z. I. Yildiz, A. Celebioglu, M. E. Kilic, E. Durgun, and T. Uyar, *Journal of Materials Science*, 53, 15837-49, 2018), Copyright (2018).

2.2.1 Introduction

Carvacrol (Figure 15a) is a phenolic monoterpene found in oregano and thyme plants essential oil [115]. It is known by its antimicrobial and antioxidant activities. Also, carvacrol is approved by US Food and Drug Administration for food use and it is accepted as flavorings in the list of the Council of Europe which make its addition to foodstuff safe [116]. However, the use of carvacrol is limited due to its high volatility, poor water solubility (1.00-1.25 mg mL^{-1}) and low stability. Besides, due to low flavor threshold, it causes change in sensory properties of food [117].

In this study, we produced ultrafine fibers from the inclusion complexes of carvacrol with two types of modified CDs, hydroxypropyl-β-cyclodextrin (HPβ CD) and hydroxypropyl-γ-cyclodextrin (HPγCD) without using any additional polymeric matrices via electrospinning. Phase solubility test was performed to investigate the solubility of carvacrol when complexed with CDs, and also the complexation stability constant (K_s) for carvacrol/CD-IC systems was also determined. Molecular modeling by ab initio computational method was performed to examine the optimal CD-IC molar ratio and the most favourable orientation of inclusion complexation between CD and carvacrol. Based on the molecular modeling data, the carvacrol/CD-ICs were prepared with molar ratio of 1:1 (carvacrol/CD). The morphological, structural and thermal characterizations of carvacrol/CD-IC electrospun fibers were performed by SEM, FTIR, XRD, ^{1}H NMR and TGA. Furthermore, antioxidant activity of carvacrol/CD-IC fibers was analyzed by 2,2-diphenyl-1-picrylhydrazyl (DPPH) radical scavenging assay. Besides, the fast-dissolving character of carvacrol/CD-IC fibrous webs was analyzed visually by exposing them to water.

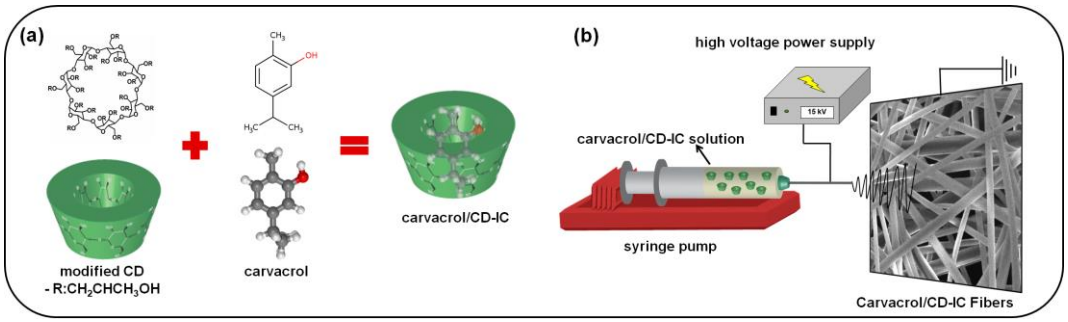

Figure 15. (a) The chemical structure of HPβCD and carvacrol; the schematic representation of carvacrol/CD-IC formation and (b) electrospinning of fibers from carvacrol/CD-IC solutions.

2.2.2 Experimental

2.2.2.1 Materials

Carvacrol (98%) and 2,2-diphenyl-1-picrylhydrazyl (DPPH) were purchased from Sigma-Aldrich. The hydroxypropyl-β-cyclodextrin (HPβCD) (degree of substitution ~ 0.6, Cavasol®W7 HP Pharma) and hydroxypropyl-γ-cyclodextrin (HPγCD) (degree of substitution ~ 0.6, Cavasol®W8 HP) were kindly donated by Wacker Chemie AG (Germany). Deuterated dimethylsulfoxide (DMSO-d6, deuteration degree min 99.8% for NMR spectroscopy) was obtained from Merck. The deionized water used was from a Millipore Milli-Q ultrapure water system. The materials were used as-supplied.

2.2.2.2 Preparation of solutions

For the preparation of carvacrol/CD-IC solutions, firstly, HPβCD (200%, w/v) and HPγCD (200%, w/v) were dissolved in water; then, carvacrol was added to these systems to get 1:1 molar ratio between carvacrol and CDs. These dispersions were stirred overnight at room temperature. At the end, the solutions of carvacrol/HPβCD-IC and carvacrol/HPγCD-IC were obtained. In addition, HPβCD and HPγCD were dissolved in water at concentration of 200% (w/v) to produce pure CD fibers (HPβCD fibers and HPγCD fibers) without carvacrol for comparative measurements [91].

2.2.2.3 Electrospinning of nanofibers

Each solution of pure CDs (HPβCD and HPγCD) and carvacrol/CD-ICs (carvacrol/ HPβCD-IC and carvacrol/HPγCD-IC) was loaded to the 1-mL syringe with a metallic needle inner diameter of 0.4, separately. Syringe pump (KD Scientific,

KDS 101) was used to pump solutions with a constant rate of 0.5-1 mL h^{-1}. Collector was placed at 10-15 cm distance from tip of needle, and high voltage at 10-15 kV was applied between tip of needle and the collector by the high voltage–power supply (Spellman, SL Series). Electrospun fibers were collected on the metal collector covered by piece of aluminum foil. Electrospin apparatus was enclosed by plexiglass box at 25 °C and 40% relative humidity.

2.2.2.4 Measurements and characterizations

Phase solubility diagram was obtained according to the method reported by Higuchi and Connors [102]. In this experiment, an excess amount of carvacrol was added to aqueous solutions of HPβCD and HPγCD in capped vials which were shaken at room temperature in the dark for 48 h and then the solutions were filtered through a 0.45-μm membrane filter. Then, concentration of carvacrol was spectrophotometrically (Varian, Cary 100) determined from filtered solutions. The experiment was carried out in triplicate, and average of three measurements was taken. The apparent stability constant (K_s) of carvacrol/CD-ICs was calculated from the phase solubility diagram according to the following equation: K_s = slope/ S_0 (1- slope)

where S_0 is the intrinsic solubility of carvacrol.

To reveal the mechanism of inclusion complex, ab initio calculations based on density functional theory were done according to our previous studies [34, 95].

The rheological behavior of the pure CDs and carvacrol/CD-IC solutions was measured by a rheometer (Anton Paar Physica MCR 301) equipped with a cone/plate accessory (spindle type CP 20-4). The constant shear rate was adjusted

as 100 s^{-1}. The conductivity of the solutions was measured by a Multiparameter InoLab Multi 720-WTW at room temperature.

Scanning electron microscope (SEM) (FEI Quanta 200 FEG) was used to perform the morphological analyses of the electrospun fibers. Each sample was sputtered with 5 nm Au/Pd prior to SEM imaging by PECS-682 to minimize charging problem. The diameter of 100 single fibers was measured to calculate average fiber diameter (AFD). Fourier transform infrared spectrometer (FTIR) (Bruker-VERTEX 70) was used to obtain the infrared spectra for pure carvacrol, pure CD fibers, and carvacrol/CD-IC fibers. Pellets were prepared by pressing the blend of potassium bromide (KBr) and samples, respectively. The 64 scans were recorded between 4000 and 400 cm^{-1} at resolution of 4 cm^{-1}. The molar ratio of carvacrol to CD was determined by using proton nuclear magnetic resonance (^{1}H NMR, Bruker D PX-400) system. The electrospun fibrous web was dissolved in d6-DMSO at the 30 g L^{-1} concentration. The spectra were recorded at 400 MHz and at 16 total scan. Thermogravimetric analyses (TGA, TA Q500, USA) were performed for carvacrol, pure CD fibers, and carvacrol/CD-IC fibers. The TGA experiments were conducted under nitrogen atmosphere by heating the samples from 25 to 600 °C at the heating rate of 20 °C min^{-1}.

2,2-Diphenyl-1-picrylhydrazyl (DPPH) radical scavenging method was used to examine antioxidant activity of samples. For this, DPPH solution in methanol (7.5×10^{-5} M) was prepared. The concentration of CD-IC fibers in water was arranged to have carvacrol ranging from 8 to 0.0625 mg mL^{-1}. On the other hand, pure carvacrol system including the highest amount of carvacrol which is 8 mg mL^{-1} concentration was prepared and undissolved part of carvacrol was filtered. Then,

200 μL of aqueous solutions of water-based carvacrol/CD-IC fibers at different concentrations and pure carvacrol were mixed with 2.3 mL of DPPH solution, and they were stirred for 1 h. DPPH solution has maximum absorption at 517 nm, and the absorption of DPPH solution disappears along with its reduction by antioxidant compound [118]. UV–Vis spectroscopy (Varian, Cary 100) was used to examine the reduction at the absorbance intensity (517 nm) for aqueous solutions of carvacrol/CD-IC fibers at different concentrations. The experiment was carried out in triplicate, and the DPPH radical scavenging efficiency was expressed as the inhibition percentage and was calculated by the following formula:

DPPH radical scavenging (%) = $((A_{blank} - A_{sample})/ A_{blank})\times 100$

Besides, carvacrol concentration providing 50% inhibition (IC50) was calculated from the graph. To investigate the stability of fibers with time in terms of antioxidant activity, the 3-year-old carvacrol/CD-IC fibers (stored at 4 C in the refrigerator) were tested as well. These 3-year-old carvacrol/CD-IC fiber samples were weighed such that their weights were the same with the fresh fibers providing IC50 value. The antioxidant activity test was also performed for the 3 years old carvacrol/CD-IC fibers, and the inhibition percentage was calculated.

The fast-dissolving character of carvacrol/CD-IC fibers in water was visually investigated. Carvacrol/HPβCD-IC fibrous web and carvacrol/HPγCD-IC fibrous web with the same weight were placed into petri dishes; then, 5 mL of water was added to these petri dishes.

2.2.3 Results and discussion

2.2.3.1 Phase solubility studies

The phase solubility profiles of carvacrol/CD-ICs are presented in Figure 16. From these profiles, it was observed that there was a linear increase in the solubility of carvacrol as CD concentration increases in a range of 0 to 16 mM. However, when the concentration of CD exceeded 16 mM, the negative deviation from linear profile was observed; in other words, the CD was proportionally less effective for solubilizing of carvacrol at higher concentrations. This type of profile is called as A_N-type [119]. The negative deviation from linearity has several explanations including CD self-association at high concentrations [120]. The stability constant (K_s) values for carvacrol/HPβCD-IC and carvacrol/HPγCD-IC were calculated from the linear part of the diagrams according to the equation mentioned experimental part. K_s values was calculated as 3321 and 288 M^{-1} (R^2>0.99) for carvacrol/HPβCD-IC and carvacrol/HPγCD-IC, respectively, which indicated that carvacrol forms more stable complex with HPβCD than HPγCD.

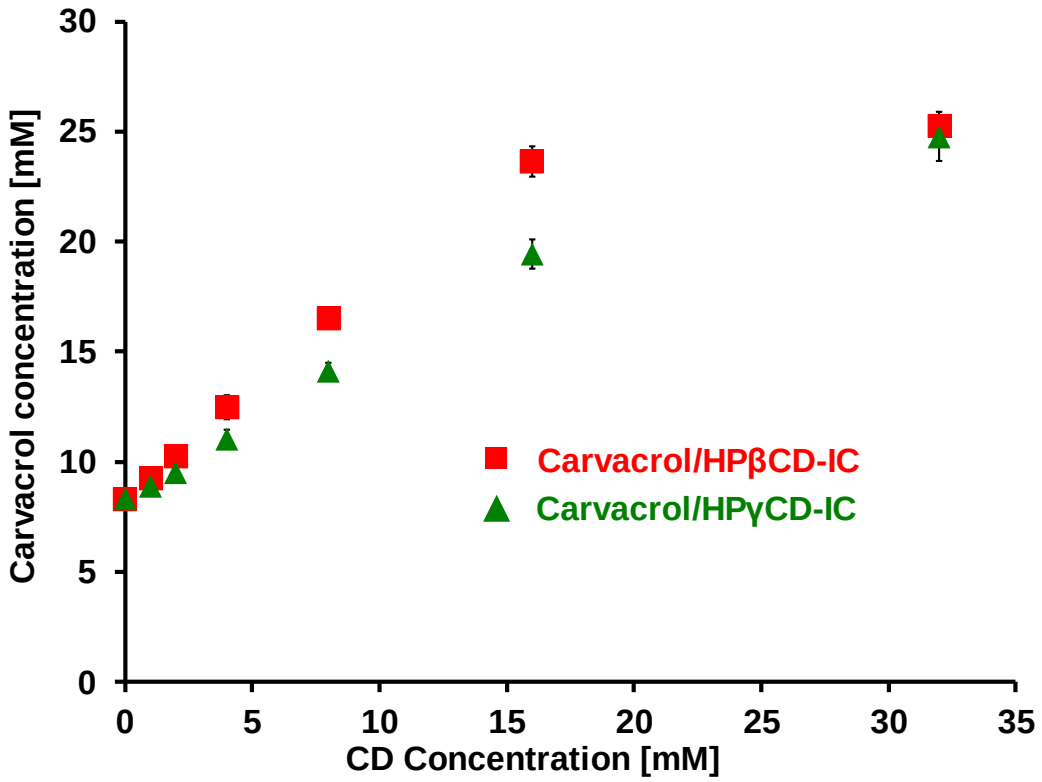

Figure 16. Phase solubility diagrams of carvacrol/HPβCD-IC and carvacrol/HPγCD-IC solutions, (n=3).

2.2.3.2 Computational modelling

In this section, we studied the interaction of carvacrol molecule with HPβCD and HPγCD by performing ab initio modeling techniques. Firstly, all the structures were relaxed without any constraint both in vacuum and in water to obtain the optimized geometries. Next, the guest molecule was approached to CD through wider rim with 1Å steps and the total energy was calculated at each step. For carvacrol, there were two possible vertical orientations which were labeled as tail (-CH_3 and -OH end) and head (-CH_3 and -CH_3 end) as shown in Figure 17. Accordingly, the interaction of carvacrol with both CDs was revealed by taking into account the position (or site) and orientation. Our calculations indicated that carvacrol molecule forms

inclusion complexes with HPβCD and HPγCD without energy barrier and the most favorable geometries are illustrated in Figure 17. In both cases, carvacrol was completely settled in CD and head and tail orientation for HPβCD and HPγCD was preferred, respectively. As width of HPγCD is larger, carvacrol shifted towards the sides to enhance the interaction while it remained at the center of HPβCD. Due to size mismatch, carvacrol cannot laterally fit into HPβCD but the cavity of HPγCD is large enough to accommodate carvacrol in lateral orientation, as well. When the results in vacuum and water are compared, a significant change in geometries cannot be noticed but the strength of interaction (or complexation energies) alters. The complexation energy (E_{comp}) for 1:1 stoichiometry can be defined as:

$$E_{comp}=E_{CD} + E_{carvacrol} - E_{IC}$$

where E_{CD}, $E_{carvacrol}$, and E_{IC} is the total energy of CD (HPβCD or HPγCD), the guest carvacrol molecule, and their inclusion complexes, respectively. Total energies were calculated both in vacuum and solvent. E_{comp} values are listed in Table 4.

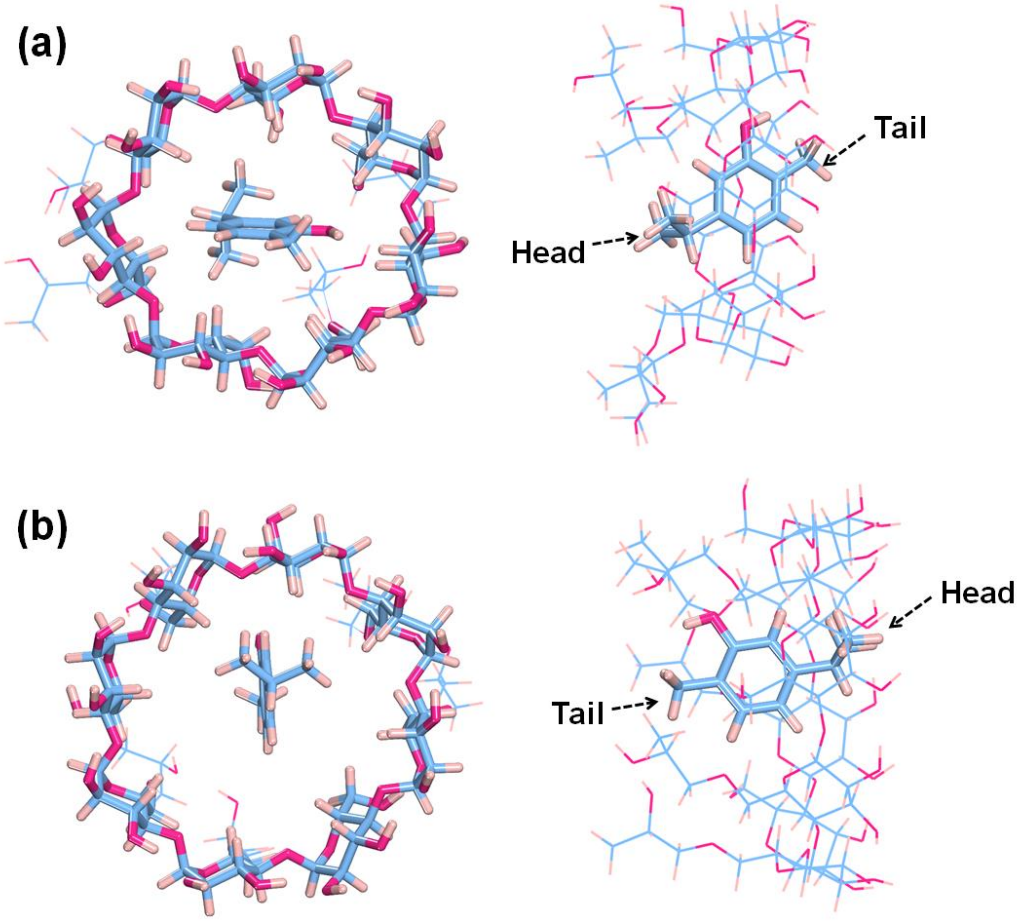

Figure 17. Top and side view of inclusion complexes of (a) HPβCD and (b) HPγCD with carvacrol. The tail and head vertical orientation of carvacrol is shown by arrows. (Blue, pink and light brown balls represent carbon, oxygen, and hydrogen atoms, respectively).

The obtained results indicated that carvacrol molecule can form stable inclusion complexes with HPβCD and HPγCD. The highest E_{comp} was obtained for carvacrol/HPβCD-IC with head orientation where the carvacrol was slightly tilted, -OH group was inside the cavity and -CH_3 groups were between hydroxypropyl arms. When compared, the energy differences between the head and tail orientations were small which suggests the possibility of complex formation with both configurations. In addition, even it is less favorable, carvacrol can laterally fit

into HPγCD with significant complexation energy. To reveal the effect of solvent environment, the calculations were repeated in water for the most favorable configurations. E_{comp} decreases for both CDs when inclusion complex is formed in water which can be attributed to interaction of phenolic functional group with the water.

As mentioned before, carvacrol has poor solubility in water but its solubility can be enhanced by complexation with CDs [117]. The change in solvation energy (E_{solv}) can be used to reveal this claim. E_{solv} is defined as:

$$E_{solv} = E_{water} - E_{vacuum}$$

E_{water} and E_{vacuum} is the total energy of carvacrol, CD, or inclusion complex in water and vacuum, respectively (Table 4). E_{solv} of carvacrol molecule was calculated as -4.31 kcal mol^{-1} confirming the low solubility in water. On the other hand, E_{solv} was -71.17 and -83.34 kcal mol^{-1} for carvacrol/HPβCD-IC and carvacrol/HPγCD-IC, suggesting a substantial increase in solubility upon complexation. This finding is also correlated with the phase solubility analyses where the water solubility of carvacrol has increased by inclusion complexation with the CDs.

Table 4. Complexation and solvation energies of the carvacrol, CDs (HPβCD and HPγCD) and carvacrol within CDs at different orientations.

Host	Guest	Orientation	E_{comp} (vacuum) kcal mol^{-1}	E_{comp} (water) kcal mol^{-1}	E_{solv} kcal mol^{-1}
HPβCD	-	-	-	-	-71.17
HPβCD	Carvacrol	Head	26.92	21.48	-70.03
HPβCD	Carvacrol	Tail	26.65	-	-
HPγCD	-	-	-	-	-83.34
HPγCD	Carvacrol	Head	17.65	-	-
HPγCD	Carvacrol	Tail	18.42	15.66	-84.88
HPγCD	Carvacrol	Lateral	23.20	-	-
-	Carvacrol	-	-	-	-4.31

2.2.3.3 Morphological analyses

The solutions of carvacrol/CD-IC and pure CD were electrospun at optimized parameters to produce bead-free fibers. The photographs and SEM images of these bead-free fibrous webs of carvacrol/CD-IC having self-standing and flexible characteristics are given in a Figure 18. The solution properties of carvacrol/CD-IC that directly have an impact on the morphology of the electrospun fibers and the fiber diameters are summarized in Table 5. The average fiber diameter (AFD) value was calculated as 1600±640 nm for carvacrol/HPβCD-IC fibers and as 2735±760 nm for carvacrol/HPγCD-IC fibers. This difference in their AFD is mostly related with the viscosity of their solutions since higher viscosity results in less stretching of the electrified jet that forms thicker fibers during electrospinning process [6, 12].

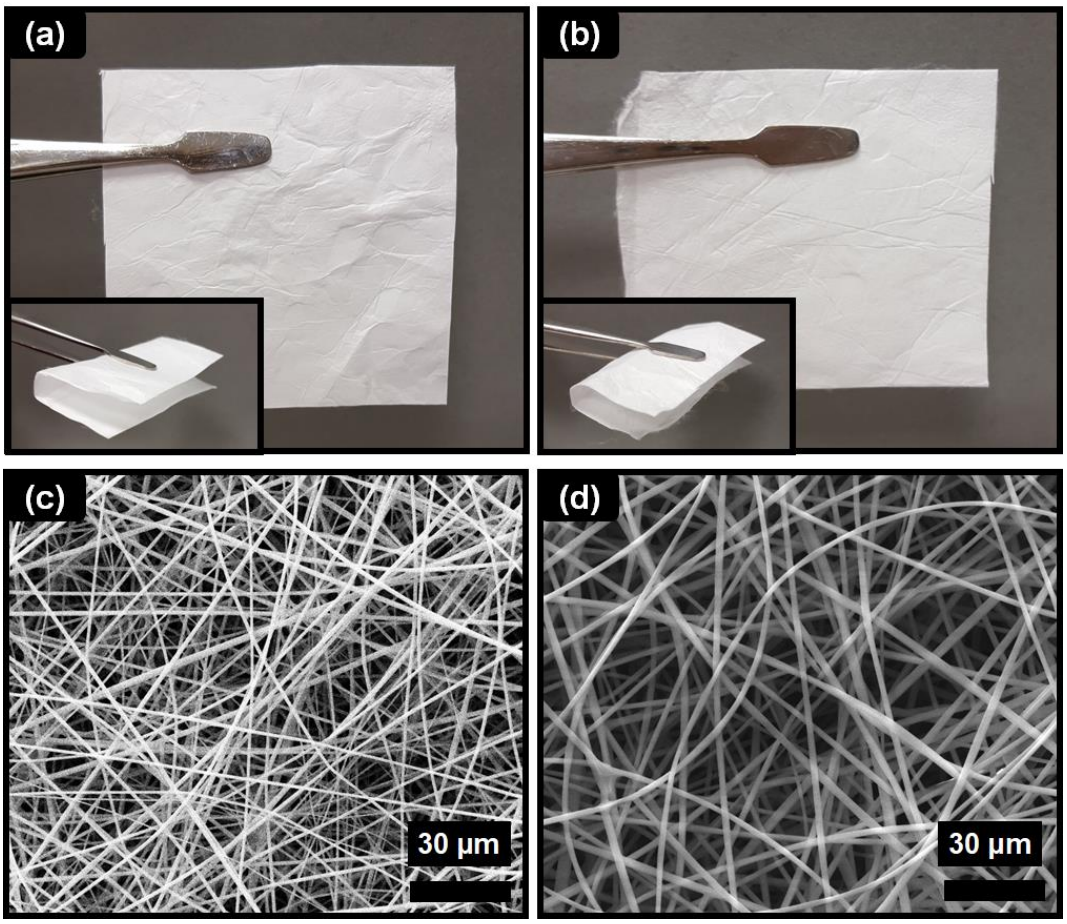

Figure 18. The photographs of (a) carvacrol/HPβCD-IC fibers and (b) carvacrol/HPγCD-IC fibers; SEM images of electrospun fibers obtained from the solutions of (c) carvacrol/HPβCD-IC and (d) carvacrol/HPγCD-IC.

Table 5. The properties of the solutions used for electrospinning and morphological characteristics of the resulting carvacrol/CD-IC fibers.

Solutions	Average fiber diameter (nm)	Fiber diameter range (nm)	Viscosity (Pa·s)	Conductivity (μS/cm)	Morphology
Carvacrol/HPβCD-IC (1:1)	1600±640	425-2938	0.95	10.98	Bead free nanofibers
Carvacrol/HPγCD-IC (1:1)	2735±760	1471-6415	1.15	2.96	Bead free nanofibers

2.2.3.4 Structural characterization

FTIR measurements were taken to characterize the carvacrol/CD-IC fibers. Besides carvacrol/CD-IC fibers, pure carvacrol and pure CD fibers were also characterized to make a comparison (Figure 19). The characteristic absorption bands of pure CD fibers were observed at around 3400 cm^{-1} (O-H stretching vibrations), 2932 cm^{-1} (C-H stretching vibrations), 1649 cm^{-1} (H-O-H bending vibrations) [110], 1155 cm^{-1} (asymmetric stretching vibration of C-O-C glycosidic bridge) 1032 and 1083 cm^{-1} (C-C, C-O stretching vibrations) [111]. The spectrum for carvacrol showed also wide absorption band at around 3400 cm^{-1} (O-H stretching vibrations), and band between 2800- 3000 cm^{-1} (stretching vibrations of C–H bonds), peaks between 1400-1650 cm^{-1} (aromatic C=C stretching), peak at around 1250 cm^{-1} (aromatic O-H stretching vibrations), peaks between 800-900 cm^{-1} (aromatic C-H bending). Absorption peaks for pure carvacrol and CD were overlapped which made the identification of each compound complicated for carvacrol/CD-IC fibers. However, there was an increase in the intensity of peaks for carvacrol/CD-IC fibers at two locations; 1250 cm^{-1} and 1585 cm^{-1} (Figure 19). This result suggested the presence of carvacrol in both carvacrol/CD-IC fibers.

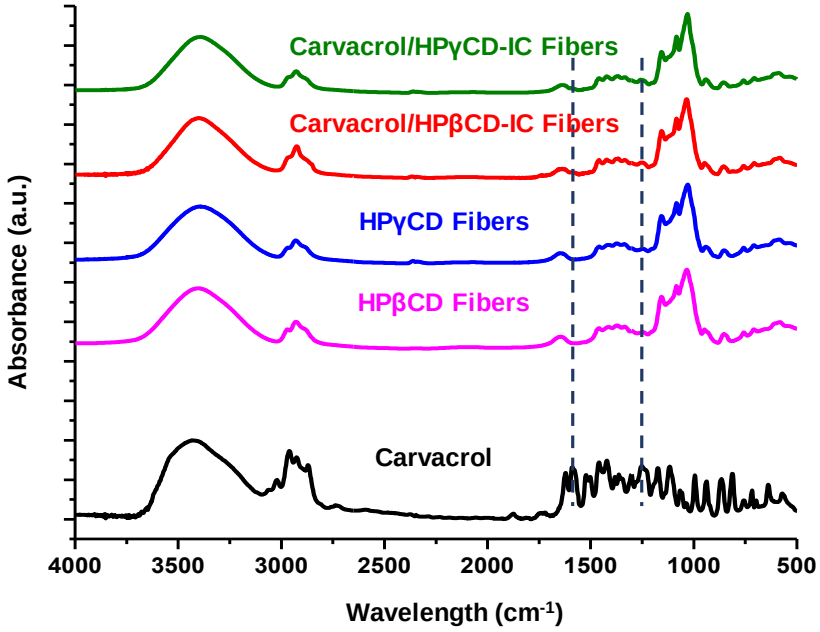

Figure 19. FTIR spectra of pure carvacrol, pure CD fibers and carvacrol/CD-IC fibers.

2.2.3.5 The molar ratio of carvacrol in carvacrol/CD-IC fibers

The molar ratio of carvacrol to HPβCD and HPγCD in carvacrol/CD-IC fibers was analysed mainly by ^{1}H-NMR study (Figure 20). In order to calculate the molar ratio, integration of characteristic peaks of carvacrol at around 1.14 ppm and CD peak at around 1.03 ppm were taken for both carvacrol/CD-IC fibers. The molar ratio of carvacrol/CD was calculated as 0.73:1.00 for carvacrol/HPβCD-IC fibers and 0.98:1.00 for carvacrol/HPγCD-IC fibers. From these results, it can be concluded that carvacrol was mostly preserved for both fibers during electrospinning process with encapsulation efficiencies of 73% for carvacrol/HPβCD-IC fibers and 98% for carvacrol/HPγCD-IC fibers. Besides, the molar ratio of 3-year-old fibers stored at 4˚C were also calculated from ^{1}H-NMR (Figure 21). The molar ratio of old fibers

was calculated as 0.70:1.00 for carvacrol/HPβCD-IC fibers and 0.94:1.00 for carvacrol/HPγCD-IC fibers. This finding confirmed that carvacrol was effectively preserved in both carvacrol/HPβCD-IC fibers and carvacrol/HPγCD-IC fibers during such long storage period. These ratios were also confirmed by molar ratio found by thermal gravimetric analysis (TGA) as discussed in the following section which were calculated as 0.88:1.00 and 0.94:1.00 for carvacrol/HPβCD-IC fibers and carvacrol/HPγCD-IC fibers, respectively.

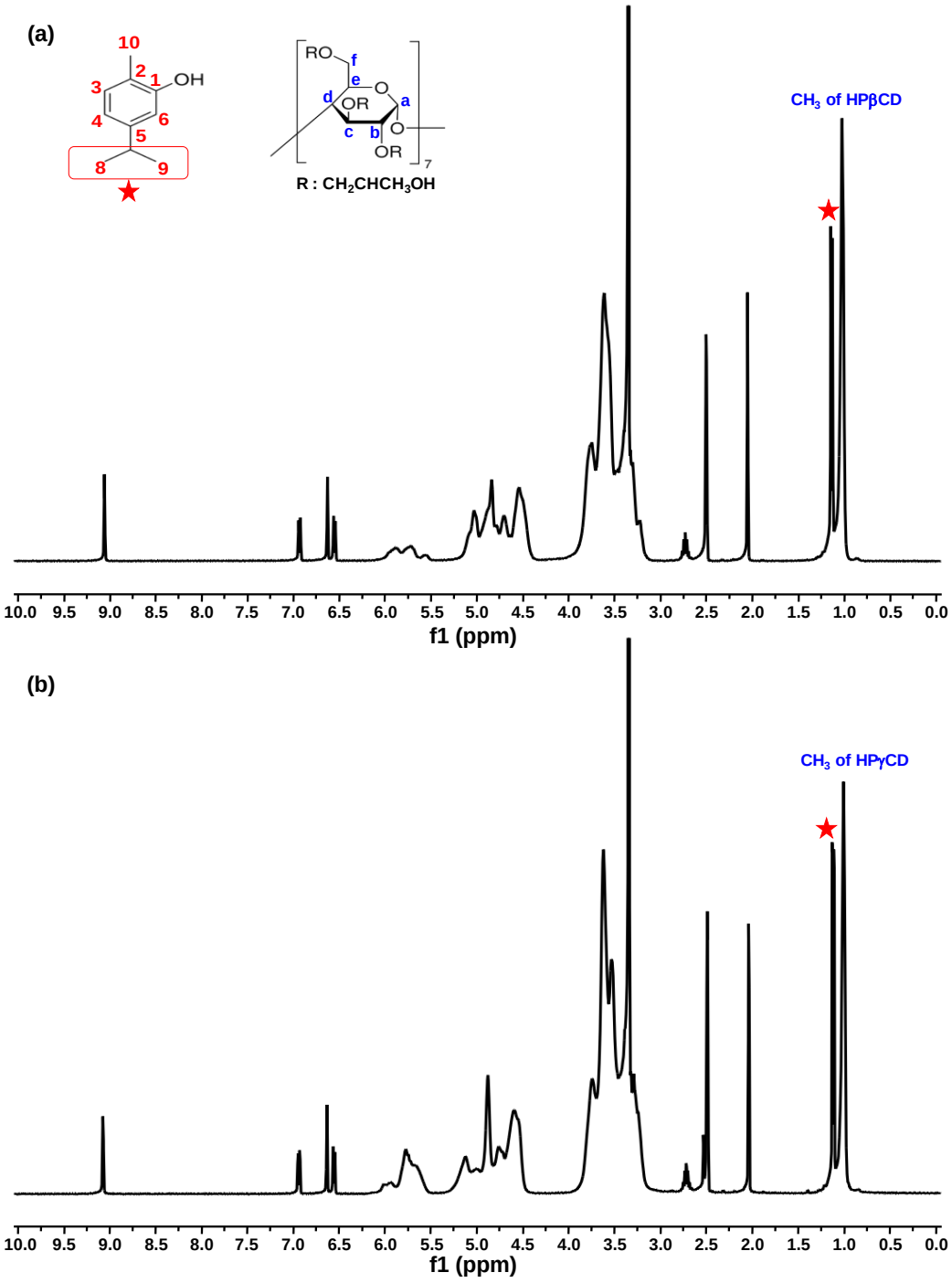

Figure 20. ^{1}H-NMR spectra of (a) carvacrol/HPβCD-IC and (b) carvacrol/HPγCD-IC fibrous web dissolved in d6-DMSO.

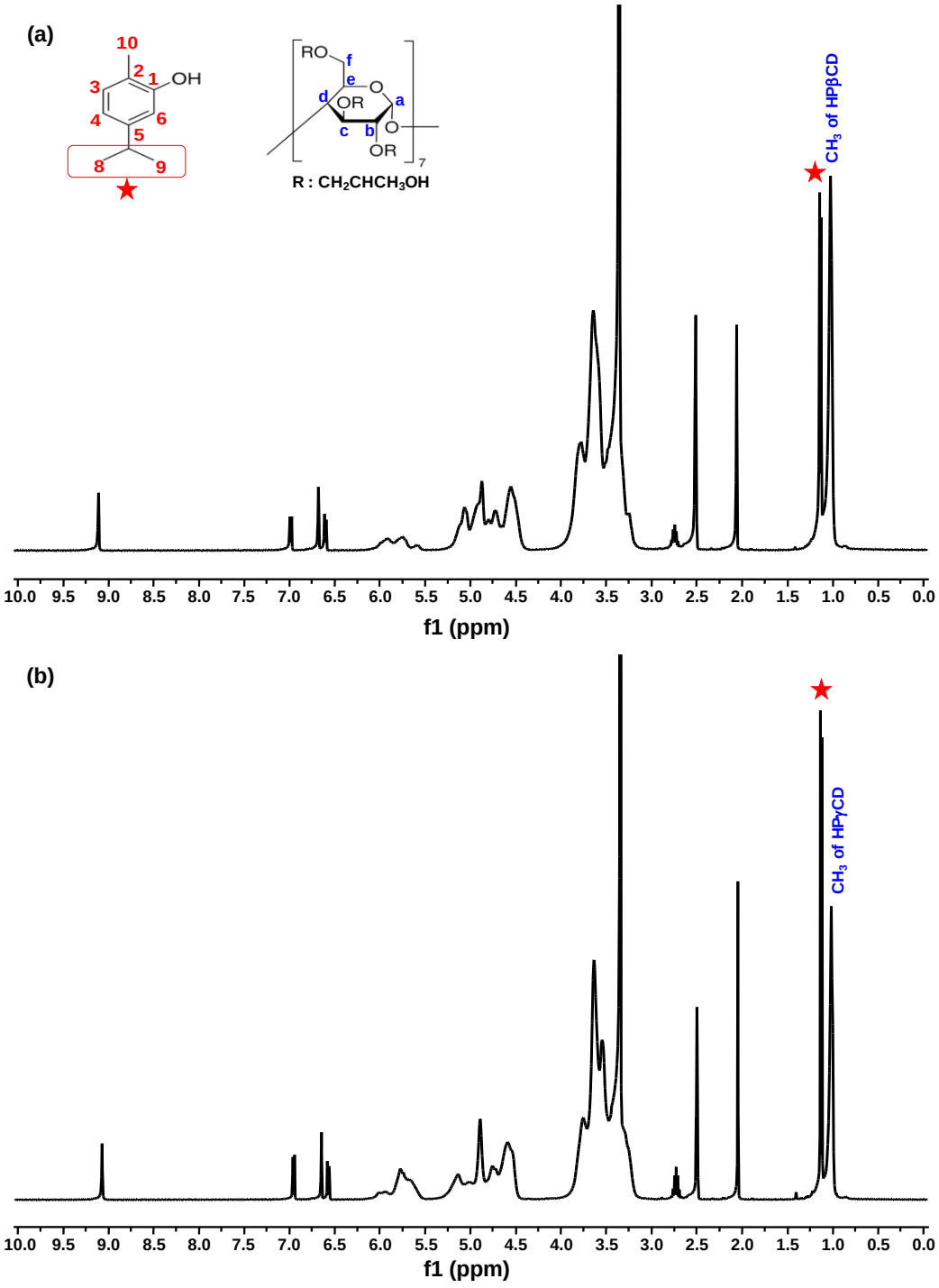

Figure 21. ^{1}H-NMR spectra of (a) carvacrol/HPβCD-IC and (b) carvacrol/HPγCD-IC fibrous web (dissolved in d6-DMSO) which were produced 3 years ago.

2.2.3.6 Thermal characterization

The TGA was performed for fibers and pure carvacrol to investigate the thermal stability and volatility of carvacrol and the obtained TGA thermograms are given in Figure 22. Pure CD fibers showed two step weight losses; the water loss below 100 °C and the main thermal degradation of CDs above 300 °C. On the other hand, both carvacrol/CD-IC fibers exhibited three steps weight losses; initial weight loss below 100 °C is due to water loses, the third weight loss which is the major one belongs to the CD degradation. For carvacrol/CD-IC fibers, the second weight loss belonging to evaporation of carvacrol starts at around 90 °C and continues till 275 °C while for pure carvacrol thermogram, it starts at around 50 °C and ends at around 185 °C. In other words, for both CD types, the second degradation that belongs to carvacrol evaporation was observed at higher degrees in temperature when compared to pure carvacrol. As a result, the higher thermal evaporation temperature was achieved for both carvacrol/CD-IC fibers confirming that the thermal stability of carvacrol was increased thanks to the interaction with CD by inclusion complex formation.

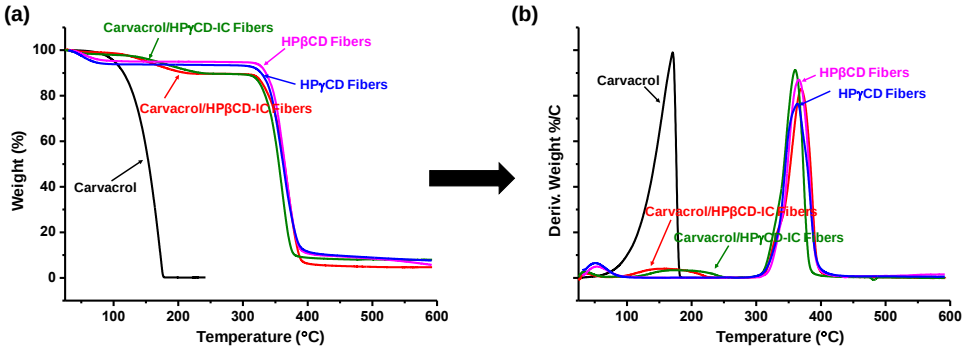

Figure 22. (a) TGA thermograms and (b) their derivatives for pure carvacrol, pure CD fibers and carvacrol/CD-IC fibers.

2.2.3.7 Antioxidant property

The antioxidant property of carvacrol was tested by DPPH radical scavenging assay. This assay is based on reduction of DPPH molecule by a hydrogen donor. As DPPH molecule is reduced, its strongest absorption band observed in UV-Vis spectrum decreases and the purple color of the solutions turns to yellow [118]. In this study, as mentioned in experimental section, antioxidant test was performed as concentration dependent in which concentration of CD-IC fibers was adjusted to have carvacrol ranging from 8 to 0.0625 mg in 1 mL of aqueous solution of fibers. On the other hand, pure carvacrol was prepared with 8 mg mL^{-1} concentration and undissolved part of carvacrol was filtered. Figure 23 shows change in the percentage of DPPH radical scavenging by carvacrol concentration and their corresponding photographs. As expected, DPPH reduction increased with increase amount of carvacrol in CD-IC fibers and DPPH was completely reduced by the 8 mg mL^{-1} carvacrol having fibers after 1 hour of incubation time. On the other hand, for pure carvacrol system prepared by 8 mg mL^{-1} carvacrol in water, the antioxidant activity was observed as 63.7 % under the same condition (Figure 24). This result confirmed that the antioxidant activity of carvacrol was enhanced by the formation of inclusion complex with CD. The reason for enhanced antioxidant activity of carvacrol is increase in water solubility by inclusion complexation with CD which was confirmed by phase solubility test and molecular modeling studies; in other words, less amount of carvacrol is required for DPPH reduction in the case of CD-IC systems. Besides, IC50 value for carvacrol/HPβCD-IC fibers and carvacrol/HPγCD-IC fibers was calculated as 0.5 mg mL^{-1} and 0.63 mg mL^{-1}, respectively. The possible reason for this difference in IC50 value is that carvacrol

formed more stable complex with HPβCD which resulted in higher degree of protection for carvacrol and so higher antioxidant activity was observed [121]. The stability of carvacrol/CD-IC fibers in terms of antioxidant activity was also investigated by using 3-year-old fibers. The 3-year-old carvacrol/CD-IC fibers showed almost same 50% inhibition activity when compared to fresh samples (Figure 25), revealing the long-term stability of the carvacrol/CD-IC fibers for their antioxidant activities. As discussed in the ^{1}H-NMR section above, the amount of carvacrol found in old samples and the fresh samples was almost same indicating that there was only very minimal loss of carvacrol during the 3-year storage (at 4˚C in the refrigerator) and this further proved that carvacrol was well protected in the fiber matrix due to inclusion complexation.

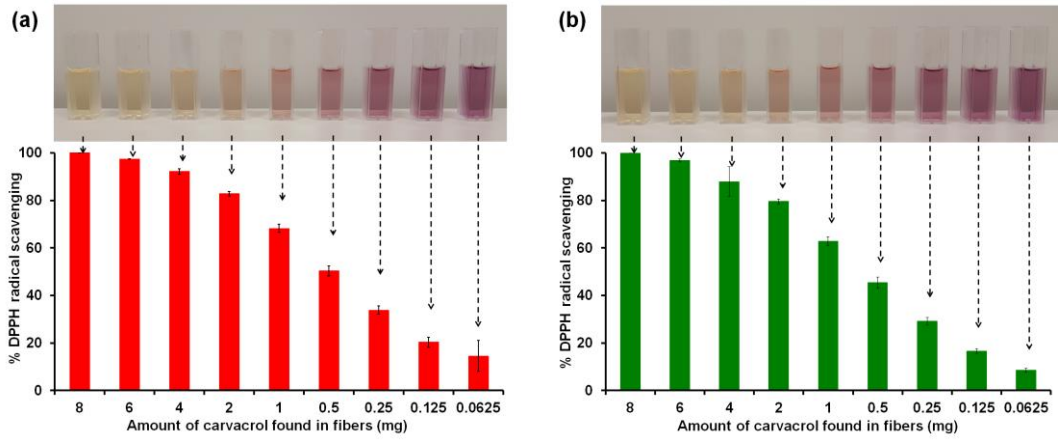

Figure 23. Carvacrol concentration dependent antioxidant test graphs and the resulting DPPH solution photographs of (a) Carvacrol/HPβCD-IC fibers and (b) Carvacrol/HPγCD-IC fibers.

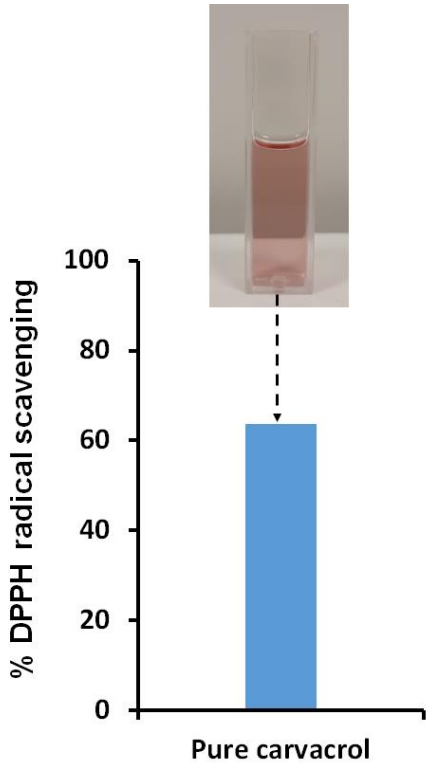

Figure 24. Concentration dependent antioxidant test graph and the resulting DPPH solution photographs of pure carvacrol.

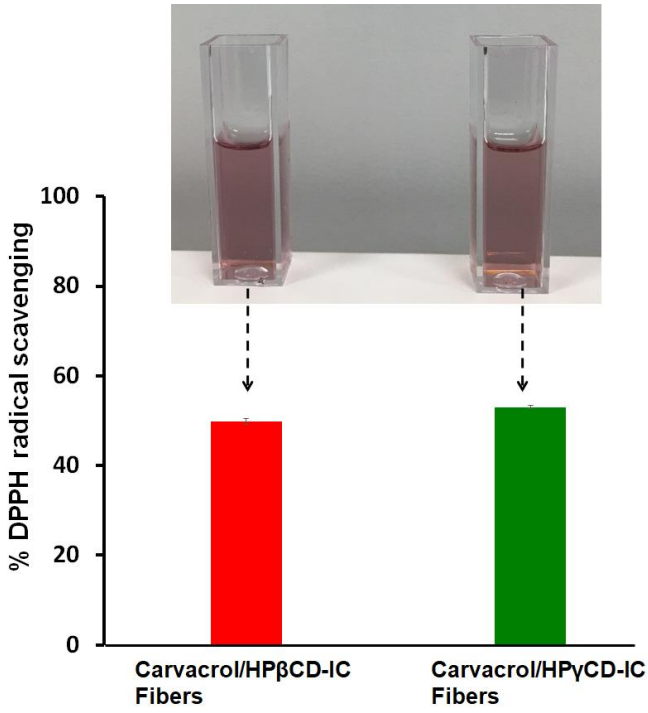

Figure 25. Carvacrol concentration dependent antioxidant test graph and the resulting DPPH solution photographs of Carvacrol/HPβCD-IC Fibers and Carvacrol/HPγCD-IC Fibers which were produced 3 years ago.

2.2.3.8 Dissolution behaviour

The fast-dissolving character of carvacrol/CD-IC fibers in water was visualized by photos (Figure 26). When the carvacrol/CD-IC fibrous webs were exposed to water, they were suddenly (< 1s) dissolved which showed the fast-dissolving character of these carvacrol/CD-IC fibrous webs. As mentioned before, carvacrol has a very low water solubility; however, carvacrol/CD-IC fibers are quite soluble which indicates the water solubility enhancement of carvacrol.

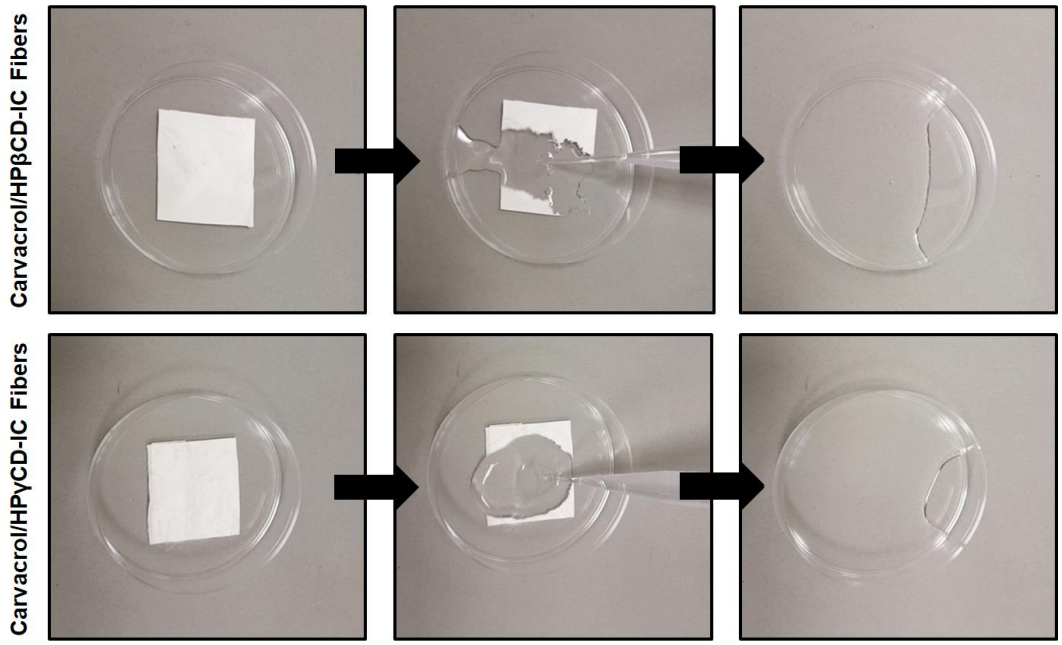

Figure 26. Presentation of the solubility behavior of carvacrol/HPβCD-IC fibrous web and carvacrol/HPγCD-IC fibrous web in water. The carvacrol/CD-IC fibrous webs are dissolved in less than a second.

2.2.4 Conclusion

Here, the production of handy, self-standing and fast-dissolving fibrous webs from carvacrol/cyclodextrin-inclusion complexes (carvacrol/CD-IC) by using the electrospinning technique was achieved. The molar ratio of carvacrol/CD was found 1:1 for both CD types (HPβCD and HPγCD) by phase solubility and molecular modeling studies. The enhanced water solubility of carvacrol due to inclusion complex formation was confirmed by the phase solubility and computational modeling studies. SEM images revealed that the carvacrol/CD-IC fibers were uniform and bead-free. FTIR, TGA and ^{1}H-NMR studies confirmed the inclusion complex formation and the presence of carvacrol in fibers. Moreover, TGA and ^{1}H-NMR studies indicated that very high amount of carvacrol (up to ~75-

95%) was preserved during/after electrospinning in carvacrol/CD-IC fibers although carvacrol has a highly volatile nature. Besides, TGA results showed that thermal stability of carvacrol in carvacrol/CD-IC fibers has increased due to the inclusion complex formation. In addition, antioxidant activity of carvacrol was enhanced due to inclusion complex formation for carvacrol/CD-IC fibers. Moreover, 3-year-old carvacrol/CD-IC fibers showed almost same antioxidant activity when compared to fresh samples, revealing the long-term stability of the carvacrol in CD-IC fibers. Also, the amount of carvacrol found in 3-year-old carvacrol/CD-IC fibrous web samples was almost same with the fresh samples, confirming that carvacrol was well protected in the fiber matrix due to inclusion complexation. In the light of all these results, it can be concluded that, main drawbacks of carvacrol like high volatility, low solubility and low stability were eliminated or minimized; besides, its antioxidant activity was enhanced by the formation carvacrol/CD-IC fibers. These promising results suggest that carvacrol/CD-IC fibrous materials may be applicable in food, cosmetic and oral care industries as fast-dissolving tablet/web/strip.

2.3 Molecular Encapsulation of Cinnamaldehyde within Cyclodextrin Inclusion Complex Electrospun Nanofibers: Fast-dissolution, Enhanced Water Solubility, High Temperature Stability and Antibacterial Activity of Cinnamaldehyde

This chapter of thesis was reprinted (adapted) with permission from [122], ("Molecular Encapsulation of Cinnamaldehyde within Cyclodextrin Inclusion Complex Electrospun Nanofibers: Fast-Dissolution, Enhanced Water Solubility, High Temperature Stability, and Antibacterial Activity of Cinnamaldehyde"; Z. I. Yildiz, M. E. Kilic, E. Durgun, and T. Uyar., *Journal of Agricultural and Food Chemistry*, 67, 11066-76, 2019). Copyright (2019) American Chemical Society.

2.3.1 Introduction

Cinnamaldehyde (Figure 27a), a primary constituent of cinnamon bark oil, is an essential oil classified as GRAS (Generally Recognized As Safe) by the U.S. Food and Drug Administration (21 CFR 182.60). Cinnamaldehyde is known to have high antibacterial, antifungal, anti-inflammatory and antioxidant activity; therefore, it is widely used in the food, drug and cosmetic industries [123-125]. For instance, cinnamaldehyde-containing films, particles and NFs have shown the advantages of use of cinnamaldehyde in various applications including pharmaceutics, food and antimicrobial packaging [126-130]. For example, Qin et al. showed that active packaging including cinnamaldehyde can lead to an increase in shelf life of fresh button mushroom [126]. In another study, it was shown that submicrometer emulsion of cinnamaldehyde can be used in clinical applications because of antitumor activity and pharmacokinetic properties [127]. In the study of Liu et al., antibacterial fish skin gelatin-based NF incorporating cinnamaldehyde was fabricated to be used in controlled-release applications [128]. In another study, electrospun chitosan/poly(ethylene oxide) mats including cinnamaldehyde having antibacterial activity against pseudomonas bacteria was engineered in order to be potentially used for alleviating nosocomial infections [129]. In a very recent study,

electrospun fibrous film was developed to be used in food industry from the pea protein isolate-polyvinyl alcohol with cinnamaldehyde cooperation to obtain a material showing antibacterial activity against both Gram-positive and -negative bacteria [130]. However, cinnamaldehyde has certain shelf-life problems due to its high volatility, low stability, low solubility and sensitivity to oxygen, light, and heat [131, 132]. Yet, molecular encapsulation of cinnamaldehyde with cyclodextrin inclusion complexation is one of the promising approaches in order to eliminate the above-mentioned drawbacks of cinnamaldehyde. For example, it was shown that enhancement of photostability and thermo-stability of cinnamaldehyde after complexation with γ-CD derivatives was possible [133]. In another related study, inclusion complexation between cinnamaldehyde and β-CD resulted in prevention of cinnamaldehyde from oxidation; besides, the cinnamaldehyde/β-CD ICs showed antioxidative properties similar to pristine cinnamaldehyde [134]. Moreover, the antimicrobial active packaging was designed by using ICs of cinnamaldehyde with β-CD in which improved stability and controlled release of cinnamaldehyde was obtained [135]. In the study of Sun et al., the inclusion mechanism and structures of cinnamaldehyde with different cyclodextrins were investigated [136] in which HP-β-CD showed higher inclusion complexation ability with cinnamaldehyde and higher solubility enhancement for cinnamaldehyde when it was compared with inclusion complexation of β-CD [136]. Moreover, several studies reported the incorporation of cyclodextrin ICs of cinnamaldehyde within the polymeric electrospun NFs for antimicrobial wound dressing and antimicrobial active food packaging [132, 137, 138]. For instance, cinnamaldehyde/β-CD-IC-incorporated polylactic acid (PLA) nanofibrous mat was fabricated as a potential candidate for

the use of wound dressing material due to its antibacterial properties and low cytotoxicity [132]. Also, a polyvinyl alcohol (PVA)/cinnamon essential oil/β-CD-IC nanofibrous film was fabricated by electrospinning for active food packaging by increasing the high-temperature stability of cinnamon essential oil by inclusion complexation and prolonging the shelf life of strawberries by showing effective antimicrobial activity [137]. Also, cinnamon essential oil/β-CD-IC was incorporated into electrospun PLA NFs for antimicrobial packaging application in which PLA/cinnamon essential oil/β-CD nanofibrous film has shown better antimicrobial activity compared to PLA/cinnamon essential oil nanofibrous film [138]. The improvement of antimicrobial activitywas attributed to cyclodextrin inclusion complexation and also, nanofibrous film obtained by the electrospinning method preserved higher amount of cinnamon essential oil when compared to film obtained by casting method [138].

In the light of these aforementioned studies and from our extensive experiences on electrospun polymer-free CD-IC NFs, we designed our study in order to electrospun NFs from purely cinnamaldehyde/CD-IC systems without using a polymeric matrix. Here, we studied inclusion complexation of cinnamaldehyde with two different hydroxypropylated CDs; hydroxypropyl-β-cyclodextrin (HPβCD) and hydroxypropyl-γ-cyclodextrin (HPγCD), in order to produce cinnamaldehyde/CD-ICs. On the basis of our computational modeling studies, cinnamaldehyde/CD-ICs were prepared in two different molar ratios between cinnamaldehyde and CDs (cinnamaldehyde:CD; 1:1 and 2:1) in aqueous solutions. Then, aqueous solutions of cinnamaldehyde/CD-IC were electrospun in which self-standing nanofibrous mats of cinnamaldehyde/CD-IC were produced successfully. In short, this study

provides a useful approach for the molecular encapsulation of cinnamaldehyde within cyclodextrin inclusion complex NFs by electrospinning, in which fast-dissolving and highly water-soluble cinnamaldehyde having higher-temperature stability along with antibacterial activity was achieved for cinnamaldehyde/CD-IC NFs.

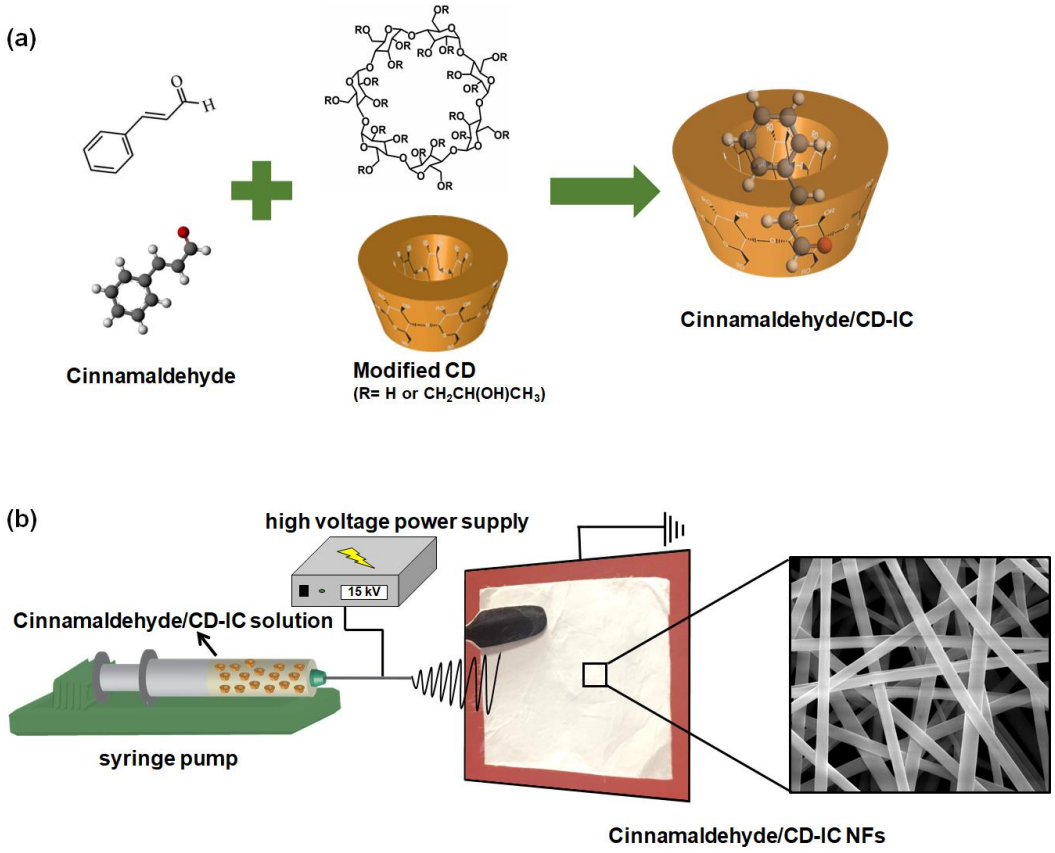

Figure 27. (a) Molecular structure of cinnamaldehyde and HP-β-CD (note: HP-γ-CD has a similar chemical structure with eight glucopyranose units), and illustration of cinnamaldehyde/CD-IC formation, (b) electrospinning process of NFs from cinnamaldehyde/CD-IC solution.

2.3.2 Experimental

2.3.2.1 Materials

Hydroxypropyl-β-cyclodextrin (HP-β-CD, CAVASOL W7 HP Pharma, degree of substitution: ~0.6, molecular weight: 1400 g/mol) and hydroxypropyl-γ-cyclodextrin (HP-γ-CD, CAVASOL W8 HP, degree of substitution: ~0.6, molecular weight: 1574 g/mol) were gift samples from Wacker Chemie AG (Germany). Cinnamaldehyde (99%, Sigma-Aldrich), 2,2-diphenyl-1-picrylhydrazyl (Sigma-Aldrich), deuterated dimethylsulfoxide (DMSO-d6, deuteration degree of minimum 99.8%, Merck), and deionized water (Millipore Milli-Q ultrapure water) were used in this study.

2.3.2.2 Preparation of electrospinning solutions

The solutions of cinnamaldehyde/CD-IC were prepared by dissolving HP-β-CD (200%, w/v, 2 g of HP-β-CD in 1 mL water) and HP-γ-CD (200%, w/v, 2 g of HP-γ-CD in 1 mL water) in water. Then, proper amount of cinnamaldehyde was mixed with aqueous CD solutions in order to obtain 1:1 and 2:1 (cinnamaldehyde/CD) molar ratio of cinnamaldehyde/CD-IC solutions. These aqueous cinnamaldehyde/CD-IC solutions were kept at room temperature under stirring for 24 h in order to obtain cinnamaldehyde/HPβCD-IC and cinnamaldehyde/HPγCD-IC solutions. In addition, pure CD solutions (HP-β-CD and HP-γ-CD) without cinnamaldehyde were also prepared at concentration of 200% (w/v, 2 g of HP-β-CD and HP-γ-CD in 1 mL water) in water for the electrospinning of pure CD NFs for comparative studies [91].

2.3.2.4 Electrospinning of nanofibers

Each cinnamaldehyde/CD-IC (cinnamaldehyde/HPβCD-IC and cinnamaldehyde/HPγCD-IC) aqueous solution was placed separately into 1 mL plastic syringes having a 27 gauge metallic needle. Then, the syringe loaded with cinnamaldehyde/CD-IC aqueous solution was placed on a syringe pump (NE-300, New Era Pump Systems, USA) in order to control the feed rate of the cinnamaldehyde/CD-IC solution for the electrospinning. The pumping rate of the cinnamaldehyde/CD-IC solution was 0.5 mL/h and the electrospinning process was performed at a voltage of ∼15 kV (AU Series of HV unit, Matsusada, Japan). The collection distance of the NFs was adjusted to 15 cm, and a stationary metal plate collector covered by aluminum foil was used. In addition, pure CD NFs (HPβCD-NFs and HPγCD-NFs) were also electrospun under the same condition for comparative study [91].

2.3.2.5 Measurements and characterizations

The phase solubility test was performed and the phase solubility diagram was plotted by which stability constants of complexes between cinnamaldehyde and the two of hydroxypropylated CDs are determined [102]. For the phase solubility test, 5 mL of the aqueous solutions of HP-β-CD and HP-γ-CD with increasing concentrations from 1 to 64 mM were prepared in capped vials; then, cinnamaldehyde with excess amount was added to these aqueous CD solutions. The cinnamaldehyde/CD solutions were shaken for 48 h at room temperature in the dark. Then, cinnamaldehyde/CD solutions were filtered by using 0.45 μm membrane filter in order to remove undissolved part if any present. After that, an UV–vis spectrophotometer (Varian, Cary 100) was used to determine the dissolved

amount of cinnamaldehyde by recording the absorption at 289 nm in the cinnamaldehyde/CD solution. The experiment was repeated three times. The phase solubility diagram was constructed by taking the average of three measurements and plotted as cinnamaldehyde concentration versus CD concentration. The stability constants (K_s) of cinnamaldehyde/CD-ICs were calculated as

K_s= slope/ S_0 (1-slope)

where S_0 is defined as the solubility of cinnamaldehyde in the absence of CD.

The ground-state properties were predicted by ab initio computational methods [105, 139] within the framework of density functional theory [103, 104]. The Perdew–Burke–Ernzerhof form of generalized gradient approximation [106] was used to calculate the exchange-correlation term. The weak intermolecular forces between molecules (van der Waals forces) were described by the Grimme approach [107]. The projector augmented-wave method [108] was implemented to describe the element potentials. The structures of HP-β-CD and HP-γ-CD were designed with 4 hydroxypropyl (HP) units (degree of substitution: ∼0.6) and 5 HP units (degree of substitution: ∼0.6), respectively. The structural relaxations were performed by using conjugate gradient optimization allowing 10–5 eV energy tolerance between two sequential steps and allowing maximum 0.005 eV/Å force on atoms. The interaction between solute and solvent was analyzed by using implicit self-consistent description [109].

The interaction energy (E_{int}) is defined as

$E_{int}=E_T(CD) + E_T(guest) – E_T(IC)$

where E_T(CD), E_T(guest), and E_T(IC) are the ground-state energy of HP-β-CD or HP-γ-CD, single cinnamaldehyde (for 1:1 stoichiometry) or pair of cinnamaldehyde molecules (for 2:1 stoichiometry), and their ICs, respectively. The inclusion complex is considered to be formed when E_{int} is maximized and maximum value of E_{int} for the given configuration is defined as complexation energy (E_{comp}).

Solvation energy (E_{solv}) is defined as

$$E_{solv} = E_T[IC]_{water} - E_T[IC]_{vacuum}$$

$E_T[IC]_{water}$ and $E_T[IC]_{vacuum}$ is the ground-state energy of cinnamaldehyde/HPβCD-IC or cinnamaldehyde/HPγCD-IC in water and vacuum, respectively.

The rheological measurement of the cinnamaldehyde/CD-IC solutions was performed via a rheometer (Anton Paar Physica MCR 301) at a 100 s^{-1} constant shear rate using a CP 20-4 spindle. The solution conductivities were measured by a conductivity meter (Multiparameter inoLab Multi 720-WTW) at room temperature.

The morphological analyses of the samples were performed by scanning electron microscopy (SEM, FEI Quanta 200 FEG). The sputtering (Gatan 682 precision etching and coating system) was done with 5 nm Au/Pd prior to SEM imaging of nanofibrous samples. About 100 fibers from different locations of the SEM images were measured for calculating the average fiber diameter (AFD) of each nanofibrous sample.

In order to determine the presence of cinnamaldehyde in cinnamaldehyde/CD-IC electrospun nanofibrous samples, nuclear magnetic resonance spectroscopy (^{1}H NMR, Bruker D PX-400) was used to record the ^{1}H NMR spectra. For each ^{1}H NMR spectrum, about 15 mg of electrospun nanofibrous mat of

cinnamaldehyde/CD-IC NFs was dissolved in 500 μL of d6-DMSO. Fourier transform infrared (FTIR) spectra of pure cinnamaldehyde, pristine CD NFs, and cinnamaldehyde/CD-IC NFs were obtained with 64 scans at resolution of 4 cm^{-1} within a range of 4000–400 cm^{-1} using a FTIR spectrometer (Bruker VERTEX 70). For the FTIR measurements, samples were blended with potassium bromide (KBr) and then pressed in order to obtain pellets. Thermogravimetric analyses (TGA, TA Instruments Q500) of the samples were performed from 25 to 600 °C at 20 °C/min heating rate under inert (nitrogen) atmosphere.

The cinnamaldehyde/CD-IC NF mats were tested for their antibacterial activities against *Escherichia coli*. The *E. coli* tested was from RSHM 888 (RSHM, National Type Culture Collection Laboratory, Ankara, Turkey). *E. coli* was grown, and 150 μL of cultures containing approximately 108 cfu mL^{-1} were spread on Luria–Bertani agar. The cinnamaldehyde/CD-IC NF mats were cut into circular pieces with 1 cm diameter and having the same weight. For comparison, the antibacterial activity of pristine CD-NF mats was also investigated. Each nanofibrous mat was placed separately on agar plate spread with *E. coli* and visualized after 24 h incubation; then, the inhibition zones (IZ) were compared.

Two different methods were used to visualize water dissolution of cinnamaldehyde/CD-IC NF mats. For the first method, the same weight of cinnamaldehyde/HPβCD-IC NF and cinnamaldehyde/HPγCD-IC NF mats was positioned in a Petri dish, and then deionized water (5 mL) was poured directly on these nanofibrous mats. For the second method, the water dissolution of cinnamaldehyde/CD-IC NF mats was visualized according to the procedure modified from the literature [140]. In this method, the bottom of the Petri dish was

covered by absorbent paper which was wetted by 10 mL of distilled water. The excess water was completely drained out. Then, cinnamaldehyde/CD-IC NF mats were placed on the wet absorbent paper, and the video was recorded to visualize dissolving behavior of the samples.

2.3.3 Results and discussion

2.3.3.1 Phase solubility studies

Figure 28 displays the phase solubility profiles of cinnamaldehyde/CD-ICs. The phase solubility diagram for cinnamaldehyde/CD-ICs shows an A type profile which indicates that solubility of cinnamaldehyde increases as a function of CD concentration [141]. The plots are classified as A_N type, negative deviation from linearity which indicates that the effect of CD on cinnamaldehyde solubility increment was less effective at higher concentrations. For A_N type profile, it is difficult to interpret the ratio between host and guest profiles [141]. On the basis of the initial linear part of the profile, the stability constant (K_s) was calculated as 140 and 110 M^{-1} ($R^2 >$ 0.99) for cinnamaldehyde/HPβCD-IC and cinnamaldehyde/HPγCD-IC, respectively. The K_s values indicated that cinnamaldehyde forms stronger binding with HP-β-CD cavity when compared to HP-γ-CD cavity. The cavity of HP-β-CD is a bit smaller than HP-γ-CD, which could be a better fit and size match for cinnamaldehyde molecules, providing stronger interactions with cinnamaldehyde in cinnamaldehyde/HPβCD-IC when compared to cinnamaldehyde/HPγCD-IC system. The stronger binding of cinnamaldehyde within the HP-β-CD cavity was also confirmed by molecular modeling studies.

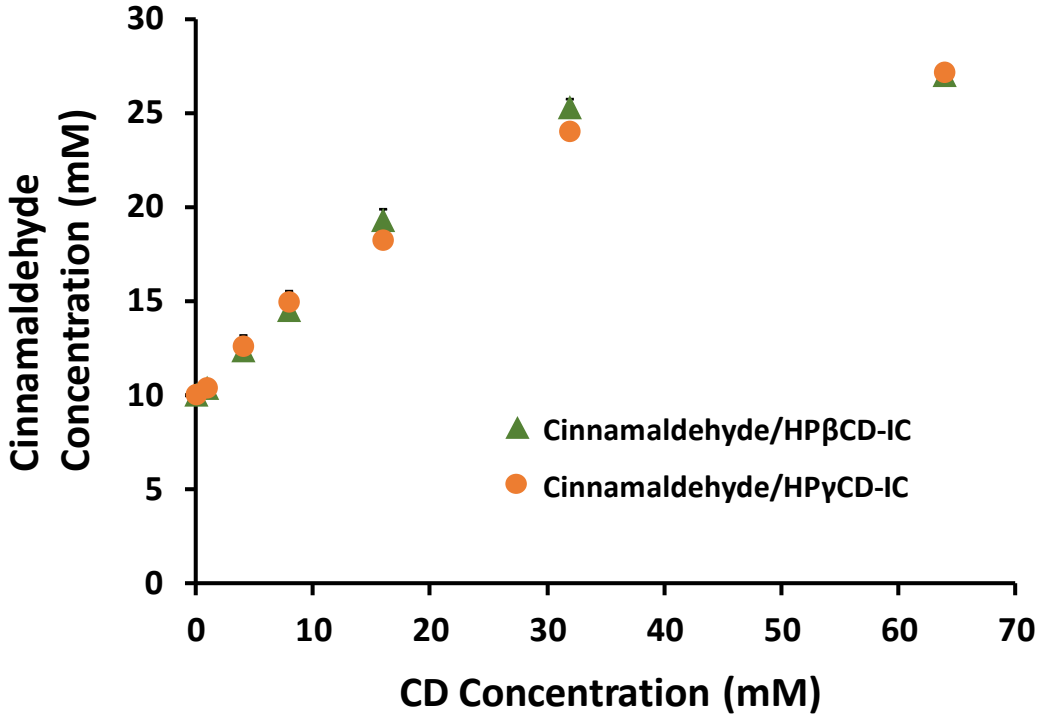

Figure 28. The phase solubility diagram of cinnamaldehyde/HPβCD-IC and cinnamaldehyde/HPγCD-IC in aqueous systems (n = 3).

2.3.3.2 Computational modeling

The molecular modeling calculations based on ab initio techniques were performed to elucidate the experimental data. Initially, HPβCD, HPγCD, and single cinnamaldehyde molecule (trans isomer) are relaxed in vacuum by minimizing the total energy and then optimized geometries are obtained. To reveal the complexation between the host and the guest molecules, cinnamaldehyde is moved toward HPβCD and HPγCD through their wider rims with 1 Å steps and the E_{int} with respect to center of mass of CD is calculated at each step (Figure 29). This procedure is repeated for two possible orientations of cinnamaldehyde which are labeled as tail (−OH group) and head (aromatic ring). As can be noticed from the Figure 29a,b(iii), E_{int} is always positive, which indicates an attractive

interaction between both CDs and cinnamaldehyde. The variation of E_{int} also demonstrates that ICs can be formed without an energy barrier and complexation is an exothermic reaction. For HPβCD, cinnamaldehyde perfectly fits the cavity and prefers the tail orientation with a tilt (Figure 29a(i)). E_{int} is maximized at 0 Å, where cinnamaldehyde/HPβCD-IC is assumed to be formed and E_{comp} is calculated as 23.18 kcal mol^{-1} (Figure 29a(iii), Table 6). For the case of HPγCD (Figure 26a(ii)), cinnamaldehyde favors head orientation where the OH-group is located in the center of CD and the benzene ring points toward hydroxypropyl tails. Cinnamaldehyde/HPγCD-IC is formed at −3 Å and E_{comp} is calculated as 15.29 kcal mol^{-1} (Figure 26a(iii), Table 6). When compared to HPγCD, stronger binding between HPβCD and cinnamaldehyde is obtained for 1:1 stoichiometry. The same analysis is performed also in water to reveal the effect of the solvent. Our results indicate that although the geometries are not altered, E_{comp} values significantly decrease for both cases upon interaction with water and become 18.43 kcal mol^{-1} versus 9.20 kcal mol^{-1} for cinnamaldehyde/HPβCD-IC and cinnamaldehyde/HPγCD-IC, respectively (Table 6).

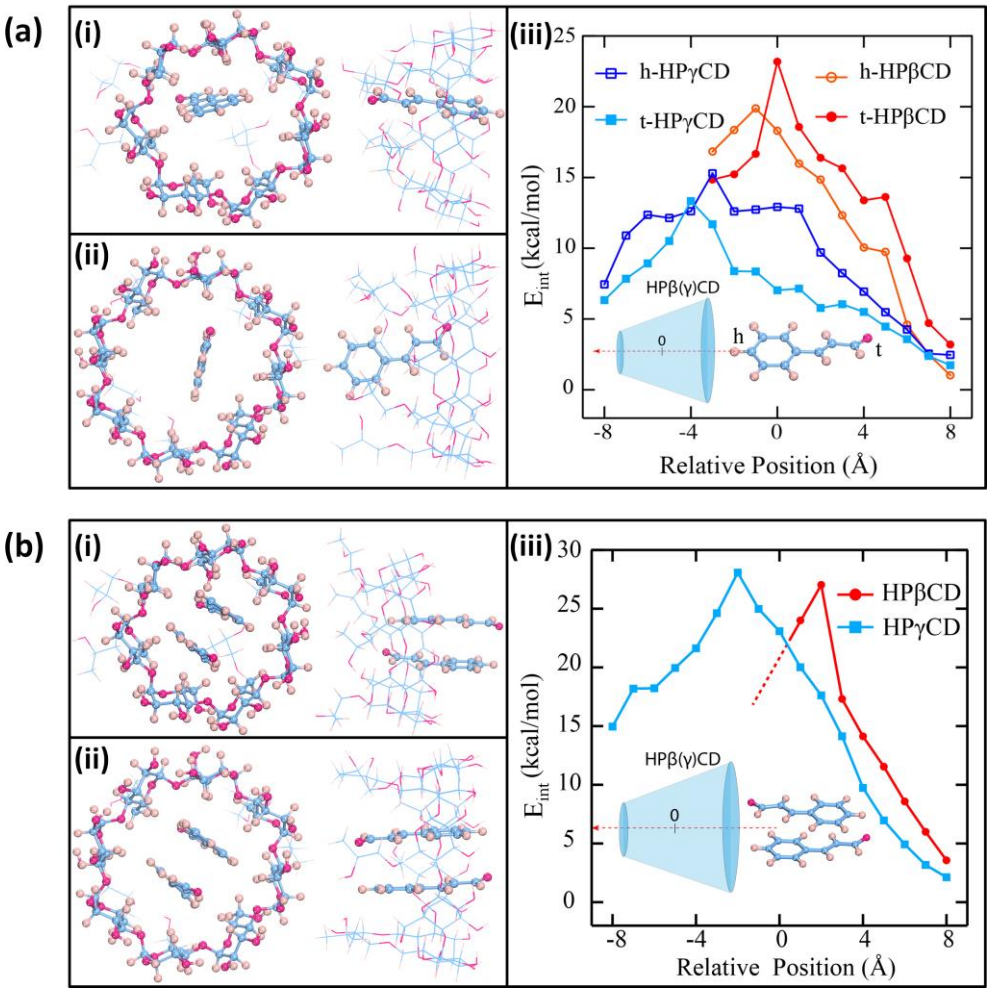

Figure 29. (a) Formation of inclusion complexes in 1:1 stoichiometry between cinnamaldehyde and CDs; (i) top and side view of cinnamaldehyde/HPβCD-IC, (ii) top and side view of cinnamaldehyde/HPγCD-IC and (iii) the variation of interaction energy of cinnamaldehyde with CD as a function of distance, and (b) Formation of inclusion complexes in 2:1 stoichiometry between cinnamaldehyde and CDs; (i) top and side view of cinnamaldehyde/HPβCD-IC, (ii) top and side view of cinnamaldehyde/HPγCD-IC and (iii) the variation of interaction energy of cinnamaldehyde with CD as a function of distance. The possible orientations of cinnamaldehyde are shown as inset. Blue, purple, and light pink balls represent carbon, oxygen, and hydrogen atoms, respectively.

Table 6. Complexation and solvation energies of the cinnamaldehyde, CDs (HPβCD and HPγCD) and cinnamaldehyde within CDs at different molar ratios and different orientations.

Host	Guest	Molar ratio (cinnamaldehyde:CD)	Orientation	E_{comp} (vacuum) kcal mol^{-1}	E_{comp} (water) kcal mol^{-1}	E_{solv} kcal mol^{-1}
HPβCD	-	-	-	-	-	-71.16
HPβCD	Cinnamaldehyde	1:1	Head	19.88	-	-
HPβCD	Cinnamaldehyde	1:1	Tail	23.18	18.43	-72.68
HPβCD	Cinnamaldehyde	2:1	Head/Tail	27.04	19.79	-75.69
HPγCD	-		-	-	-	-83.32
HPγCD	Cinnamaldehyde	1:1	Head	15.29	9.20	-83.49
HPγCD	Cinnamaldehyde	1:1	Tail	13.34	-	-
HPγCD	Cinnamaldehyde	2:1	Head/Tail	28.08	24.77	-91.21
-	Cinnamaldehyde	-	-	-	-	-6.27

Next, we investigate the possibility of inclusion complex formation in the 2:1 stoichiometry (Figure 29b). The most favorable orientation for the cinnamaldehyde pair is shown in Figure 29b. Our results indicate that inclusion complex formation for 2:1 stoichiometry is also an exothermic process for both type of the CDs. For HPβCD, inclusion complex is formed at +2 Å which is partially outside the rim. HPβCD started to deform, if the cinnamaldehyde pair is pushed inside (Figure 29b(i)). Ecomp slightly increases with respect to the 1:1 case and becomes 27.04 kcal mol^{-1} (Figure 29b(iii), Table 6). As the cavity of HPγCD is larger than that of HPβCD, the cinnamaldehyde pair perfectly fits and inclusion complex is formed at −2 Å (Figure 29b(ii)). Ecomp drastically increases (almost doubled) and becomes 28.08 kcal mol^{-1} (Figure 29b(iii), Table 6). Similar to 1:1 stoichiometry, when calculations are repeated in water, no significant effect on geometries is noticed but E_{comp} decreases for both cases and becomes 19.79 and 24.77 kcal mol^{-1} for cinnamaldehyde/HPβCD-IC and cinnamaldehyde/HPγCD-IC, respectively (Table 6).

Finally, solvation energies (E_{solv}) are calculated to reveal the solubility trends (Table 6). The obtained results show that although the cinnamaldehyde molecule is almost insoluble in water (−6.27 kcal mol^{-1}), inclusion complex formation significantly increases the E_{solv}. These results suggest a substantial increase in cinnamaldehyde solubility. E_{solv} is calculated as −72.68 and −83.49 kcal mol^{-1} for cinnamaldehyde/HPβCD-IC and cinnamaldehyde/HPγCD-IC, respectively in the 1:1 stoichiometry. E_{solv} further increases in the 2:1 stoichiometry and becomes −75.69 and −91.21 kcal mol^{-1} for cinnamaldehyde/HPβCD-IC and cinnamaldehyde/HPγCD-IC, respectively.

2.3.3.3 Morphological analyses

Optimization for the parameters of the electrospinning process was done to produce uniform NFs from cinnamaldehyde/CD-IC systems. Figure 30 displays the digital photographs of cinnamaldehyde/CD-IC mats along with their SEM images. The cinnamaldehyde/CD-IC NFs without any beaded morphology were successfully electrospun, and the nanofibrous mats of cinnamaldehyde/CD-IC NFs were obtained having self-standing, easy-to-handle, lightweight, and flexible features. Table 7 summarizes the conductivity and viscosity of the highly concentrated cinnamaldehyde/HPβCD-IC and cinnamaldehyde/HPγCD-IC aqueous solutions and the AFD of the resulting electrospun cinnamaldehyde/HPβCD-IC NFs and cinnamaldehyde/HPγCD-IC NFs for 1:1 and 2:1 molar ratios. It is a known fact that the conductivity and viscosity of the solutions noticeably affect the electrospinnability and resulting diameter of the electrospun NFs. Typically, less stretching occurs during the electrospinning process when the solution has higher viscosity and lower conductivity, and therefore, much thicker fibers are electrospun [12]. When compared to other cinnamaldehyde/CD-IC NFs, cinnamaldehyde/HPγCD-IC NFs (1:1) have the highest value of AFD which was measured as 825 ± 330 nm, as its solution has the highest viscosity (2.18 ± 0.65 Pa s) and the lowest conductivity (4.53 ± 0.30 μS cm^{-1}) among other cinnamaldehyde/CD-IC solutions. The cinnamaldehyde/HPγCD-IC NFs (2:1) has AFD value of 805 ± 275 nm which is slightly higher than AFD of NFs obtained from cinnamaldehyde/HPβCD-ICs in both 1:1 (700 ± 260 nm) and 2:1 (545 ± 175 nm) molar ratios. The reason for this difference in AFD is that solution of cinnamaldehyde/HPγCD-IC (2:1) has higher viscosity (1.84 ± 0.30 Pa

s) and lower conductivity (5.00 ± 0.16 μS cm^{-1}) than solutions of cinnamaldehyde/HPβCD-IC. In contrast, cinnamaldehyde/HPβCD-IC NFs (2:1) has the lowest AFD value (545 ± 175 nm) due to its lowest viscosity which is 1.15 ± 0.16 Pa s and higher conductivity which is 12.18 ± 0.25 μS cm^{-1}. Overall, the trends in AFD values of cinnamaldehyde/CD-IC NFs were well correlated with the electrospun polymeric NFs, where lower conductivity and higher viscosity resulted in much bigger fibers [12].

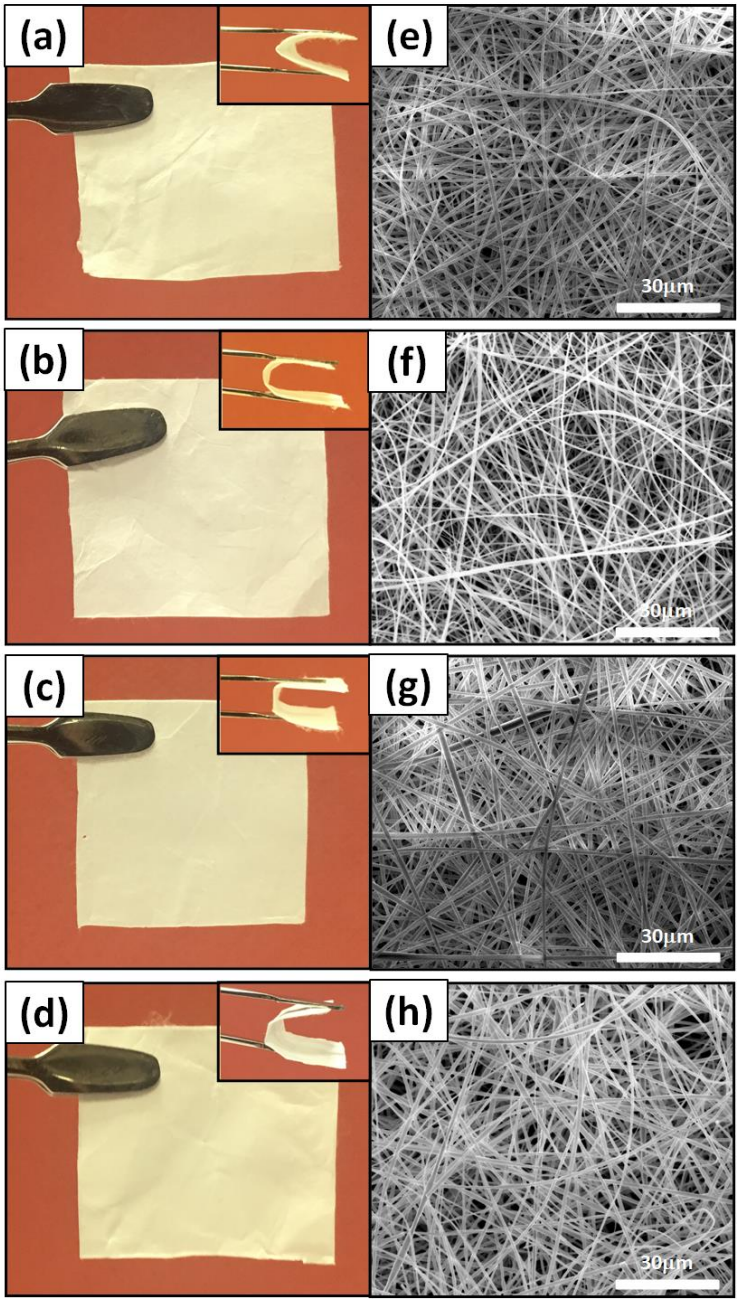

Figure 30. The digital photograph of (a) cinnamaldehyde/HPβCD-IC NF mat (1:1), (b) cinnamaldehyde/HPβCD-IC NF mat (2:1), (c) cinnamaldehyde/HPγCD-IC NF mat (1:1), and (d) cinnamaldehyde/HPγCD-IC NFs (2:1) mat. The representative SEM images of (e) cinnamaldehyde/ HPβCD-IC NFs (1:1), (f) cinnamaldehyde/HPβCD-IC NFs (2:1), (g) cinnamaldehyde/HPγCD-IC NFs (1:1), (h) cinnamaldehyde/HPγCD-IC NFs (2:1).

Table 7. The properties of the solutions used for electrospinning and diameter of the resulting cinnamaldehyde/CD-IC NFs.

Samples	Viscosity (Pa·s)	Conductivity (μS cm^{-1})	Average fiber diameter (nm)	Fiber diameter range (nm)
Cinnamaldehyde/HPβCD-IC (1:1)	1.76± 0.29	12.66± 0.65	700±260	280-1925
Cinnamaldehyde/HPβCD-IC (2:1)	1.15± 0.16	12.18± 0.25	545±175	225-1160
Cinnamaldehyde/HPγCD-IC (1:1)	2.18± 0.65	4.53± 0.30	825±330	240-1895
Cinnamaldehyde/HPγCD-IC (2:1)	1.84± 0.30	5.00± 0.16	805±275	345-1630

2.3.3.4 Structural characterization

The presence of cinnamaldehyde in electrospun cinnamaldehyde/HPβCD-IC NFs was validated by ^{1}H NMR study (Figure 31). The specific peaks of cinnamaldehyde were detected in ^{1}H NMR spectra of all cinnamaldehyde/CD-IC NFs samples (Figure 31) confirming the presence of cinnamaldehyde in these samples. Although cinnamaldehyde is highly volatile, the ^{1}H NMR study clearly elucidated that cinnamaldehyde was effectively preserved in all cinnamaldehyde/CD-IC NFs samples during the whole process, including preparation of CD-IC solutions as well as during the electrospinning process of cinnamaldehyde/CD-IC NFs and their storage.

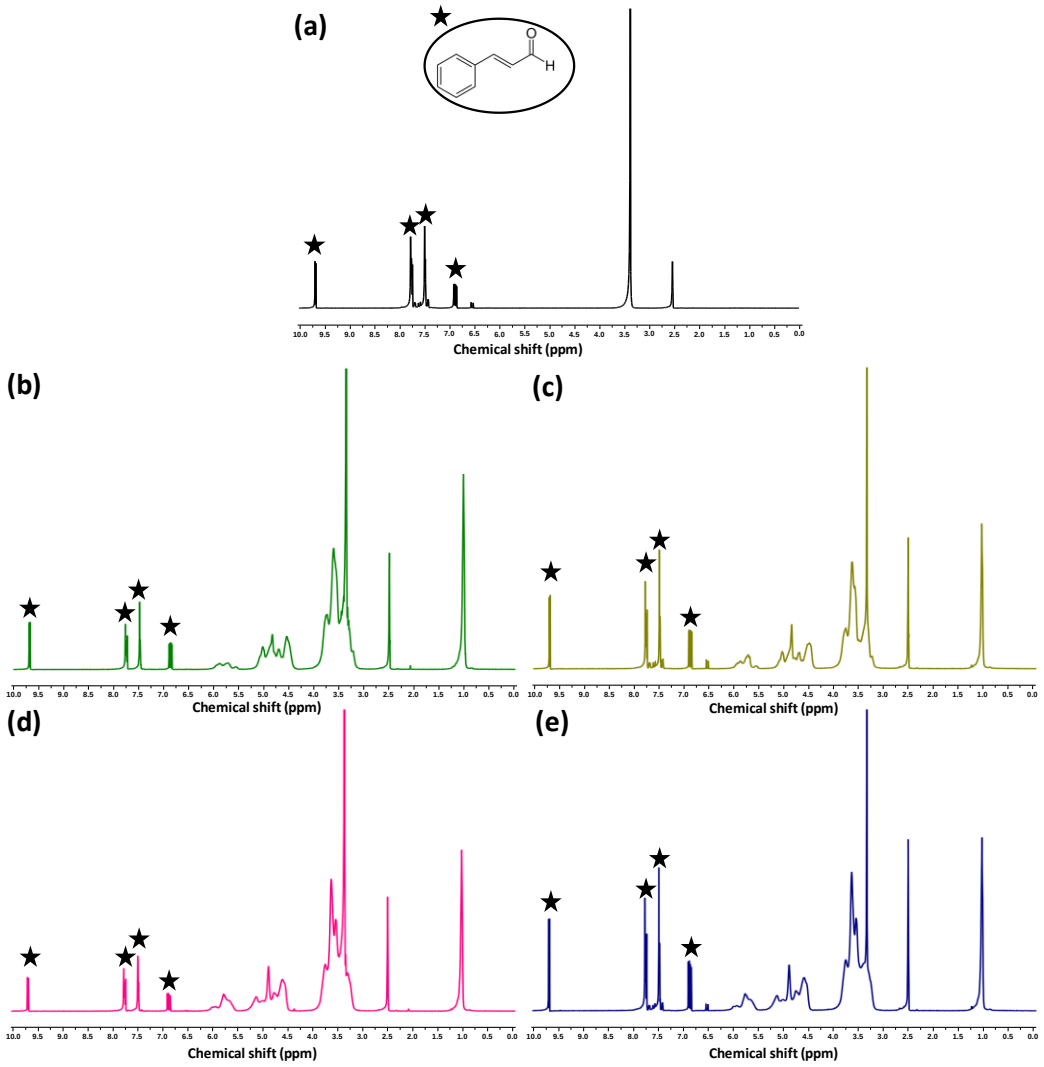

Figure 31. ^{1}H-NMR spectra of (a) pure cinnamaldehyde, (b) cinnamaldehyde/HPβCD-IC NFs (1:1), (c) cinnamaldehyde/HPβCD-IC NFs (2:1), (d) cinnamaldehyde/HPγCD-IC NFs (1:1), (e) cinnamaldehyde/HPγCD-IC NFs (2:1). The ^{1}H-NMR spectra were recorded by dissolving the samples in d6-DMSO. The characteristic peaks of cinnamaldehyde are shown by black stars.

FTIR spectroscopy is a useful technique to study the cyclodextrin inclusion complexation between host and guest molecules [111]. Moreover, FTIR spectroscopy can also verify the presence of guest molecules in the CD-IC samples. In FTIR analysis, inclusion complex formation can cause variations for the peak

position and peak intensity for the guest molecules when they are in the complexation state with the host CD cavity. The FTIR spectrum of cinnamaldehyde, pristine CD NFs, and cinnamaldehyde/CD-IC NFs are shown in Figure 32. The characteristic peaks for cinnamaldehyde at 1625 cm^{-1} belonging to the C═C double bond and 1676 cm^{-1} belonging to the C═O double bond were detected clearly. In the case of ICs, these peaks were present and the intensity of these peaks were suppressed; besides, the peak at 1676 cm^{-1} for the C═C double bond was shifted to 1670 cm^{-1}, whereas they were not observed at the spectra of pristine CD NFs. This type of peak position shift and peak intensity suppression is typically observed for CD-IC systems. Therefore, FTIR results suggested that the guest cinnamaldehyde molecules are in the complexation state with the host CDs (HP-β-CD and HP-γ-CD, 1:1 and 2:1 molar ratio) in all cinnamaldehyde/CD-IC NFs samples.

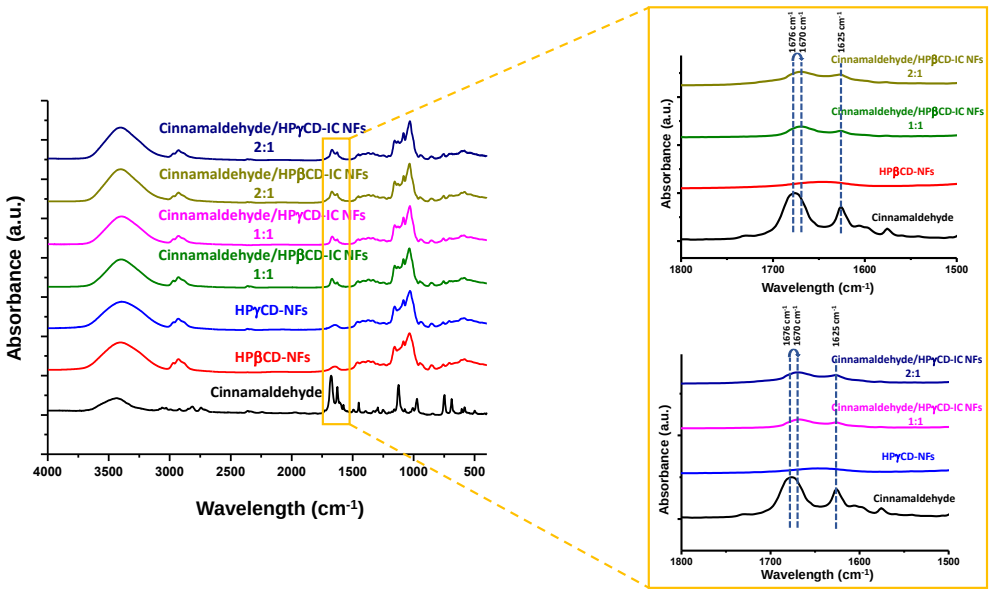

Figure 32. The FTIR spectra of pure cinnamaldehyde, pristine CD NFs, and cinnamaldehyde/CD-IC NFs.

2.3.3.5 Thermal characterization

The TGA data of pure cinnamaldehyde, cinnamaldehyde/HPβCD-IC NFs (1:1 and 2:1 molar ratio), and cinnamaldehyde/HPγCD-IC NFs (1:1 and 2:1 molar ratio) are given in Figure 33. As cinnamaldehyde is a volatile organic compound, the evaporation of pure cinnamaldehyde starts at a low temperature (below 50 °C) and it completely vaporized before the temperature of 200 °C. For cinnamaldehyde/CD-IC NFs samples, there are three weight losses observed; the weight loss below ~100 °C is due to water loss, and the weight loss above 300 °C is due to main thermal decomposition of hydroxypropylated CD molecules. The weight loss step observed between 100 and 300 °C is due to vaporization of cinnamaldehyde in cinnamaldehyde/CD-IC NFs. For cinnamaldehyde/HPβCD-IC NFs (1:1), the evaporation of cinnamaldehyde started at ~85 °C and completed at ~240 °C, whereas for cinnamaldehyde/HPβCD-IC NFs (2:1), the evaporation of cinnamaldehyde was observed between ~75 and 270 °C. On the other hand, for cinnamaldehyde/HPγCD-IC NFs (1:1), the evaporation of cinnamaldehyde was observed between ~85 and ~260 °C, whereas the evaporation of cinnamaldehyde was observed between ~75 and ~270 °C for cinnamaldehyde/HPγCD-IC NFs (2:1). The TGA studies clearly showed that the evaporation of cinnamaldehyde takes place at a much higher temperature for cinnamaldehyde/CD-IC NFs samples compared to pure cinnamaldehyde. The higher evaporation temperature of cinnamaldehyde in cinnamaldehyde/CD-IC NF mats elucidates the inclusion complexation between guest cinnamaldehyde and host CD molecules. Also, the presence of guest–host inclusion complexation in these cinnamaldehyde/CD-IC NF samples provides much higher thermal stability for the cinnamaldehyde.

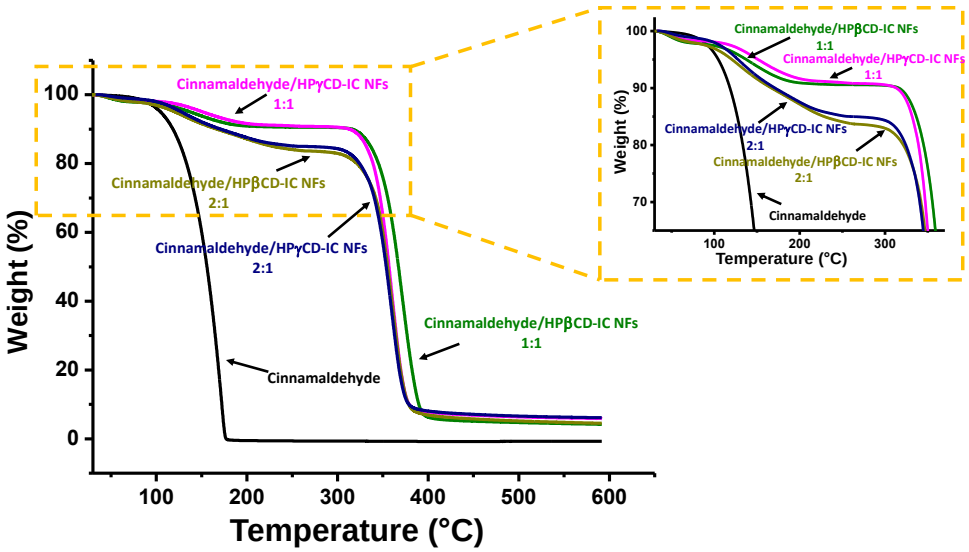

Figure 33. The TGA thermogram of pure cinnamaldehyde and cinnamaldehyde/CD-IC NFs.

The weight percentage of cinnamaldehyde present in cinnamaldehyde/CD-IC NF mats was calculated from TGA thermograms. The amount of cinnamaldehyde was calculated as 7.30% (w/w), 7.20% (w/w), 14.30% (w/w), and 13.70% (w/w) for cinnamaldehyde/HPβCD-IC NFs (1:1), cinnamaldehyde/HPγCD-IC NFs (1:1), cinnamaldehyde/HPβCD-IC NFs (2:1), and cinnamaldehyde/HPγCD-IC NFs (2:1), respectively. The initial theoretical amount of cinnamaldehyde is 8.25% (w/w) in cinnamaldehyde/HPβCD-IC NFs (1:1), 7.32% (w/w) in cinnamaldehyde/HPγCD-IC NFs (1:1), 15.25% (w/w) in cinnamaldehyde/HPβCD-IC NFs (2:1), and 13.79% (w/w) in cinnamaldehyde/HPγCD-IC NFs (2:1), respectively. Therefore, it was concluded that cinnamaldehyde was mostly preserved with a very high efficiency (~90%, w/w) within the cinnamaldehyde/CD-IC NFs, although cinnamaldehyde is a highly volatile organic compound.

2.3.3.6 Antibacterial activity

The antibacterial activities of cinnamaldehyde/HPβCD-IC NFs and cinnamaldehyde/HPγCD-IC NFs for both molar ratios (1:1 and 2:1 molar ratio) were investigated against strains of *E. coli* by the agar diffusion method. *E. coli* is a Gram-negative bacteria which is one of the significant food-borne pathogens that can cause serious disease outbreaks all over the world [142]. There is an increasing demand on the use of natural sterilization to prevent possible infections caused by *E. coli* or some other undesirable food-related microorganisms instead of the use of chemical food preservatives [142, 143]. The use of essential oils derived from plants have received great attention as a natural source to inhibit food-borne pathogens [142-145]. Among plant essential oils, cinnamaldehyde was reported as one of the effective essential oils against *E. Coli* [145-147]. The pristine CDs do not show antibacterial activity against *E. coli*, and so the NFs purely based on CDs are not expected to show any antibacterial activity [148]. Nevertheless, in our study, the antibacterial activity test against *E. coli* for pristine CD NFs was also done as a control test in order to see the differences caused by the presence of cinnamaldehyde in cinnamaldehyde/CD-IC NF mats (Figure 34). As expected, pristine CD NFs did not show any inhibition against *E. coli* growth. When the antibacterial activity against *E. coli* was tested for cinnamaldehyde/CD-IC NFs samples, the diameter of the IZs was observed as 4.83 ± 0.12, 4.89 ± 0.18, 4.50 ± 0.22, and 4.56 ± 0.06 cm for cinnamaldehyde/HPβCD-IC NFs (1:1), cinnamaldehyde/HPβCD-IC NFs (2:1), cinnamaldehyde/HPγCD-IC NFs (1:1), and cinnamaldehyde/HPγCD-IC NFs (2:1), respectively. These results indicated that

cinnamaldehyde/CD-IC NFs has certain amount of cinnamaldehyde which still effectively shows antibacterial activity against *E. coli*.

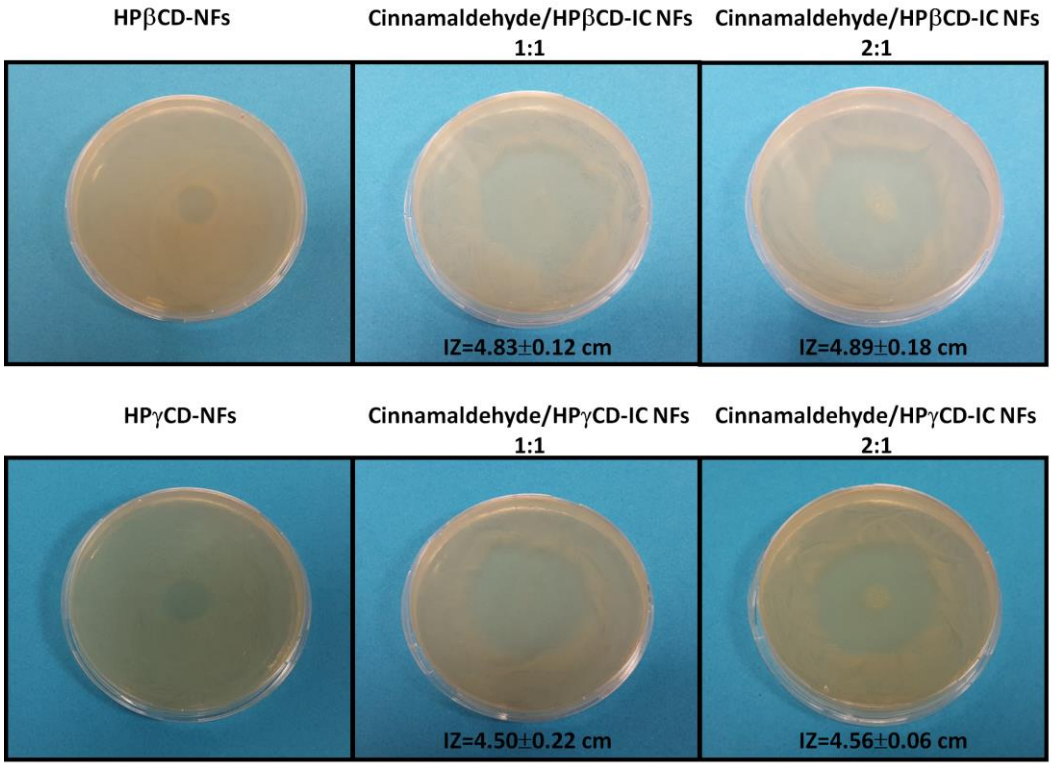

Figure 34. Representative digital photographs of antibacterial test plates of pristine CD NF mats and cinnamaldehyde/CD-IC NF mats against *E. coli*. The average IZ obtained from agar diffusion method (n = 3).

2.3.3.7 Dissolution behaviour

The water solubility of cinnamaldehyde is quite low (1.35 g L^{-1}) [149] which sometimes limits its applications. However, as revealed from phase solubility and molecular modeling studies, CD-IC formation significantly enhanced the water solubility of cinnamaldehyde. Here, two different methods were used to visualize the water solubility enhancement and fast-dissolution behavior of cinnamaldehyde/CD-IC NF mats. For the first method, distilled water was directly

added to the cinnamaldehyde/CD-IC NF mats. As seen from Figure 35, both cinnamaldehyde/HPβCD-IC NFs (1:1 and 2:1 molar ratio) and cinnamaldehyde/HPγCD-IC NFs (1:1 and 2:1 molar ratio) samples show very fast-dissolution behavior with the addition of water. Because of the nanofibrous structure providing very high surface area, cinnamaldehyde/CD-IC NF mats were dissolved in water very quickly (less than a second), which proves the fast-dissolving character of cinnamaldehyde/CD-IC NF mats. For the second method, absorbent paper was soaked by distilled water, then cinnamaldehyde/CD-IC NF mats were placed onto this paper. Figure 6 shows the dissolution character of cinnamaldehyde/CD-IC NF mats. The cinnamaldehyde/CD-IC NF mats were dissolved instantly when they were placed onto the distilled water-soaked absorbent paper. This result clearly shows that these cinnamaldehyde/CD-IC NF mats have ultrafast dissolution behavior even in the presence of a small amount of water such as saliva. These results are very promising that the cinnamaldehyde/CD-IC NF mats can be used in variety of applications including fast-dissolving oral care products. In both dissolution tests, it was observed that cinnamaldehyde/CD-IC NFs samples having 2:1 (cinnamaldehyde/CD) molar ratio have shown slightly slower dissolution behavior compared to cinnamaldehyde/CD-IC NFs samples having 1:1 (cinnamaldehyde/CD) molar ratio. This is possibly because of the higher content of the cinnamaldehyde present in cinnamaldehyde/CD-IC NFs samples having 2:1 molar ratio which may slightly decrease the dissolution rate of these nanofibrous mats.

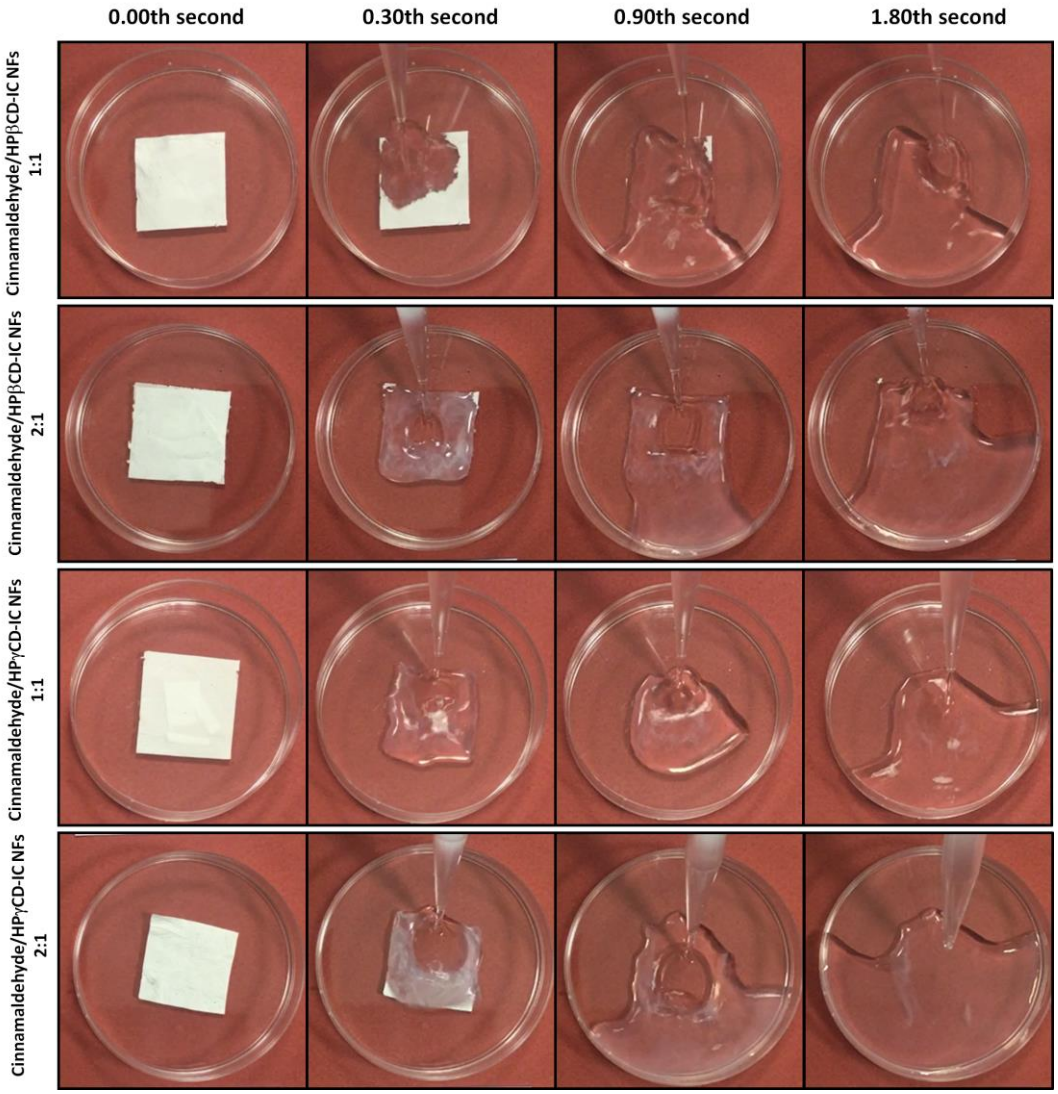

Figure 35. Representation of dissolution behavior of cinnamaldehyde/CD-IC NF mats when exposed to distilled water. The cinnamaldehyde/CD-IC NF mats are dissolved completely in a few seconds.

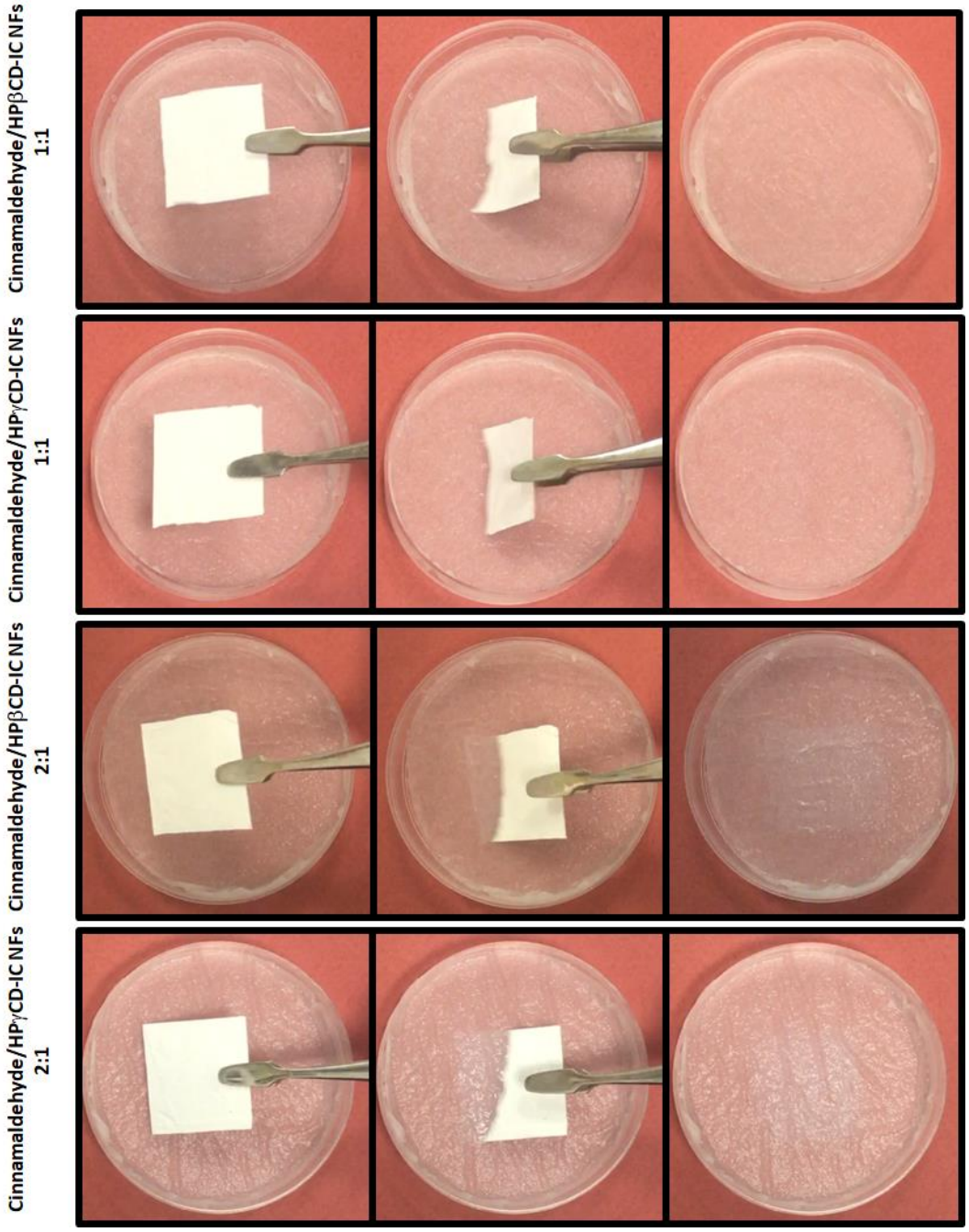

Figure 36. Representation of dissolution behavior of cinnamaldehyde/CD-IC NF mats when contacted to water soaked absorbent paper. The cinnamaldehyde/CD-IC NF mats are dissolved instantly.

2.3.4 Conclusion

In brief, cinnamaldehyde was inclusion complexed with two different type of hydroxypropylated CDs (HPβCD and HPγCD) at two different molar ratios (1:1 and 2:1, cinnamaldehyde/CD). The inclusion complexation of cinnamaldehyde with HPβCD and HPγCD was investigated by phase solubility and molecular modeling studies. The electrospinning of NFs from cinnamaldehyde/CD-IC was successfully performed. Although cinnamaldehyde is a highly volatile organic compound, because of the inclusion complexation within the CD cavity, cinnamaldehyde was effectively preserved with high efficiency in electrospun cinnamaldehyde/CD-IC NFs during the whole process including preparation, electrospinning, and storage. Cinnamaldehyde has shown much higher temperature stability in cinnamaldehyde/CD-IC NFs when compared to its pure form due to the inclusion complexation. The cinnamaldehyde/CD-IC NFs have shown antibacterial activity when tested against *E. coli*. Even though cinnamaldehyde is not soluble in water, cinnamaldehyde/CD-IC NF mats have shown fast-dissolving character in water. These promising results suggest that cinnamaldehyde/CD-IC NF mats may be quite applicable in food, oral-care, healthcare, pharmaceutics, cosmetics, and so forth, due to their fast-dissolution, enhanced water solubility, high temperature stability, and promising antibacterial activity.

2.4 β-carotene/cyclodextrin inclusion complex nanofibers: Antioxidant activity and enhanced photostability

2.4.1 Introduction

Carotenoids are natural pigments found in many plants, animals and microorganisms [150]. β-carotene (Figure 37a) is one of the carotenoids found in fruits and vegetables, and giving them red-orange colour. It is known to be a natural precursor of vitamin A and also be a strong antioxidant. These properties may account for its ability to reduce the risk of cardiovascular disease, eye diseases and certain cancers [150, 151]. Therefore, there is considerable interest in use of β-carotene in food products as a nutraceutical agent and a natural pigment [151]. However, very high hydrophobic nature and high degree of unsaturation of β-carotene which leads to extremely low water solubility and chemical instability restrict its incorporation into products [150-152].

In this study, inclusion complexes of β-carotene was prepared by two hydroxpropylated CDs, HPβCD and HPγCD, and nanofibers were produced from its CD-ICs by electrospinning method (Figure 37). The nanofibers were characterized by scanning electron microscope (SEM), Fourier transform infrared (FTIR) spectroscopy and X-Ray Diffraction (XRD). The antioxidant activity of β-carotene/CD-IC nanofibers was investigated by using 2,2-diphenyl-1-picrylhydrazyl (DPPH) method. In order to test light stability of encapsulated β-carotene, the nanofibers including β-carotene were exposed to ultraviolet (UV) light and then the antioxidant properties of these nanofibers were analysed by using UV-Vis spectrscopy. The light stability of carotenoids after formation of CD-IC nanofibers were decided by comparing UV light exposed nanofibers with nanofibers which are not exposed to.

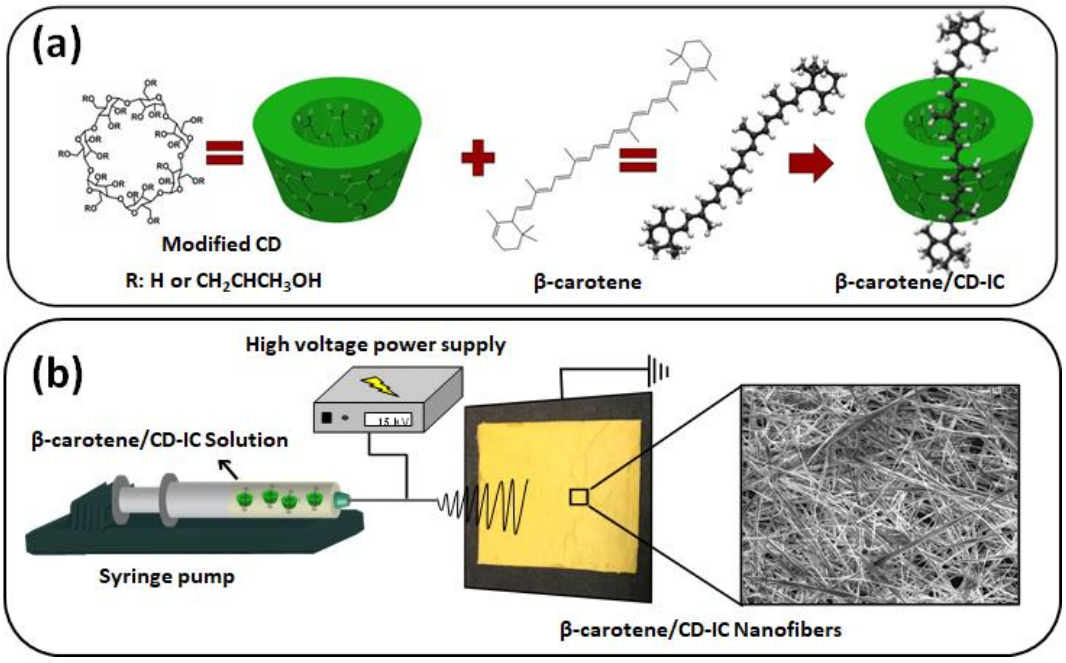

Figure 37. (a) Molecular structure of β-carotene and HPβCD (note: HPγCD has a similar chemical structure with eight glucopyranose units), and illustration of β-carotene/CD-IC formation, (b) electrospinning process of NFs from β-carotene/CD-IC solution.

2.4.2 Experimental

2.4.2.1 Materials

β-carotene (≥95%) was received from Cayman Chemical. The hydroxypropyl-β-cyclodextrin (HPβCD) (Cavasol®W7 HP) and hydroxypropyl-γ-cyclodextrin (HPγCD) (Cavasol®W8 HP) were kindly given by Wacker Chemie AG (Germany). The Millipore Milli-Q ultrapure water system was used for the distilled water used in the experiments. N,N-Dimethylformamide (DMF, anhydrous, 99.8%) and 2,2-diphenyl-1-picrylhydrazyl (DPPH) were purchased from Sigma-Aldrich. Deuterated dimethylsulfoxide (d6-DMSO, deuteration degree min. 99.8% for NMR spectroscopy) were purchased from Merck. All the materials were used as-received.

2.4.2.2 Preparation of electrospinning solution

The inclusion complex solutions of β-carotene with two modified CDs (HPβCD and HPγCD) were prepared by 6:1 molar ratio (CD: β-carotene) for water as a solvent and 1:1 molar ratio (CD: β-carotene) for DMF as a solvent. First, β-carotene was dispersed in both solvent system, respectively. Then, HPβCD and HPγCD at 180% concentration (1.8 g of CD in 1 mL water) were added to the β-carotene dispersion prepared in water. For β-carotene dispersion prepared in DMF, HPβCD and HPγCD at 130% concentration (1.3 g of CD in 1 mL DMF) were added. The resulting solutions were stirred at room temperature for overnight. Besides, to make comparison, highly concentrated HPβCD and HPγCD solution without β-carotene were also prepared for the electrospinning of pure CD nanofibers [91].

2.4.2.3 Electrospinning of nanofibers

The CD-IC solutions of β-carotene and solutions of pure CDs were seperately loaded in 1 mL syringe with metallic needle having 0.4 mm inner diameter. These syringes were placed on pump (KD Scientific, KDS-101, USA) having rate of 0.5-1.0 mL/h. High voltage at 15 kV was applied between tip of needle and grounded metal collector by high voltage power supply (Spellman, SL Series). The distance between needle and collector was arranged as 15-20 cm.

2.4.2.4 Measurements and characterizations

Phase solubility diagram was plotted and stability constants of complexes between β-carotene and CDs were determined according to the method reported by Higuchi and Connors [102]. For the test, excess amount of β-carotene was added to 5 mL of the aqueous solution of HPβCD and HPγCD with increasing concentration from 1

to 36 mM. The β-carotene/ CD solutions were shaken at room temperature for 48 h in the dark. Then, solutions were filtered to remove undissolved part through a 0.45 μm membrane filter. After that, dissolved amount of β-carotene in the β-carotene/CD solutions was determined by UV-Vis spectrophotometer (Varian, Cary 100) by recording the absorption at 278 nm. The experiment was repeated three times and average was taken. β-carotene concentration versus CD concentration graph was plotted. The apparent stability constant (K_s) was calculated from the graph according to the following equation:

K_s = slope/ S_0 (1- slope)

where S_0 is the intrinsic solubility of β-carotene.

Inclusion complexation between β-carotene and CDs was also studied by ab initio computational method depending on density functional theory (DFT) [103-105]. Generalized gradient approximation including van der waals correction was used to express the exchange-correlation functional [106, 107]. The projector augmented-wave method was applied to describe the element potentials [108]. Implicit solvent method using continuum dielectric description was applied to examine solvent effect [109]. The interaction energy (E_{int}) of resulting complexes can be defined as:

$E_{int} = E_{CD} + E_{\beta\text{-carotene}} - E_{IC}$

where E_T (CD), E_T(guest), and E_T(IC) is the total energy of HPβCD or HPγCD, single β-carotene and their inclusion complexes (for 1:1 and 2:1 stoichiometry), respectively.

The solvation energy (E_{solv}) of inclusion complexes can be calculated by the following formula:

$E_{solv} = E_{water} - E_{vacuum}$

E_{water} and E_{vacuum} is the total energy of β-carotene, CD, or β-carotene/CD-IC in water and vacuum, respectively.

Rheological behaviour of β-carotene/CD solutions was measured by a rheometer (Anton paar, physica CR 301) equuipped with a CP 20-4 spindle at a constant shear rate of 100 s^{-1} at 25 °C.

Scanning electron microscope (SEM, FEI Quanta 200 FEG) was used to perform morphological analyses of electrospun nanofibers. 5 nm Au/Pd sputtering was done prior to SEM imaging of nanofibers by Gatan 682 PECS. Average fiber diameter (AFD) of each samples was calculated by measuring diameter of 100 fibers from different locations of the SEM images.

Crystalline structure of β-carotene, pure CD NFs and β-carotene/CD-IC NFs was determined by X-Ray diffraction instrument (XRD, PANalytical X'Pert powder diffractometer) applying Cu Kα radiation in a range of 2θ = 5-30°.

Fourier transform infrared spectrometry (FTIR, Bruker- VERTEX70) was used to obtain FTIR spectra of β-carotene, pure CD NFs and β-carotene/CD-IC NFs. Potassium bromide (KBr) was used to prepare pellets required for instrument. 64 scans were recorded at resolution of 4 cm^{-1} within a range of 4000-400 cm^{-1}.

The antioxidant activity of β-carotene/CD-IC NFs was examined by 2,2-Dipheniy-1-picrylhydrazyl (DPPH) radical scavenging method. For this, DPPH solution in methanol (1.25×10^{-4}M) was prepared. In this assay, β-carotene/CD-IC NFs prepared in water system were used, since water is more friendly for food and drug based applications than DMF. 3 mL of 1.25×10^{-4}M DPPH solution was added on

10 mg of β-carotene/HPβCD-IC NFs and β-carotene/HPγCD-IC NFs. To make comparison, DPPH solution was also added to the β-carotene in the maximum amount found in nanofibers. After the addition of the DPPH stock solution on the samples, a reduction at the absorbance intensity (517 nm) was recorded at different time intervals by using UV-Vis spectroscopy (Varian, Carry 100). The experiment was repeated three times for each sample. The DPPH radical scavenging efficiency was expressed as the inhibition percentage and was calculated by the following formula:

DPPH radical scavenging (%) = $((A_{blank} - A_{sample})/ A_{blank})\times 100$.

It is known that β-carotene has extremely low light stability [152]. In order to analyse the effect of CD-IC NFs formation on β-carotene, β-carotene/CD-IC NFs (10 mg) were exposed to UV- light (300 W, Osram Ultra-Vitalux, E27/ES) from a distance of 15 cm for 6h. The photostability of β-carotene, β-carotene/HPβCD-IC NFs and β-carotene/HPγCD-IC NFs were investigated by performing antioxidant activity test according to procedure explained in the previous section. The results were compared with the results obtained from antioxidant activity analyses (1h measurements) of non-treated nanofibers. These experiments were conducted in triplicate.

2.4.3 Results and discussion

2.4.3.1 Phase solubility studies

Phase solubility profiles of β-carotene/CD-IC are displayed in Figure 38. From these profiles it was observed that the β-carotene concentration increased linearly

by increasing CD concentration which shows increase of solubility of β-carotene by CD-IC formation.

Stability constant (K_s) was calculated as 27 M^{-1} and 36 M^{-1} for β-carotene/HPβCD-IC and β-carotene/HPγCD-IC, respectively.

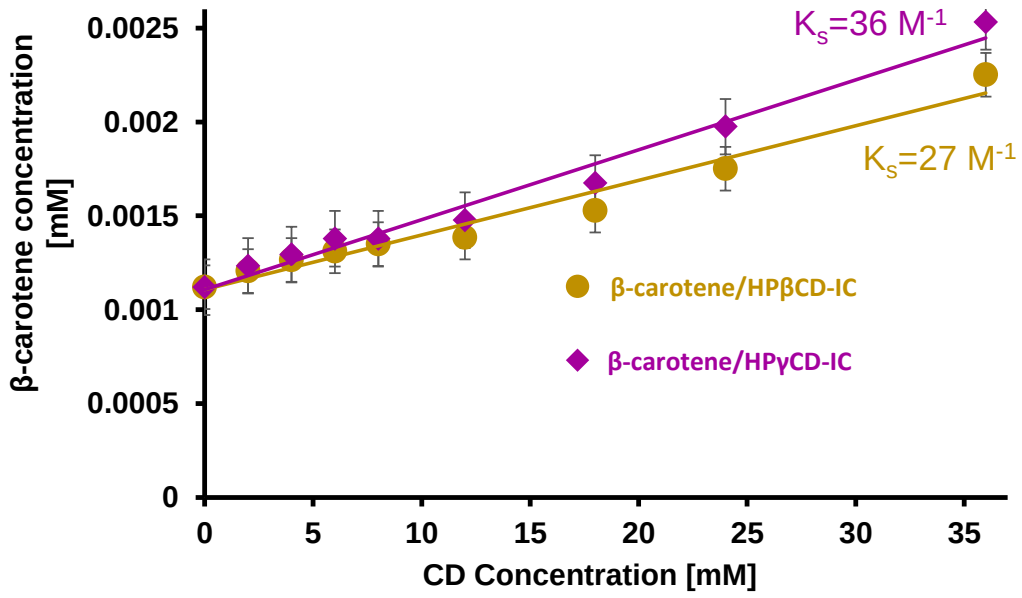

Figure 38. Phase solubility diagrams of β-carotene/HPβCD-IC and β-carotene/HPγCD-IC, (n = 3).

2.4.3.2 Computational modeling

Initially, HPβCD, HPγCD, and single β-carotene molecule are relaxed in vacuum by minimizing the total energy and optimized geometries are obtained (Figure 39a). To reveal the complexation of the host CD and the guest molecule, β-carotene is moved towards HPβCD and HPγCD in different molar ratios (1:1 and 2:1, CD: β-carotene). It was shown that β-carotene molecule can form inclusion complexes with both HPβCD and HPγCD at 1:1 molar ratios (Figure 39b). Besides, since there is size mismatch observed in inclusion complexes with HPβCD at 2:1 molar ratio

(CD: β-carotene), the formation of complexes in this ratio is only favored for HPγCD at different configurations (Figure 39c).

The inclusion complex is considered to be formed when E_{int} is maximized and maximum value of E_{int} for the given configuration is defined as complexation energy (E_{comp}). High complexation energy indicates strong binding for both CDs. The results are given in Table 8 in which it was seen that HPγCD forms stronger binding with β-carotene than HPβCD which is correlated with the previous data obtained from phase solubility analysis.

Solvation energies (E_{solv}) were also calculated to reveal the solubility trends (Table 8). Obtained results show that although β-carotene molecule is almost insoluble in water (-0.10 kcal mol^{-1}), inclusion complex formation significantly increases the E_{solv}. This results suggest a substantial increase in β-carotene solubility. E_{solv} is calculated as -67.76 kcal mol^{-1} and -81.81 kcal mol^{-1} for β-carotene/HPβCD-IC and β-carotene/HPγCD-IC, respectively in 1:1 stoichiometry. E_{solv} further increases in 2:1 stoichiometry and becomes -162.69 kcal mol^{-1} and -163.99 kcal mol^{-1} for AB-AB and AB-BA configurations of β-carotene/HPγCD-IC, respectively.

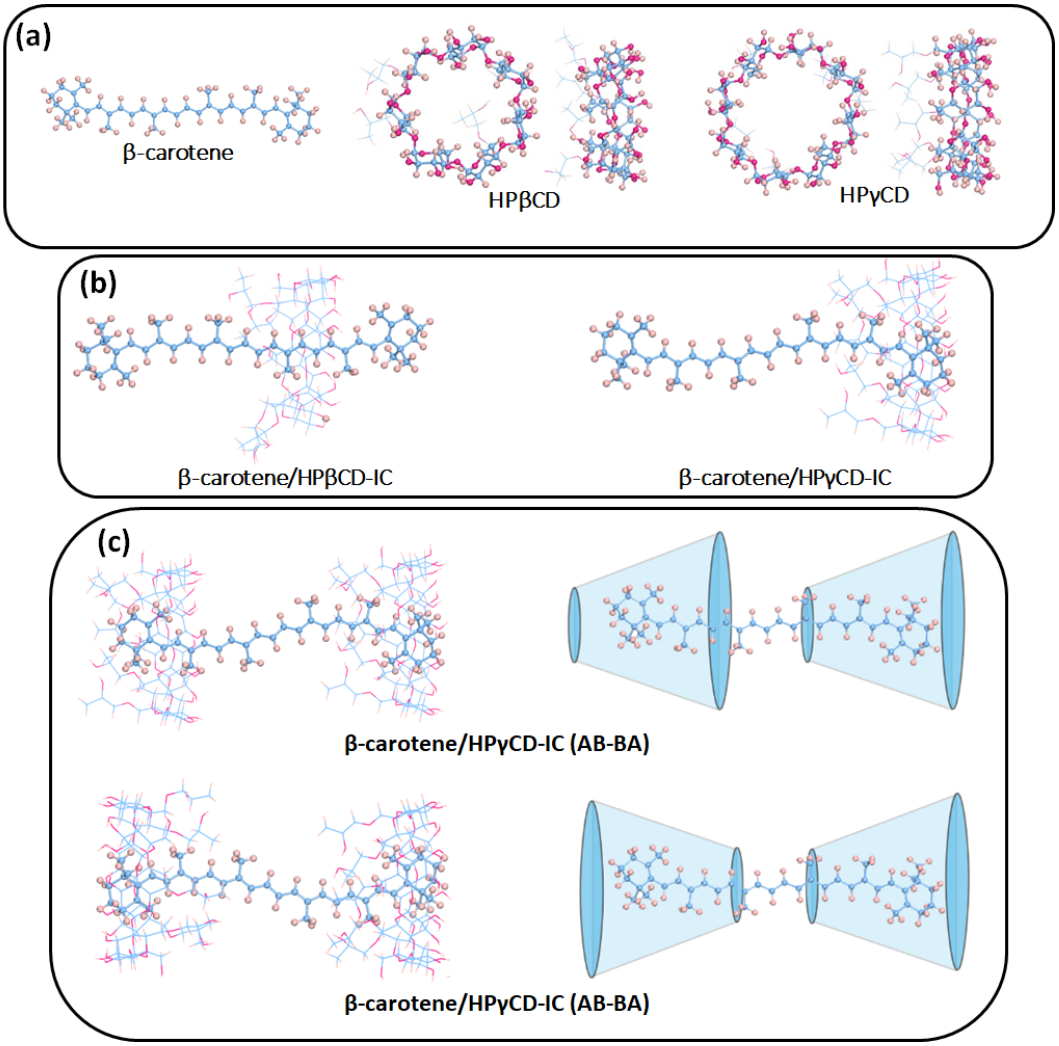

Figure 39. (a) optimized structures of β-carotene, HPβCD and HPγCD, (b) formation of inclusion complexes in 1:1 stoichiometry between CDs and β-carotene, and (c) formation of inclusion complexes in 2:1 stoichiometry between HPγCD and β-carotene with two different configurations.

Table 8. Complexation and solvation energies of the β-carotene, CDs (HPβCD and HPγCD) and β-carotene within CDs at different molar ratios and different orientations.

Host	Guest	Molar ratio (host:guest)	Configuration	E_{comp} (vacuum) kcal mol^{-1}	E_{comp} (water) kcal mol^{-1}	E_{solv} kcal mol^{-1}
HPβCD	β-carotene	1:1	-	21.34	15.58	-67.76
HPγCD	β-carotene	1:1	-	23.54	19.87	-81.81
HPβCD	β-carotene	2:1	-	-	-	-
HPγCD	β-carotene	2:1	AB-AB	45.26	19.29	-162.69
HPγCD	β-carotene	2:1	AB-BA	45.25	20.58	-163.99
-	β-carotene	-	-	-	-	-0.10

2.4.3.3 Morphological analyses

Parameters of electrospinning process was optimized to produce uniform nanofibers from β-carotene/HPβCD-IC and β-carotene/HPγCD-IC solutions. Digital photographs and their representative SEM images of β-carotene/CD-IC mats were displayed in Figure 40.

The average fiber diameter (AFD) was measured as 250±195 for β-carotene/HPβCD-IC NFs (water), 320±175 for β-carotene/HPγCD-IC NFs (water), 665±465 for β-carotene/HPβCD-IC NFs (DMF) and 1130±575 for β-carotene/HPγCD-IC NFs (DMF) (Table 9). The difference in AFD can be explained by differences in the viscosity of solutions. Since its well-known that higher solution viscosity results in less stretching of the electrified jet that forms thicker fibers during electrospinning process [12].

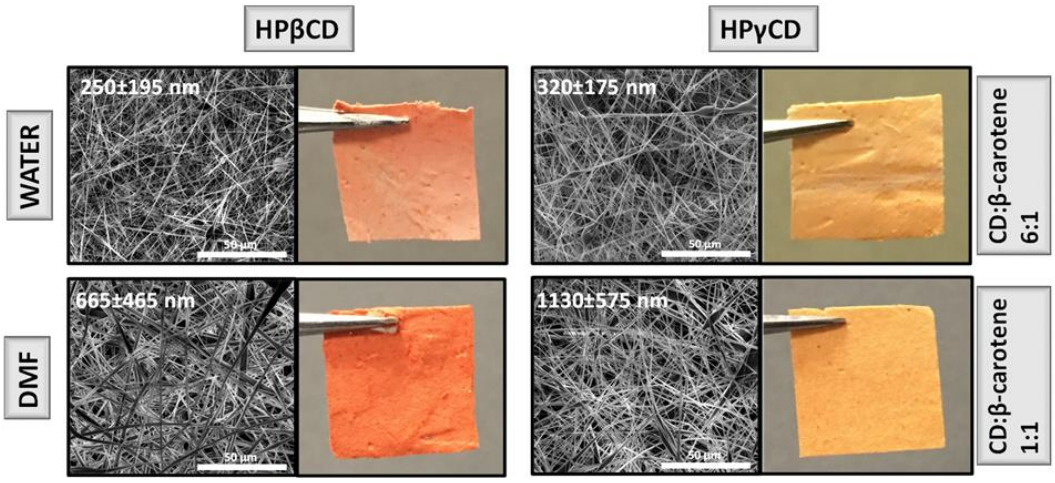

Figure 40. The photographs and SEM images of optimized β-carotene /CD-IC NFs.

Table 9. The properties of the solutions used for electrospinning and diameter of the resulting β-carotene/CD-IC NFs.

Solutions	Solvent	% CD[a] (w/v)	Molar ratio CD:β-carotene	Viscosity (Pa·s)	Average fiber diameter (AFD) (nm)
β-carotene/HPβCD-IC	Water	180	6:1	2.84	250±195
β-carotene/HPγCD-IC	Water	180	6:1	3.43	320±175
β-carotene/HPβCD-IC	DMF	130	1:1	7.15	665±465
β-carotene/HPγCD-IC	DMF	130	1:1	10.21	1130±575

2.4.3.4 Structural characterization

The crystalline structures of β-carotene, CD NFs and β-carotene/CD-IC NFs were investigated by XRD (Figure 41). The crystalline structure of β-carotene was transformed into amorphous after β-carotene/CD-IC NFs formation which verifies that β-carotene molecules were encapsulated by CDs and so they cannot form crystalline aggregates. It is known that compounds in crystalline forms are more stable so they have lower solubility [153]. In other words, the change in structure of β-carotene from crystalline to amorphous after CD-IC formation confirmed the increase in its solubility.

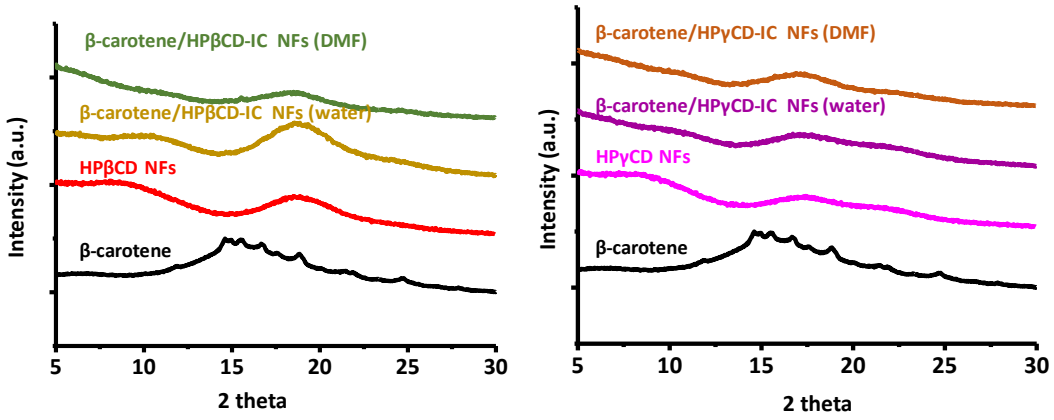

Figure 41. The XRD patterns of β-carotene, CD NFs and β-carotene/CD-IC NFs obtained in different solvents.

Fourier-transform infrared spectroscopy (FTIR) was used to confirm the formation of inclusion complex. Chemical variations caused by inclusion complex formation show the variation of peak shape, position and intensity. Figure 42 shows the FTIR spectra of β-carotene, pure CD NFs and β-carotene/CD-IC NFs prepared in different CD: β-carotene molar ratios. This type of peak intensity suppression seen

in Figure 42 suggested the formation of inclusion complexes between CD and β-carotene.

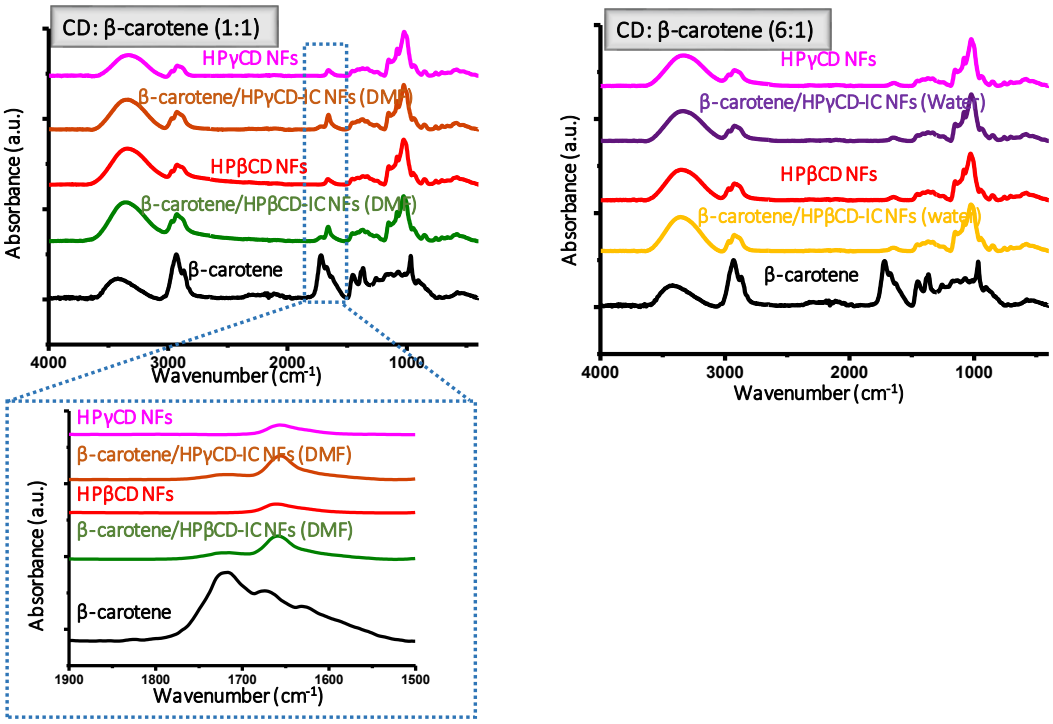

Figure 42. FTIR spectra of β-carotene, CD NFs and β-carotene/CD-IC NFs obtained in different solvents.

2.4.3.5 Antioxidant activity

The antioxidant capacity of β-carotene was obtained by DPPH radical scavenging assay. This assay is based on reduction of DPPH molecule by a hydrogen donor. As DPPH molecule is reduced, its strongest absorption band observed in UV-Vis spectrum decreases and the purple color of the solutions turns to yellow. In this assay, β-carotene/CD-IC NFs prepared in water system were used, since water is more friendly for food and drug based applications than DMF. Here, time dependent radical scavenging tests were carried out to discover the antioxidant performances differences between samples more precisely. The results are given in

Figure 43. These results indicated that β-carotene continues to show antioxidant activity after formation of its CD-IC NFs.

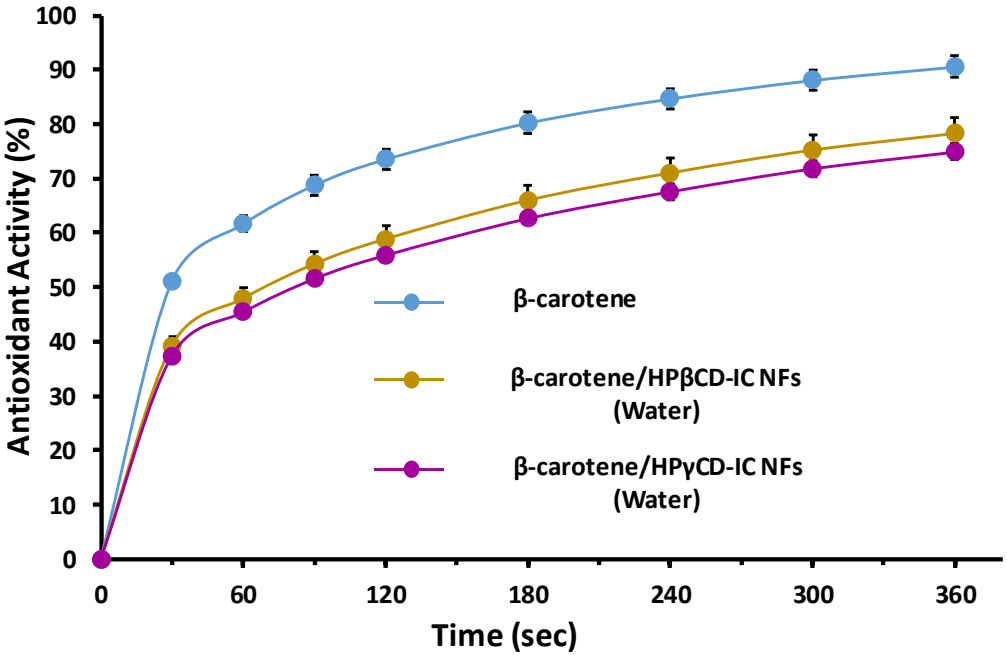

Figure 43. Time dependent antioxidant test graphs of β-carotene and β-carotene/CD-IC NFs.

2.4.3.6 Photostability

Antioxidant tests was repeated for β-carotene/CD-IC NFs which were exposed to UV-light to analyze change in their stability under light. The results are given in Figure 44. The results showed that, although β-carotene was highly affected by UV exposure, its CD-IC nanofibrous webs were not affected that much. This means that formation of CD-IC NFs of β-carotene provides protection against light.

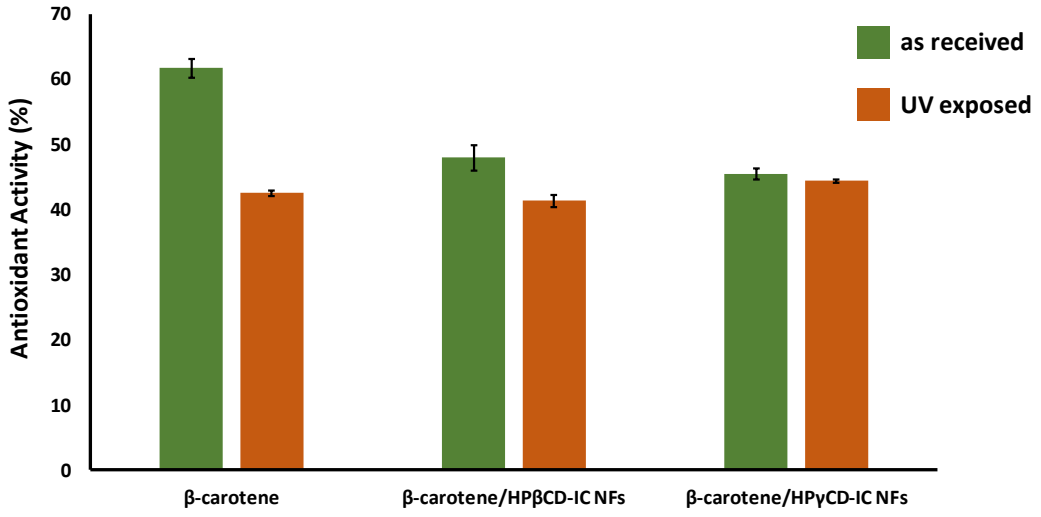

Figure 44. Antioxidant test graphs of β-carotene and β-carotene/CD-IC NFs after exposure to UV-light.

2.4.4 Conclusion

In this study, handy and self-standing nanofibrous webs of β-carotene/HPβCD-IC and β-carotene/HPγCD-IC were successfully produced at different CD: β-carotene molar ratios (1:1 and 6:1). The enhanced water solubility of β-carotene was confirmed by phase solubility and molecular modeling studies. SEM images showed the formation of uniform nanofibers. Presence of β-carotene in nanofibers and the formation of inclusion complexes were confirmed by XRD and FTIR studies. Antioxidant activity test revealed that antioxidant activity of β-carotene was preserved after formation of CD-IC nanofibers. Finally, enhancement of light stability of β-carotene after formation of CD-IC nanofibers was shown by photostability test. These results suggest that β-carotene in the form of CD-IC nanofibers may be applicable in food and pharmaceutics due to its enhanced light stability.

CHAPTER 3

ENCAPSULATION OF DRUGS BY CYCLODEXTRIN FUNCTIONALIZED ELECTROSPUN NANOFIBERS

3.1. Polymer-free electrospun nanofibers from sulfobutyl ether$_7$-beta-cyclodextrin (SBE$_7$-β-CD) inclusion complex with sulfisoxazole: Fast-dissolving and enhanced water solubility of sulfisoxazole

This part of thesis was reprinted (adapted) by permission from Elsevier [154], (“Polymer-free electrospun nanofibers from sulfobutyl ether(7)-beta-cyclodextrin (SBE7-β-CD) inclusion complex with sulfisoxazole: Fast-dissolving and enhanced water-solubility of sulfisoxazole”, Z. I. Yildiz, A. Celebioglu, and T. Uyar, *International Journal of Pharmaceutics*, 531, 550-8, 2017), Copyright (2017) Elsevier.

3.1.1 Introduction

Sulfonamides are synthetic drugs known by their antimicrobial effects on different pathogenic microorganisms [155]. However, the use of these types of drugs is

sometimes limited due to their poor water-solubility. The oxazole subtituted sulfonamide is called as sulfisoxazole (Figure 45a). Sulfisoxazole is a weak acid and slightly soluble in water. In this study, our aim was to develop nanofibrous sulfisoxazole-cyclodextrin inclusion complex system (Figure 45a) in order to have fast-dissolving character and enhance the water-solubility of sulfisoxazole. Here, we prepared a highly concentrated aqueous solution of inclusion complex between sulfisoxazole and sulfobutyl ether$_7$-beta-cyclodextrin (SBE$_7$-β-CD), and then, without using any polymeric matrix, sulfisoxazole/ SBE$_7$-β-CD-IC was electrospun into nanofibrous structure to obtain a free-standing and handy solid form (Figure 45b). We observed that sulfisoxazole/ SBE$_7$-β-CD-IC nanofibrous web was readily soluble in water and the water-solubility of sulfisoxazole was enhanced significantly. Our findings suggested that sulfisoxazole/ SBE$_7$-β-CD-IC in the form of nanofibrous webs can be quite useful in fast-dissolving tablet formulations for drug delivery.

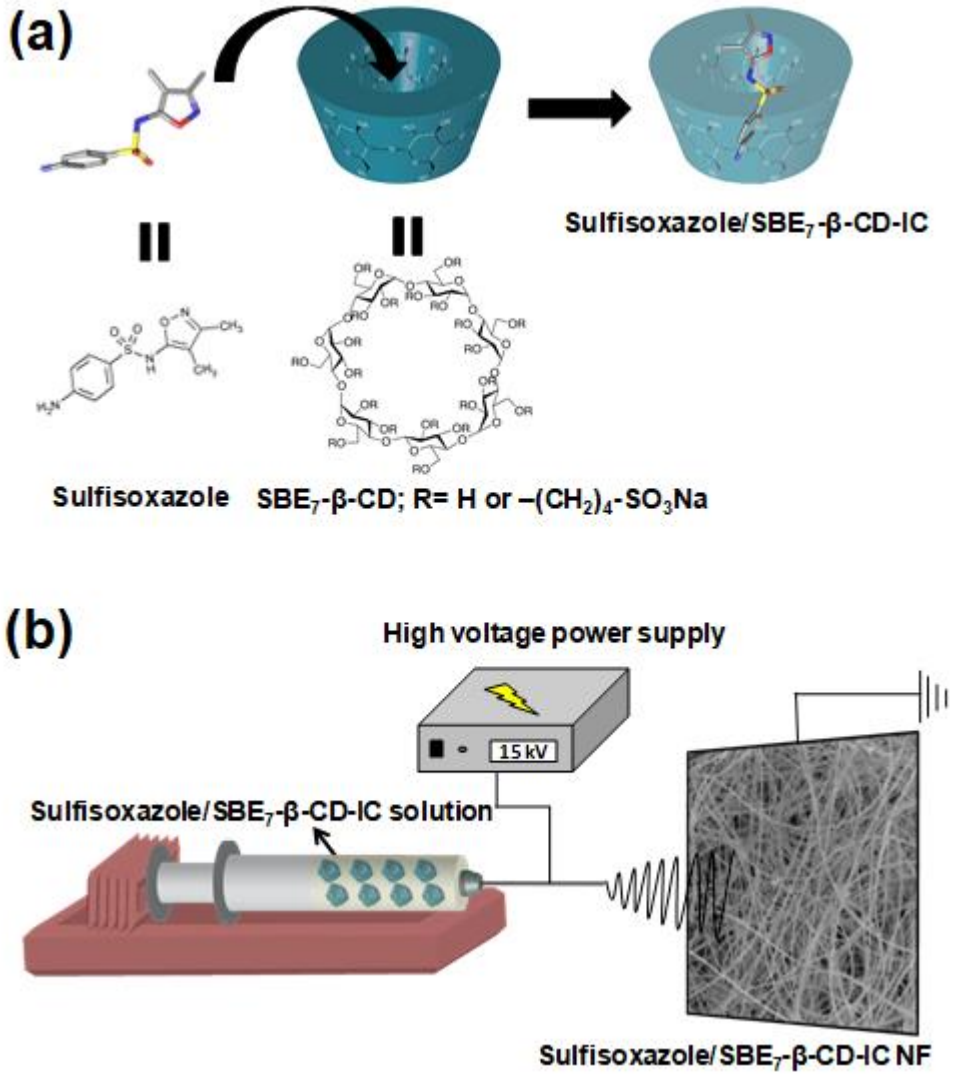

Figure 45. (a) The chemical structure of sulfisoxazole and SBE7-β-CD with a schematic representation of sulfisoxazole, SBE7-β-CD and their IC, (b) Schematic representation of the electrospinning of sulfisoxazole/SBE7-β-CD-IC nanofibers (NF).

3.1.2 Experimental

3.1.2.1 Materials

Sulfisoxazole (99%) was obtained from Sigma-Aldrich commercially. SBE7-β-CD (Captisol®, average degree of substitution=6.6) was kindly donated by Cydex

Pharmaceuticals Inc. (Kansas, USA). Potassium bromide (KBr, 99%, FTIR grade, Sigma-Aldrich), deuterated dimethylsulfoxide (d6-DMSO, deuteration degree min. 99.8% for NMR spectroscopy, Merck) were used in this study. The water used was from a Millipore Milli-Q ultrapure water system. The materials were used as-received without any further purification process.

3.1.2.2 Preparation of solutions

The inclusion complex solution of sulfisoxazole with SBE_7-β-CD was initially prepared by 1:1 molar ratio of sulfisoxaole:SBE_7-β-CD. However, the molar ratio was changed to 1:2 (sulfisoxazole:SBE_7-β-CD) since electrospinning of uniform nanofiber cannot be obtained from 1:1 complex solution. Firstly, sulfisoxazole powder was dispersed in water then SBE_7-β-CD (200% (w/v)) was added to the dispersion. After that, the solution was stirred 24 h until clear and homogenous solution was obtained. Besides, to make comparison, highly concentrated SBE_7-β-CD (200% (w/v)) solution without sulfisoxazole was also prepared in water for the electrospinning of pure SBE_7-β-CD nanofibers. Sulfisoxazole/ SBE_7-β-CD-IC was also obtained in the powder form in order to compare with sulfisoxazole/ SBE_7-β-CD-IC NF in terms of the dissolving rate and water solubility. Sulfisoxazole powder was dispersed in water and then SBE_7-β-CD was added with the molar ratio of 1:2 (sulfisoxazole: SBE_7-β-CD). After 24 h stirring, this inclusion complex solution was frozen at -80 °C for two days and then lyophilized in a freeze-dryer for 24 h to obtain sulfisoxazole/ SBE_7-β-CD-IC powder.

3.1.2.3 Electrospinning of nanofibers

Sulfisoxazole/SBE_7-β-CD-IC solution was loaded to the 1 mL syringe fitted with a 0.4 mm inner diameter having needle. The syringe was placed horizontally on the syringe pump (KD Scientific, KDS 101) and the solution was pumped with rate of 0.5-1 mL/h. A grounded metal collector covered by aluminum foil was placed at 10-15 cm from the tip of the needle and the applied voltage was 10-15 kV. The electrospinning of pristine SBE_7-β-CD NF was performed with the same conditions/parameters. The electrospinning system was enclosed by Plexiglass box and electrospinning was performed at 25 ºC and 30% relative humidity.

3.1.2.3 Measurements and characterizations

Phase solubility measurement was carried out according to Higuchi and Connors (1965) [102]. An excess amount of sulfisoxazole was added to 5 mL of aqueous solutions containing increasing concentration of SBE_7-β-CD ranging from 0 to 7.4 mM. The suspensions were shaken for 48 h at room temperature to reach equilibrium. Then, all suspensions were filtered by a 0.45 μm membrane filter to remove undissolved parts and all suspensions were diluted with water. Sulfisoxazole concentration with respect to increasing SBE_7-β-CD concentration was determined by UV-Vis spectroscopy (Varian, Cary 100) at 260 nm. The result of phase solubility was given as a plot of the molar concentration of sulfisoxazole versus molar concentration of SBE_7-β-CD. The apparent stability constant (K_s) of sulfisoxazole/SBE_7-β-CD-IC were calculated from the phase solubility diagram according to the following equation:

K_s= slope/ S_0 (1-slope)

where S_0 is the intrinsic solubility of sulfisoxazole.

The samples of electrospun nanofibers (SBE_7-β-CD-IC NF and sulfisoxazole/SBE_7-β-CD-IC NF) were investigated morphologically by scanning electron microscopy (SEM, FEI-Quanta 200 FEG). Nanofibers were sputtered with 5 nm Au/Pd layer to minimize charging by PECS-682. Average fiber diameter (AFD) for both nanofibrous web was calculated from SEM images of 100 fibers.

The proton nuclear magnetic resonance (^{1}H-NMR, Bruker D PX-400) system was used to determine molar ratio between sulfisoxazole and SBE_7-β-CD. In addition, SBE_7-β-CD powder was also analyzed by ^{1}H-NMR to see if there is any change due to degradation in chemical structure of SBE_7-β-CD after electrospinning process. 30 g L^{-1} concentration of pure sulfisoxazole, SBE_7-β-CD powder, SBE_7-β-CD NF, sulfisoxazole/SBE_7-β-CD-IC NF and sulfisoxazole/SBE_7-β-CD-IC powder was dissolved in d6-DMSO separately for the preparation of solution for ^{1}H NMR measurements.

Thermogravimetric analysis (TGA, TA Q500, USA) was carried out to determine the thermal properties of sulfisoxazole, SBE_7-β-CD NF and sulfisoxazole/SBE_7-β-CD-IC NF. These studies of the samples were performed from 25 to 600 °C with a heating rate of 20 °C/min under nitrogen gas flow.

Differential scanning calorimetry (DSC, TA Q2000, USA) was used to analyze inclusion complex formation between sulfisoxazole and SBE_7-β-CD. DSC measurement was performed for sulfisoxazole, SBE_7-β-CD NF, sulfisoxazole/SBE_7-β-CD-IC NF and sulfisoxazole/SBE_7-β-CD-IC powder under

N_2. Samples were equilibrated at 50 ºC and heated to 220 ºC with a rate of 10 ºC /min.

X-ray diffraction (XRD) (PANalytical X'Pert powder diffractometer) measurements of pure sulfisoxazole, SBE_7-β-CD NF, sulfisoxazole/SBE_7-β-CD-IC NF and sulfisoxazole/SBE_7-β-CD-IC powder were recorded by applying Cu Kα radiation in a range of 2θ = 5-30° to determine the crystalline structure of the samples.

Fourier transform infrared spectrometry (FTIR, Bruker-VERTEX70) was used to obtain the infrared spectra of the samples. The samples were mixed with potassium bromide (KBr) and pressed as pellets. 64 scans were recorded between 4000 and 400 cm^{-1} at a resolution of 4 cm^{-1}.

The water solubility of sulfisoxazole is quite limited [156]. Here, excess amount of sulfisoxazole (1.3 mg mL^{-1}), and sulfisoxazole/SBE_7-β-CD-IC NF and sulfisoxazole/SBE_7-β-CD-IC powder having the same amount of sulfisoxazole were added to the water and stirred overnight. To make comparison, the solution of sulfisoxazole with concentration of its water solubility (about 0.2 mg mL^{-1}) was also prepared and stirred overnight. After that, all samples were filtered through a 0.45 μm membrane filter to remove undissolved sulfisoxazole. Then, absorbance versus wavelength plots of four samples was obtained from UV-Vis spectroscopy (Varian, Cary 100). In addition, to show the fast-dissolving character and water-solubility enhancement of the drug visually, the water is directly added to solid sulfisoxazole, and sulfisoxazole/SBE_7-β-CD-IC NF and sulfisoxazole/SBE_7-β-CD-IC powder samples. The videos and pictures have been taken in which,

sulfisoxazole powder and the sulfisoxazole/SBE_7-β-CD-IC NF were placed into petri dishes separately and then, 5 mL of water was added to petri dishes. Then, to make comparison, powdered sulfisoxazole/SBE_7-β-CD-IC powder was also placed into petri dish and then, 5 mL of water was added.

3.1.3 Results and discussion

3.1.3.1 Phase solubility studies

Phase solubility diagram plotted by sulfisoxazole concentration versus SBE_7-β-CD concentration was given in Figure 46 which corresponds that with increase in SBE_7-β-CD concentration, sulfisoxazole concentration also increases. The complex showed linear trend (A_L-type) demonstrating 1:1 complex formation tendency of sulfisoxazole and SBE_7-β-CD molecules. The stability constant (K_s) was calculated as 880 M^{-1} from the diagram and this value indicates better stability when compared to the previously done study on HPβCD by Gladys et al. (2003) [156].

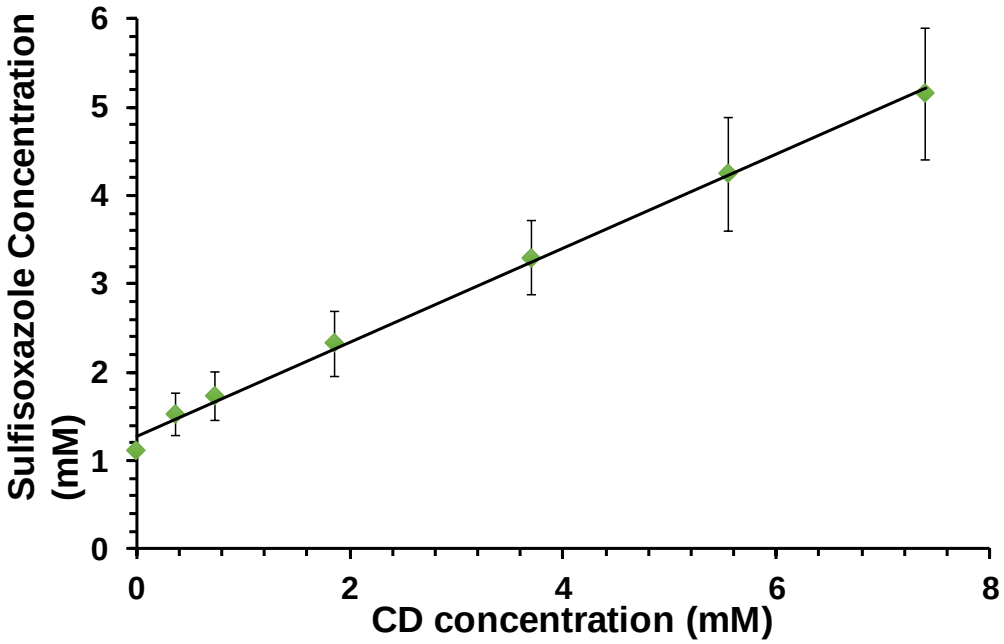

Figure 46. Phase solubility diagram of sulfisoxazole/ SBE$_7$-β-CD systems in water (n=3).

3.1.3.2 Morphological analyses

Since the phase solubility studies indicated 1:1 (sulfisoxazole:SBE$_7$-β-CD) complex formation tendency between sulfisoxazole and SBE$_7$-β-CD, first, we prepared 1:1 molar ratio inclusion complex between sulfisoxazole and SBE$_7$-β-CD by using highly concentrated SBE$_7$-β-CD (200% (w/v)) aqueous solution for the complexation. However, the electrospinning of uniform nanofibers from 1:1 molar ratio of sulfisoxazole/SBE$_7$-β-CD-IC system was not successful under the applied electrospinning conditions/parameters. Hence, we optimized the CD-IC solutions and found out that sulfisoxazole/SBE$_7$-β-CD-IC solution having 1:2 (sulfisoxazole:SBE$_7$-β-CD) molar ratio was more favorable for the electrospinning of uniform nanofibers. As a control sample, pristine SBE$_7$-β-CD NF was also

electrospun and we obtained bead-free and uniform nanofiber morphology for the free-standing nanofibrous web of SBE_7-β-CD. The optimized parameters for the electrospinning of the bead-free nanofibers from pristine SBE_7-β-CD and sulfisoxazole/SBE_7-β-CD-IC systems were given in detail in experimental section. The photos of free-standing and flexible electrospun nanofibrous samples were given in Figure 47a-b for pristine SBE_7-β-CD NF and sulfisoxazole/SBE_7-β-CD-IC NF. The representative SEM images of these SBE_7-β-CD NF and sulfisoxazole/SBE_7-β-CD-IC NF samples were given in Figure 47c-d, respectively. From the SEM images, the average fiber diameter (AFD) for sulfisoxazole/SBE_7-β-CD-IC NF and pristine SBE_7-β-CD NF was calculated as 650±290 nm and 890±415 nm, respectively.

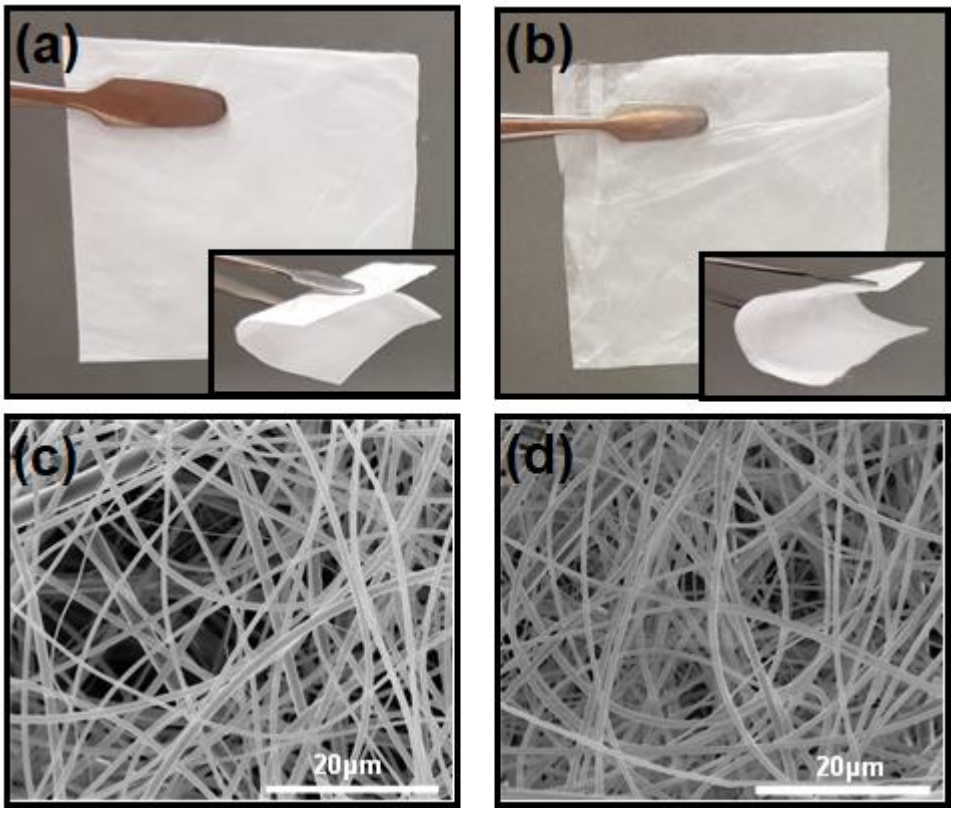

Figure 47. Photographs of electrospun (a) SBE_7-β-CD NF, (b) sulfisoxazole/SBE_7-β-CD-IC NF, and SEM images of (c) SBE_7-β-CD NF, (d) sulfisoxazole/SBE_7-β-CD-IC NF.

3.1.3.3 The molar ratio of sulfisoxazole in sulfisoxazole/CD-IC NFs

^{1}H-NMR spectroscopy is used to obtain molar ratio of sulfisoxazole to SBE_7-β-CD in the sulfisoxazole/SBE_7-β-CD-IC NF matrix. The ^{1}H-NMR spectra of sulfisoxazole, SBE_7-β-CD powder, SBE_7-β-CD NF, sulfisoxazole/SBE_7-β-CD-IC NF and sulfisoxazole/SBE_7-β-CD-IC powder were evaluated (Fig. 48a-d). Protons of SBE_7-β-CD NF and as-received powder SBE_7-β-CD were appeared in the range of δ 1.5-5.8 ppm which is correlated with previous literature [157, 158]. As shown in Figure 48b, the ^{1}H NMR spectra of SBE_7-β-CD powder and SBE_7-β-CD NF present the same characteristic shifts which indicated that the electrospinning

process did not cause any chemical degradation to the structure of SBE7-β-CD. The molar ratio was calculated from integration of peak ratio between peak of sulfisoxazole at around 7.35 (H-a) and SBE7-β-CD peak at around 5.00 ppm (H-1) as 0.28:1.00 for both sulfisoxazole/SBE7-β-CD-IC NF and sulfisoxazole/SBE7-β-CD-IC powder (Fig. 48c-d). This suggests that more than 50 % (w/w) of initial sulfisoxazole amount was preserved for both nanofibrous web and powder form.

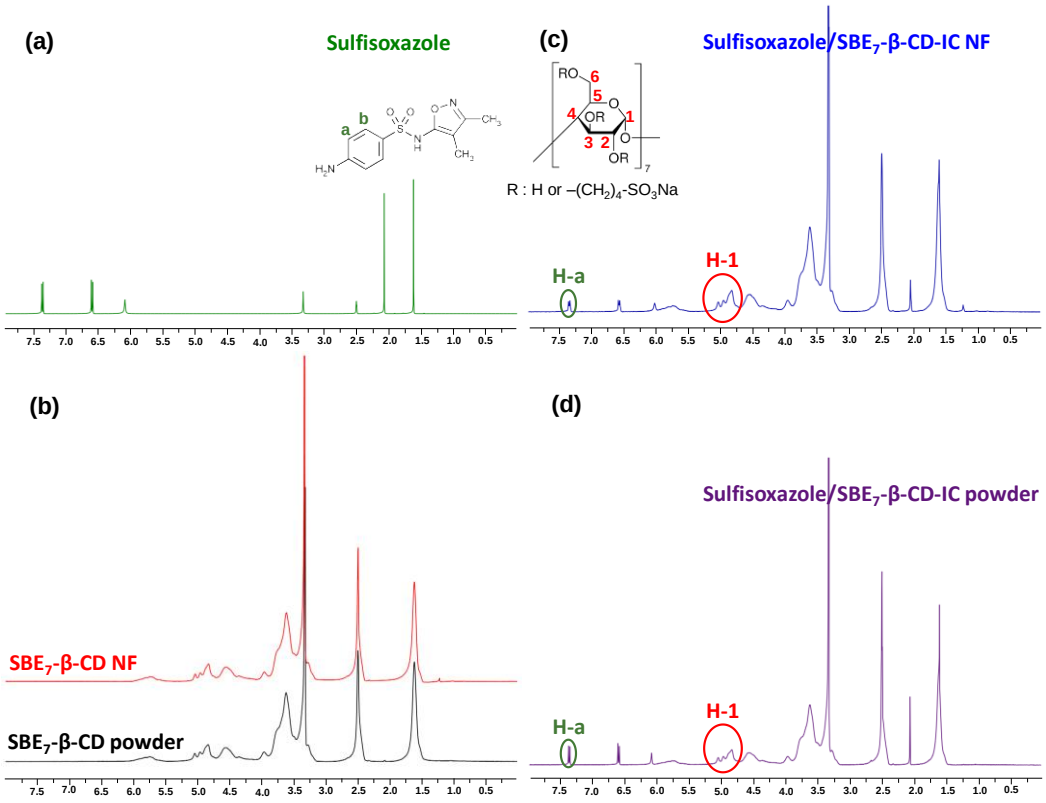

Figure 48. ^{1}H NMR spectra of (a) sulfisoxazole powder, (b) SBE7-β-CD NF and SBE7-β-CD powder, (c) sulfisoxazole/SBE7-β-CD-IC NF, (d) sulfisoxazole/SBE7-β-CD-IC powder.

3.1.3.4. Thermal characterization

The thermal decomposition of sulfisoxazole, SBE7-β-CD NF and sulfisoxazole/SBE7-β-CD-IC NF were investigated by thermal gravimetric analysis

(TGA) (Figure 49). The weight losses below 100 °C belong to the water loss for all samples. Pure sulfisoxazole decomposition occured between 190- 400 ºC while SBE7-β-CD NF exhibited main degredation between 250 and 500 ºC. Along with this, thermal decomposition of sulfisoxazole/SBE7-β-CD-IC NF started at 220 ºC and continued up to 500 ºC. There are two differences between SBE7-β-CD NF and sulfisoxazole/SBE7-β-CD-IC NF degradation. First one is the small step starting at 220 ºC which possibly belong to the sulfisoxazole. The shifting of thermal decomposition onset of sulfisoxazole from 190 ºC to 220 ºC showed the IC formation between sulfisoxazole and SBE7-β-CD. The second difference is the intensity of peak at 300 ºC which also proves the formation of inclusion complexes.

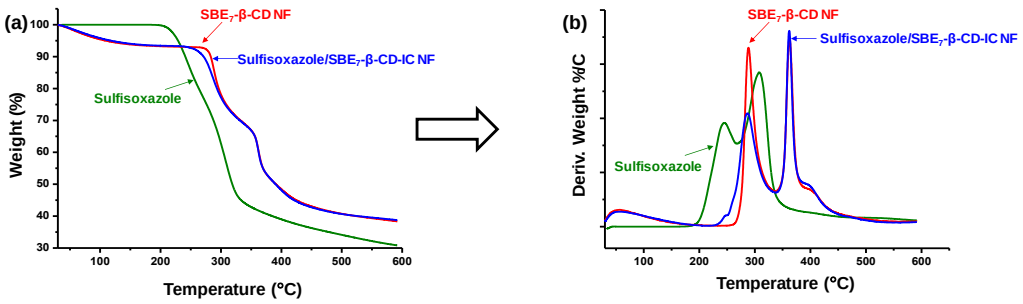

Figure 49. (a) TGA thermograms and (b) their derivatives of sulfisoxazole, SBE7-β-CD NF and sulfisoxazole/SBE7-β-CD-IC NF.

DSC is one of the widely used techniques to evaluate IC formation between CD and guest molecule in such a way that the melting point of guest molecules is not observed if guest molecules fully complexed within CD cavities [159]. The DSC scans of pure sulfisoxazole, SBE7-β-CD NF, sulfisoxazole/SBE7-β-CD-IC NF and sulfisoxazole/SBE7-β-CD-IC powder were given in Figure 50. The pure sulfisoxazole DSC scan exhibited a melting point at 197 ºC, whereas no melting

point was observed for sulfisoxazole for the samples of sulfisoxazole/SBE7-β-CD-IC NF and sulfisoxazole/SBE7-β-CD-IC powder.The DSC results further confirm that the sulfisoxazole molecules are fully complexed with SBE7-β-CD in the samples of sulfisoxazole/SBE7-β-CD-IC NF and sulfisoxazole/SBE7-β-CD-IC powder.

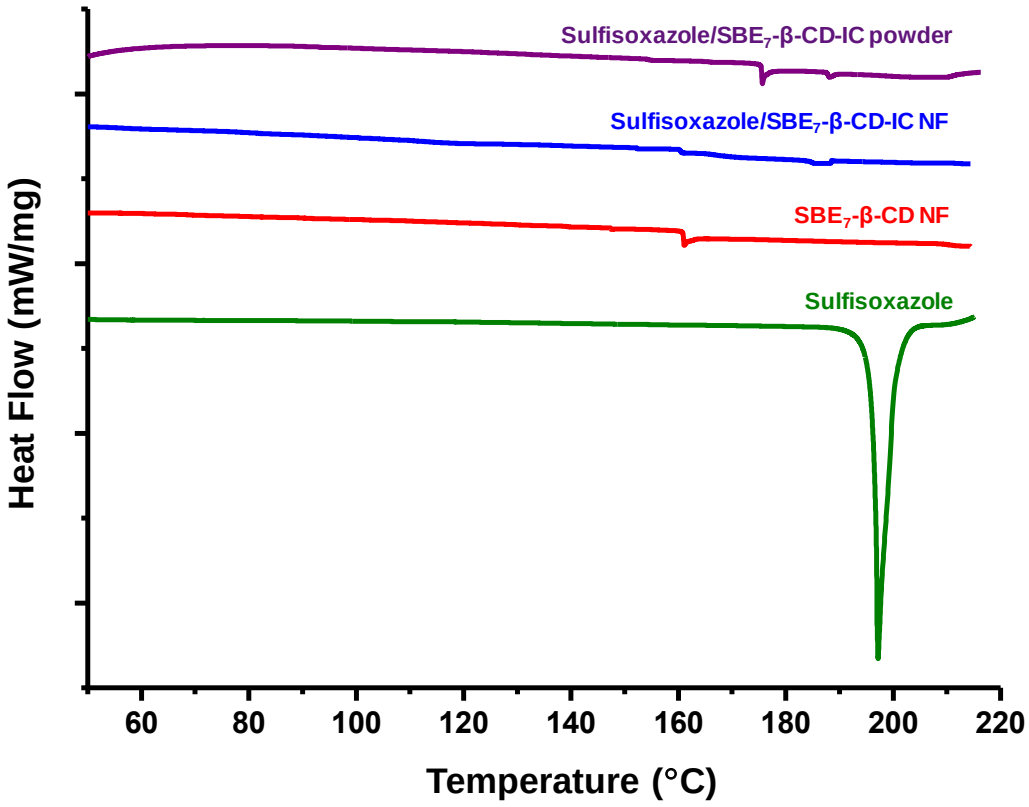

Figure 50. DSC thermogram of sulfisoxazole, SBE7-β-CD NF, sulfisoxazole/SBE7-β-CD-IC NF and sulfisoxazole/SBE7-β-CD-IC powder.

3.1.3.5 Structural caharcterization

The structural characterization of SBE7-β-CD NF, sulfisoxazole/SBE7-β-CD-IC NF and sulfisoxazole/SBE7-β-CD-IC powder samples was done by using the different methods. The crystalline structures of pure sulfisoxazole, SBE7-β-CD NF,

sulfisoxazole/SBE$_7$-β-CD-IC NF and sulfisoxazole/SBE$_7$-β-CD-IC powder were investigated by XRD to show the evidence of IC formation between sulfisoxazole and SBE$_7$-β-CD. Sulfisoxazole is a crystalline material having a sharp diffraction peaks at different 2θ values; however, the XRD pattern of SBE$_7$-β-CD NF, sulfisoxazole/SBE$_7$-β-CD-IC NF and sulfisoxazole/SBE$_7$-β-CD-IC powder are very similar which have amorphous structures. The IC nanofiber and IC powder do not show any diffraction peaks of sulfisoxazole (Figure 51). In other words, XRD results revealed the IC formation between sulfisoxazole and SBE$_7$-β-CD in the samples of sulfisoxazole/SBE$_7$-β-CD-IC NF and sulfisoxazole/SBE$_7$-β-CD-IC powder. The XRD result suggests that sulfisoxazole molecules are isolated from each other by entering into SBE$_7$-β-CD cavities and cannot form any crystalline aggregates. Since drugs in crystalline forms are more stable, their solubility decreases [153]; however, CD-IC formation prevent crystallization of drugs. Therefore, the solubility of sulfisoxazole increases by SBE$_7$-β-CD-IC formation since the crystallization of sulfisoxazole was prevented as confirmed by the XRD pattern.

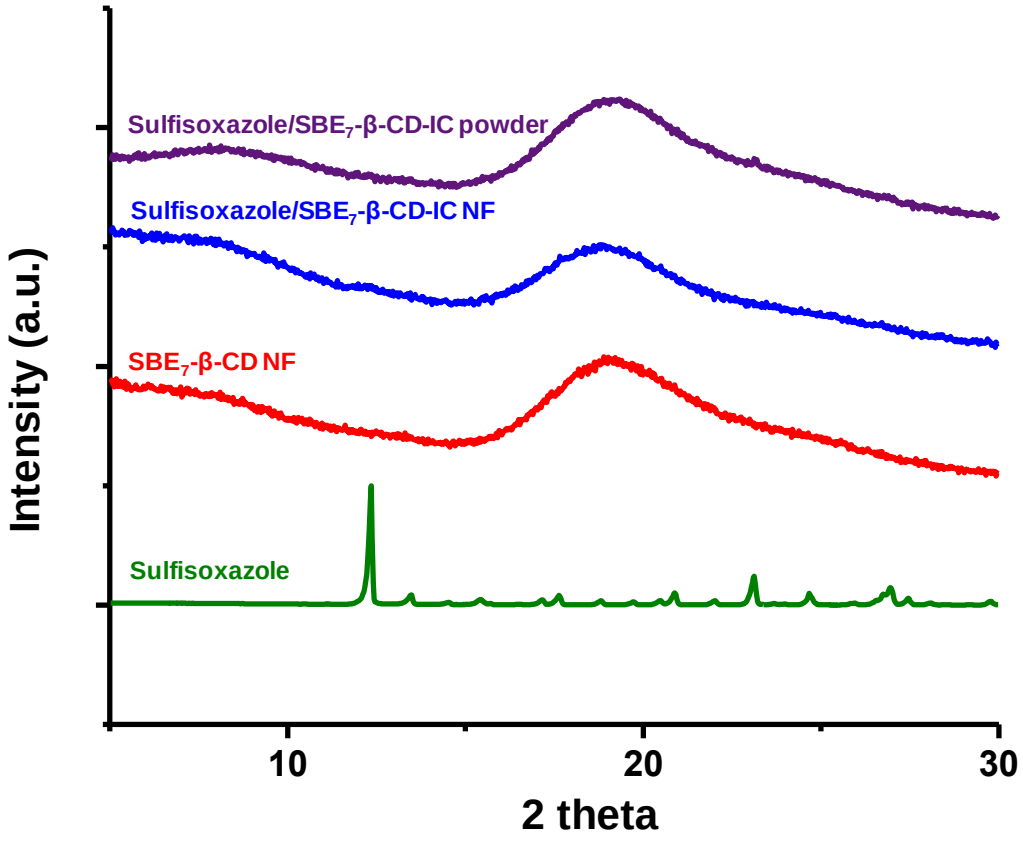

Figure 51. XRD patterns of sulfisoxazole, SBE7-β-CD NF sulfisoxazole/SBE7-β-CD-IC NF and sulfisoxazole/SBE7-β-CD-IC powder.

The presence of guest molecule in structure and the formation of inclusion complexes between host and guest molecule can be proved by FTIR analysis. The FTIR spectra of pure sulfisoxazole, SBE_7-β-CD NF and sulfisoxazole/SBE_7-β-CD-IC NF are represented in Figure 52. The FTIR spectrum of sulfisoxazole displayed salient peaks at 876–688 cm^{-1} range (C-H bending), at 1347 cm^{-1}, (SO_2 stretching); at 1326 cm^{-1} (aromatic ring stretching); at 1597 cm^{-1} (C=C stretching); at 1632 cm^{-1} (NH_2 deformation vibrations). The FTIR spectrum of SBE_7-β-CD showed a broad peak at between 3015-3760 cm^{-1} (O-H stretching vibration); a peak at 2931 cm^{-1} (C-H stretching vibrations); peaks at 1159 cm^{-1} and 1043 cm^{-1} (C-H

and C-O stretching vibrations). Sulfisoxazole peaks were overlapped by CD peaks which makes the identification of each compounds complicated at the spectra of inclusion complex nanofibers. However, the sharpest absorption peak of sulfisoxazole at about 1597 cm^{-1} corresponding to C-H stretching vibration causes increase in intensity at that wavelength of inclusion complex nanofiber. This result suggested that sulfisoxazole is present in inclusion complex nanofibers.

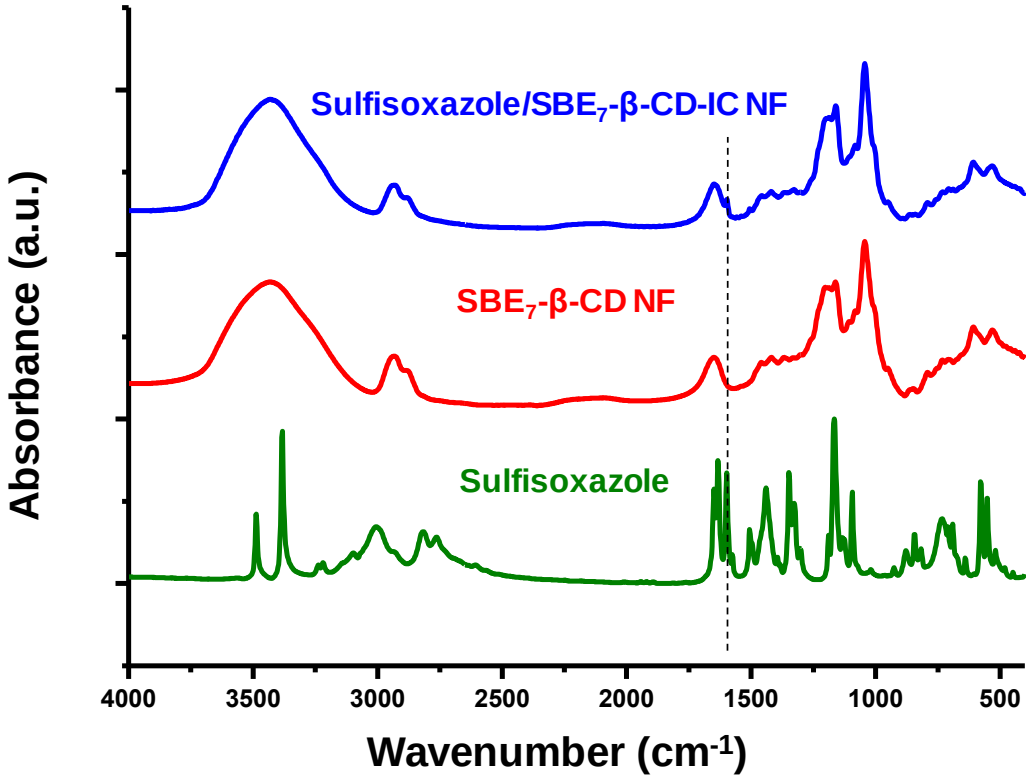

Figure 52. FTIR spectra of sulfisoxazole, SBE7-β-CD NF and sulfisoxazole/SBE7-β-CD-IC NF.

3.1.3.4 Dissolution behaviour

As mentioned experimental section, excess amount of sulfisoxazole (1.3 mg mL^{-1}) and sulfisoxazole/SBE_7-β-CD-IC NF and sulfisoxazole/SBE_7-β-CD-IC powder having the same amount of sulfisoxazole were added to water. In order to make

comparison, the solution of sulfisoxazole with concentration of its water solubility (about 0.2 mg mL^{-1}) was also prepared to see water-solubility enhancement. The plot (Figure 53) shows that the solutions of sulfisoxazole with 0.2 mg mL^{-1} concentration and of sulfisoxazole with 1.3 mg mL^{-1} demonstrated peak at almost the same absorbance. On the other hand, sulfisoxazole/SBE_7-β-CD-IC NF sample solution having 1.3 mg mL^{-1} of sulfisoxazole concentration showed peak at 10 times higher absorbance. This shows that the solubility of sulfisoxazole was increased by 10 times with sulfisoxazole/SBE_7-β-CD-IC NF formation. As seen from Figure 53, sulfisoxazole/SBE_7-β-CD-IC powder also enhances water solubility of sulfisoxazole due to formation of CD-IC, however sulfisoxazole/SBE_7-β-CD-IC NF shows higher absorbance than sulfisoxazole/SBE_7-β-CD-IC powder. The high surface area to volume ratio, high porosity of nanofibers structure contribute to the enhancement of water solubility of the drug [160]; therefore, the water solubility enhancement in sulfisoxazole/SBE_7-β-CD-IC NF become higher compared to sulfisoxazole/SBE_7-β-CD-IC powder. The fast-dissolving property and water-solubility enhancement of the sulfisoxazole in sulfisoxazole/SBE_7-β-CD-IC NF and sulfisoxazole/SBE_7-β-CD-IC powder were also visually proven (Figure 54). After addition of 5 mL water to the petri dishes, while sulfisoxazole/SBE_7-β-CD-IC NF was dissolved immediately, the dissolution of sulfisoxazole/SBE_7-β-CD-IC powder took place a little bit slower than sulfisoxazole/SBE_7-β-CD-IC NF sample and pure sulfisoxazole remain undissolved. This clearly showed the fast-dissolving property of sulfisoxazole/SBE_7-β-CD-IC NF along with highly-increased water-solubility of sulfisoxazole by sulfisoxazole/SBE_7-β-CD-IC NF formation.

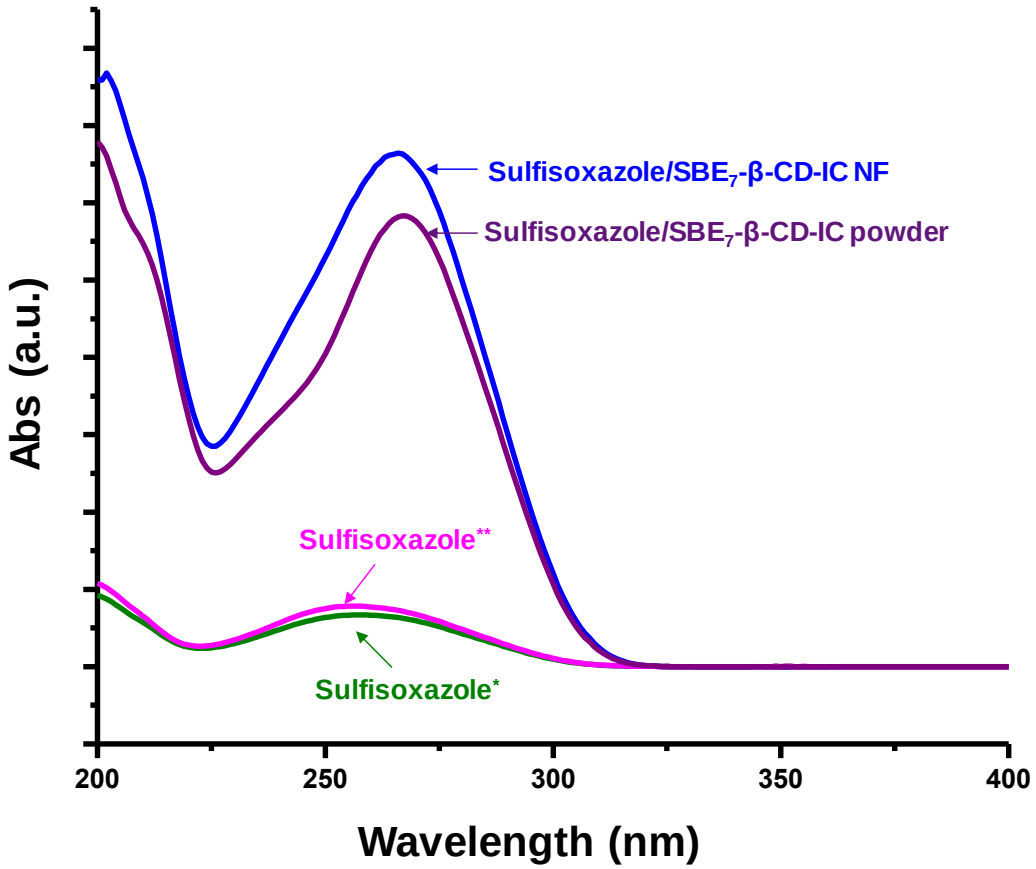

Figure 53. Water solubility diagram of *sulfisoxazole with concentration of its water solubility (green), **excess amount of sulfisoxazole (pink), sulfisoxazole/SBE7-β-CD-IC NF having the same excess amount of sulfisoxazole (blue), sulfisoxazole/SBE7-β-CD-IC powder having the same excess amount of sulfisoxazole (purple).

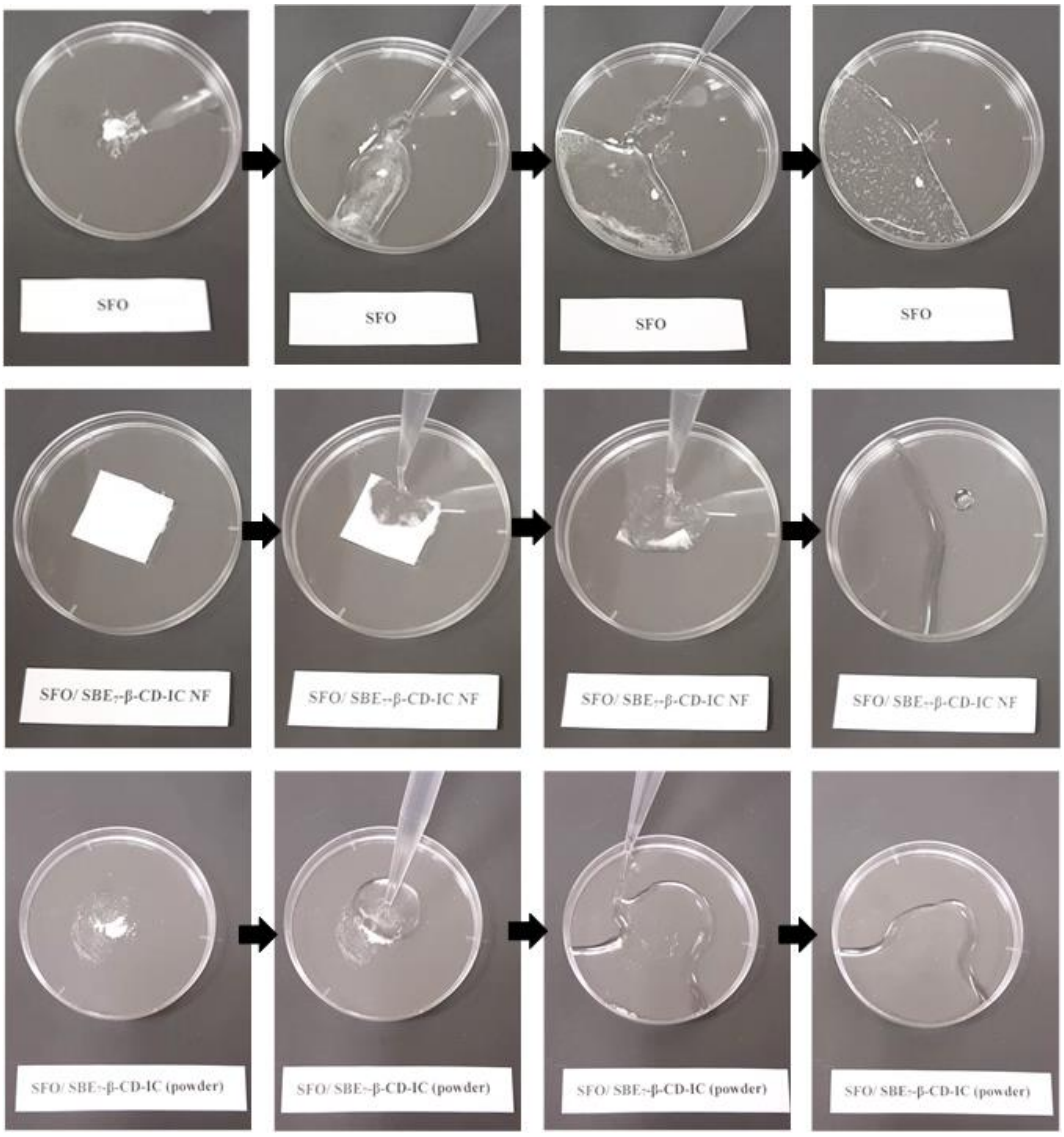

Figure 54. Presentation of the solubility behaviour of sulfisoxazole (represented by "SFO"), sulfisoxazole/SBE7-β-CD-IC NF and sulfisoxazole/SBE7-β-CD-IC powder for a few seconds of water exposure.

3.1.4 Conclusions

In this study, free-standing and easily handled nanofibrous web of sulfisoxazole/SBE$_7$-β-CD-IC was successfully produced by using electrospinning technique. The electrospun sulfisoxazole/SBE$_7$-β-CD-IC nanofibrous web has

shown the fast-dissolving property as well as the providing enhanced water-solubility to sulfisoxazole. Based on our results, it is concluded that SBE_7-β-CD is a good candidate to form ICs with sulfisoxazole to increase its water-solubility to a great extent. Moreover, electrospinning of nanofibers from sulfisoxazole/SBE_7-β-CD-IC system having high surface area to volume ratio and nano-scale porosity provides fast-dissolving property. In brief, electrospinning of nanofibers/nanowebs from drug/CD-ICs systems may provide novel approaches for enhanced water-solubility and fast-dissolving tablet formulations for drug delivery systems.

3.2 Fast-dissolving electrospun nanofibrous films of paracetamol/cyclodextrin inclusion complexes

This part of thesis was reprinted (adapted) by permission from Elsevier [161], ("Fast-dissolving electrospun nanofibrous films of paracetamol/cyclodextrin inclusion complexes", Z. I. Yildiz, and T. Uyar, *Applied Surface Science*, 492, 626-33, 2019), Copyright (2019) Elsevier.

3.2.1 Introduction

Paracetamol (N-acetyl-para-aminophenol, also known as acetaminophen, Figure 55a) is an antipyretic and analgesic agent which is used to relieve pain in the body and to reduce body temperature [162]. Although it has no significant anti-inflammatory activity compared to aspirin or ibuprofen, it is widely used since it is generally safe at recommended doses even for children and pregnant women [163]. There are studies in literature focusing on CD-ICs of paracetamol due to effects of CD-ICs on solubility, dissolution rate, absorption and chemical stability of drugs

[163, 164]. In one of those studies, it was shown that paracetamol can form stable ICs with native CDs; α-CD, β-CD and γ-CD [164]. In another study, ICs of paracetamol with β-CD, hydroxypropyl-β-CD (HPβCD) and methylated-β-CD (MβCD) were prepared in 1:1 molar ratio and the higher complexation stability with the two modified CDs (HPβCD and MβCD) was observed when compared to native β-CD [163]. There are also studies in the literature related to encapsulation of paracetamol into hydrophilic polymeric electrospun nanofiber matrix to increase the water solubility and dissolution rate of paracetamol [162, 165-168]. In a related study, the electrospun nanofiber based solid dispersion of paracetamol was prepared by using polyvinylpyrrolidone (PVP) as a hydrophilic fiber matrix and compared with conventional processes and the study showed that electrospun nanofibrous system has shown a better performance than conventional processes in terms of improving dissolution rate of paracetamol [165]. In another study, PVP nanofibers loaded with paracetamol and caffeine were fabricated by electrospinning and such hydrophilic nanofibrous matrix encapsulating paracetamol and caffeine has exhibited fast-dissolving character. However, in this system a flavoring agent was added to system in order to mask bitterness of drugs [162]. The literature shows that encapsulation of paracetamol by formation of CD-ICs and by electrospun nanofibers provide advantages on bioavailability of paracetamol especially in terms of its dissolution rate. However, in the literature, there is no example of electrospun nanofibers including CD-IC and the possible effects of this combination on bioavailability of paracetamol. Based on the literature and our previous experience, it is expected that formation of paracetamol/CD-IC nanofibers by using two

modified CDs provides enhanced properties for paracetamol especially for its dissolving character in water.

In this study, nanofibers (NFs) from CD-IC of paracetamol (paracetamol/CD-IC NFs) were produced via electrospinning. Here, paracetamol was separately complexed with two different modified CDs; HPβCD and sulfobutylether-β-CD (SBE-β-CD), and then paracetamol/CD-IC aqueous systems were electrospun into nanofibers without using additional polymeric matrix. The polymer-free electrospun paracetamol/CD-IC NFs were obtained as a free-standing webs having fast-dissolving character in water.

3.2.2 Experimental

3.2.2.1 Materials

Paracetamol (99%) was obtained from Sigma-Aldrich commercially. Sulfobutylether-beta-cyclodextrin (SBE-β-CD, Captisol®) was kindly donated by Cydex Pharmaceuticals Inc. (Kansas, USA) and hydroxypropyl-beta-cyclodextrin (HPβCD) (Cavasol W7 HP Pharma) was donated by Wacker Chemie (Germany). Potassium bromide (KBr, 99%, FTIR grade, Sigma-Aldrich), deuterated dimethylsulfoxide (d6-DMSO, deuteration degree min. 99.8% for NMR spectroscopy, Merck) were used as received. The water used was from a Millipore Milli-Q ultrapure water system.

3.2.2.2 Preparation of electrospinning solutions

Paracetamol was dispersed in 0.5 mL of water and then HPβCD ((200%, w/v) and SBE-β-CD (240%, w/v) was added to get 1:1 (paracetamol:CDs) molar ratio, respectively (Figure 55a). The solutions were stirred at room temperature for 24h.

For comparative studies, solutions for pure CDs were also prepared in water with concentration of 200%, w/v for HPβCD and 240%, w/v for SBE-β-CD.

3.2.2.3 Electrospinning of nanofibers

The solutions of pure CDs and paracetamol/CD-ICs were separately loaded in 1 mL syringe having metallic needle of 0.4 mm inner diameter. These solutions were pumped through a syringe pump (KD Scientific, KDS-101, USA) at 0.5-1.0 mL/h rate. Grounded metal covered with aluminum foil, a collector, was placed 15-20 cm from the tip of needle. High voltage at 15-20 kV was applied between tip of needle and collector by high voltage power supply (Spellman, SL Series) (Figure 55b).

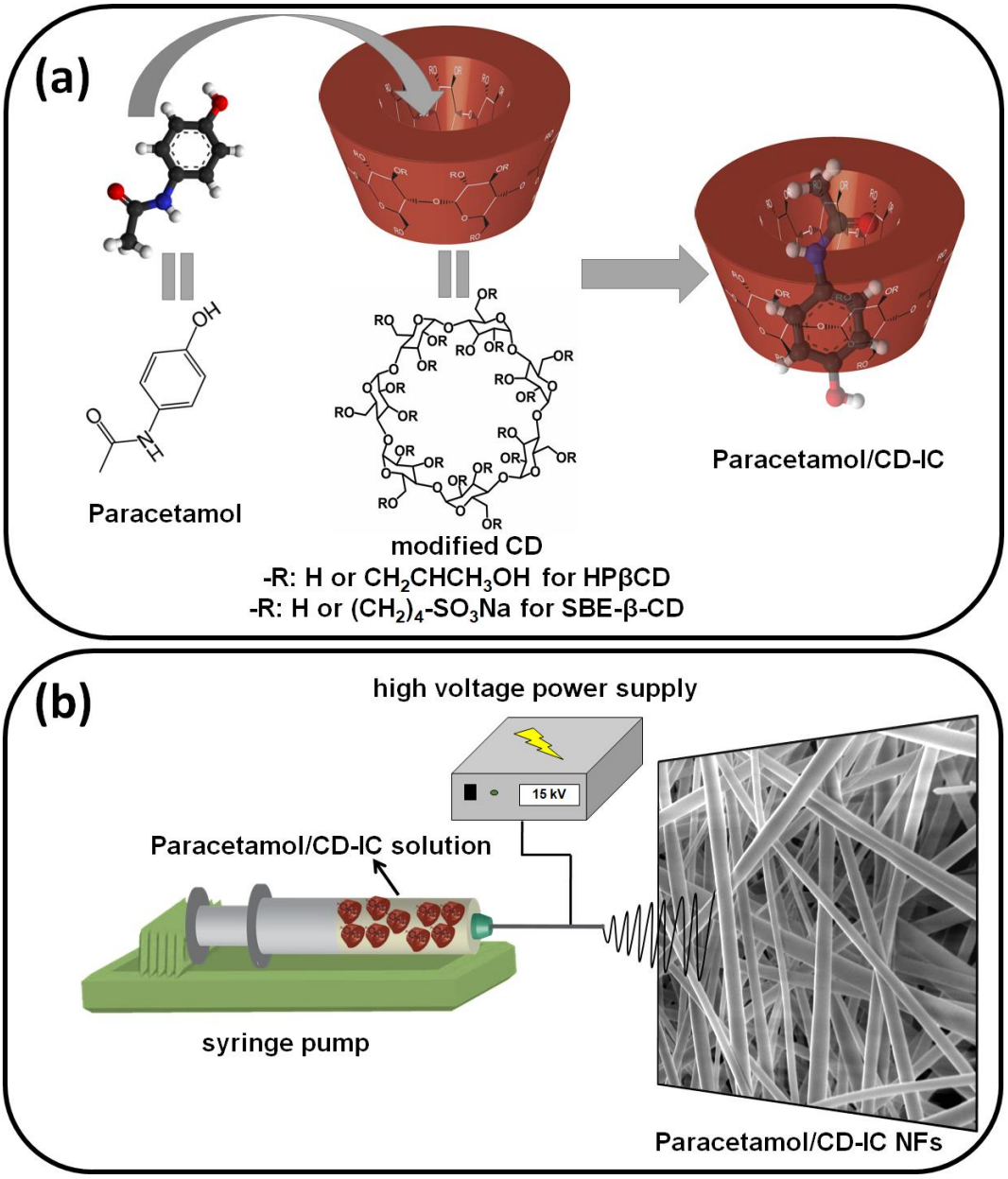

Figure 55. The schematic representation and chemical structure of (a) Paracetamol, CDs and paracetamol/CD-ICs; (b) electrospinning of paracetamol/CD-IC solution.

3.2.2.3 Measurements and characterizations

The viscosity of paracetamol/CD-IC solutions were measured by rheometer equipped with a cone/plate accessory (CP 20−4 spindle type, Anton Paar Physica

MCR 301) under constant shear rate of 100 s^{-1} at RT. The Inolab pH/Cond 720-WTW was used to determine the conductivity of solutions at RT.

Scanning electron microscopy (SEM; Quanta 200 FEG; FEI) was used to perform morphological characterization of electrospun paracetamol/HPβCD-IC NFs and paracetamol/SBE-β-CD-IC NFs. Au/Pd was sputtered on the nanofibers before SEM imaging to eliminate charging problems. Average fiber diameter (AFD) of nanofibrous films were calculated directly from SEM images by measuring the diameter of about 100 fibers.

The molar ratio between paracetamol and CDs was determined by using proton nuclear magnetic resonance (^{1}H NMR; DPX-400, Bruker) spectra at 400 MHz and 25 °C by dissolving about 20 g/L sample in d6-DMSO.

Fourier transform infrared spectrometry (FTIR, Bruker-VER-TEX70) was used to obtain the infrared spectra of paracetamol, pure CD NFs and paracetamol/CD-IC NFs. The pellets of samples were prepared by mixing them with potassium bromide (KBr). The scans (64) were recorded between 4000 and 400 cm^{-1} at a resolution of 4 cm^{-1}.

The crystalline structure of paracetamol, pure CD NFs and paracetamol/CD-IC NFs was recorded by X-ray diffractometry (XRD; X'Pert powder diffractometer; PANalytical) applying Cu Kα radiation in a 2θ range 5–30°.

Differential scanning calorimetry (DSC) (TA Q2000, USA) and thermogravimetric analysis (TGA) (TA Q500, USA) were used for the investigation of the thermal properties of the samples. DSC analyses were carried out under N_2; initially, samples were equilibrated at 25 °C and then heated to 200 °C at a heating rate of

20 °C /min. TGA measurements were performed from room temperature to 600 °C at a heating rate of 20 °C/min under N_2 atmosphere.

The dissolution behavior of paracetamol/CD-IC nanofibrous films during water exposure was analyzed with two different ways. In the first one, nanofibrous films with equal weight were placed into petri dishes and 5 mL of distilled water was added onto the nanofibrous films. In the second one, absorbent paper was placed into petri dishes and thoroughly wetted with distilled water (10 mL). The excess water was completely drained out and the nanofibrous films were placed on the wet paper.

3.2.3 Results and discussion

3.2.3.1 Morphological analyses

Electrospinning of paracetamol/CD-ICs was conducted under optimized parameters to obtain bead-free and uniform nanofibers. Besides optimization on electrospinning setup like voltage, distance between tip and collector, humidity and temperature, adjustment of solution concentration is quite essential for proper electrospinning process. In this study, high concentration of paracetamol/CD-ICs solutions was prepared for both CDs and bead-free and uniform nanofibers were obtained. The image of nanofibrous films with their representative SEM images were given in Figure 56. The nanofibers of paracetamol/CD-ICs are self-standing, easy to handle and flexible. The average fiber diameter (AFD) was calculated as 775 ± 285 nm for paracetamol/HPβCD-IC NFs and 610 ± 365 nm for paracetamol/SBE-β-CD-IC NFs (Table 10). Although the AFD value for both nanofibers was not very different from each other, the slight difference was possibly

due to the variation in viscosity of the CD-IC solutions (Table 10). The higher viscosity causes the formation of thicker nanofibers due to the greater resistance to stretching of solution [6]. Here, the viscosity of paracetamol/HPβCD-IC NFs is higher than paracetamol/SBE-β-CD-IC NFs, therefore, this system resulted in thicker fibers.

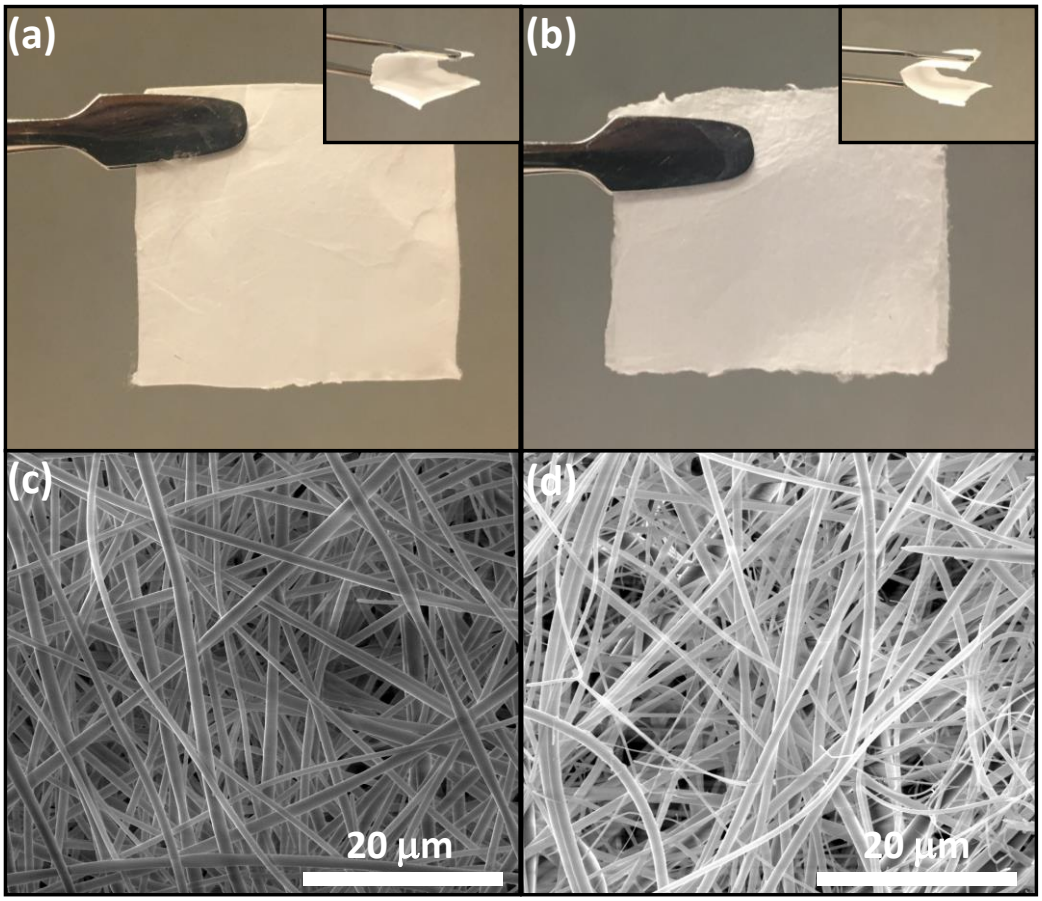

Figure 56. The photographs of (a) paracetamol/HPβCD-IC NFs and (b) paracetamol/SBE-β-CD-IC NFs; SEM images of electrospun (c) paracetamol/HPβCD-IC NFs and (d) paracetamol/SBE-β-CD-IC NFs.

Table 10. The properties of the solutions used for electrospinning and morphological characteristics of the resulting paracetamol/CD-IC NFs.

Solutions	Average fiber diameter (nm)	Fiber diameter range (nm)	Viscosity (Pa·s)	Conductivity ($\mu S\ cm^{-1}$)	Morphology
Paracetamol/HPβCD-IC	775±285	261-1426	2.37±0.23	7.57±0.41	Bead-free nanofibers
Paracetamol/SBE-β-CD-IC	610±365	125-1854	2.06±0.12	6.42±0.12	Bead-free nanofibers

3.2.3.2 The molar ratio of paracetamol in paracetamol/CD-ICs

Proton nuclear magnetic resonance (^{1}H NMR) was employed to find the molar ratio of paracetamol to CDs for paracetamol/HPβCD-IC and paracetamol/SBE-β-CD-IC NFs. The molar ratio was calculated by integrating peaks of paracetamol (at around 6.65 ppm), HPβCD (at 1 ppm) and SBE-β-CD (at around 5 ppm) (Figure 57). The molar ratio was calculated as ~0.85:1.00 (paracetamol:CD) for paracetamol/HPβCD-IC NFs and as ~0.80:1.00 (paracetamol:CD) for paracetamol/SBE-β-CD-IC NFs. When compared with initial molar ratio which is 1.00:1.00, it is concluded that the paracetamol was mostly preserved for both CD types with similar ratios in these electrospun nanofibrous films.

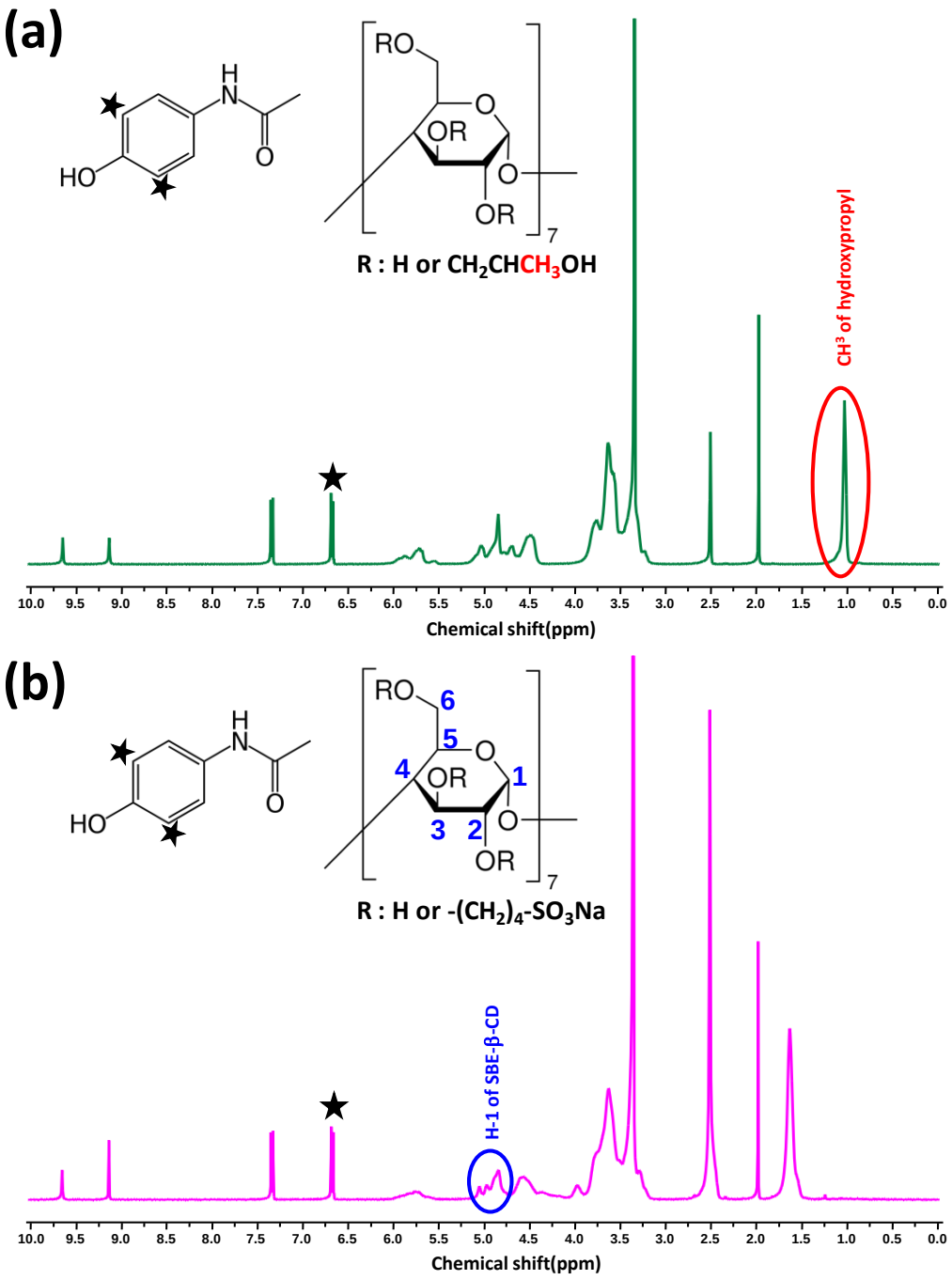

Figure 57. The ^{1}H-NMR spectra of (a) paracetamol/HPβCD-IC NFs and (b) paracetamol/SBE-β-CD-IC NFs which was dissolved in d6-DMSO.

3.2.3.3 Structural characterization

FTIR is widely used characterization technique to verify the formation of inclusion complexes between CD host and guest materials and to verify presence of both guest and host molecules in their inclusion complexes. The infrared spectra of paracetamol, pure CD NFs and paracetamol/CD-ICs NFs were obtained and presented in Figure 58. The IR spectrum of paracetamol is characterized by absorption bands at 3326 cm^{-1} (N-H amide stretching), 3160 cm^{-1} (free –OH stretching), 1655 cm^{-1} (C=O stretching), 1610 cm^{-1} (C=C stretching), 1565 cm^{-1} (N-H amide II bending), 1507 cm^{-1} (asymmetrical C-H bending), 1443 cm^{-1} (C-C stretching), 1368-1328 cm^{-1} (symmetrical C-H bending) and 1260-1227 cm^{-1} (C-N stretching) [169, 170]. Some peaks of paracetamol become invisible due to the extensive overlap of these bands with those of the cyclodextrins. However, there is decrease in intensity of peaks at 1565, 1507 and 1260 cm^{-1}. Besides, the absorption peaks at 1565 cm^{-1} shifted to 1554 cm^{-1} for paracetamol/HPβCD-IC and to 1558 cm^{-1} for paracetamol/SBE-β-CD-IC and at 1507 cm^{-1} shifted to 1514 cm^{-1} for both CD-ICs. These results suggested that there is an interaction between paracetamol and CDs, and paracetamol was included into the cavity of CDs.

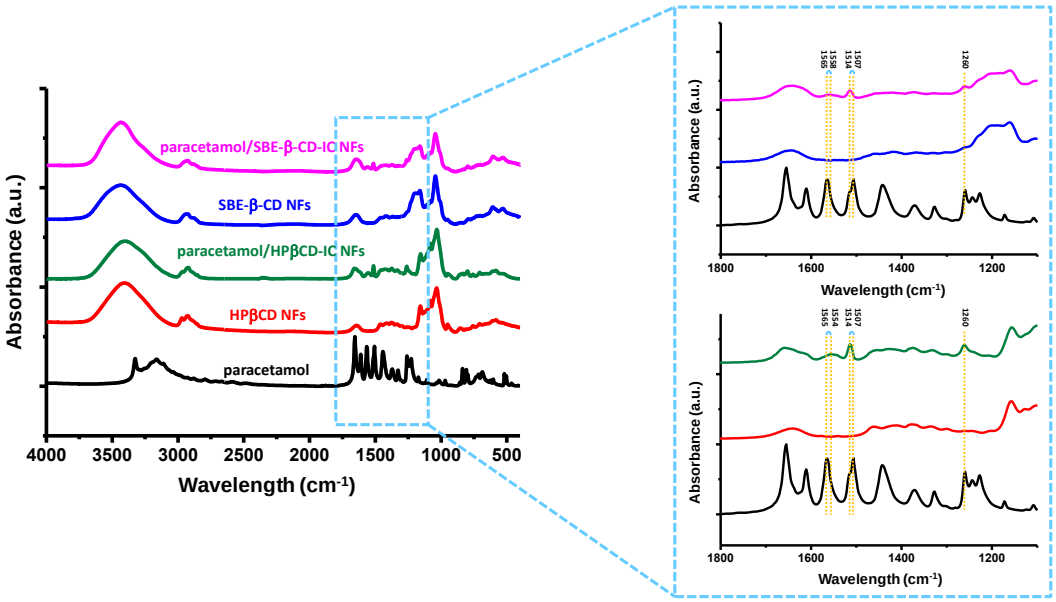

Figure 58. The FTIR spectra of paracetamol, pure CD NFs and paracetamol/CD-IC NFs.

The crystalline behavior of paracetamol, pure CD NFs and paracetamol/CD-ICs NFs was evaluated by XRD (Figure 59a). Paracetamol is a crystalline material showing sharp diffraction peaks appearing at 2θ 15.30°, 18.00°, 20.19°, 24.17° and 26.36° [165, 171]. In the literature, there is a study in which electrospun nanofibers including paracetamol has shown amorphous character due to spreading of paracetamol molecules through nanofibrous films and these films have shown highly rapid dissolution in water [162]. In another study, formation of CD-IC of paracetamol with a modified CD caused change in its crystalline structure into amorphous due to isolation of paracetamol molecules by CD-IC formation [163]. In this study, similar results with the literature has been obtained; the XRD pattern of pure CD NFs and paracetamol/CD-ICs NFs are similar and do not exhibit any crystalline peak confirming their amorphous state. This verifies that paracetamol molecules in the paracetamol/CD-ICs were isolated from each other by the CD

cavity so they cannot form crystalline aggregates. This change in crystalline structure of drug results in solubility increment since drugs in crystalline forms are more stable that decreases their solubility [153].

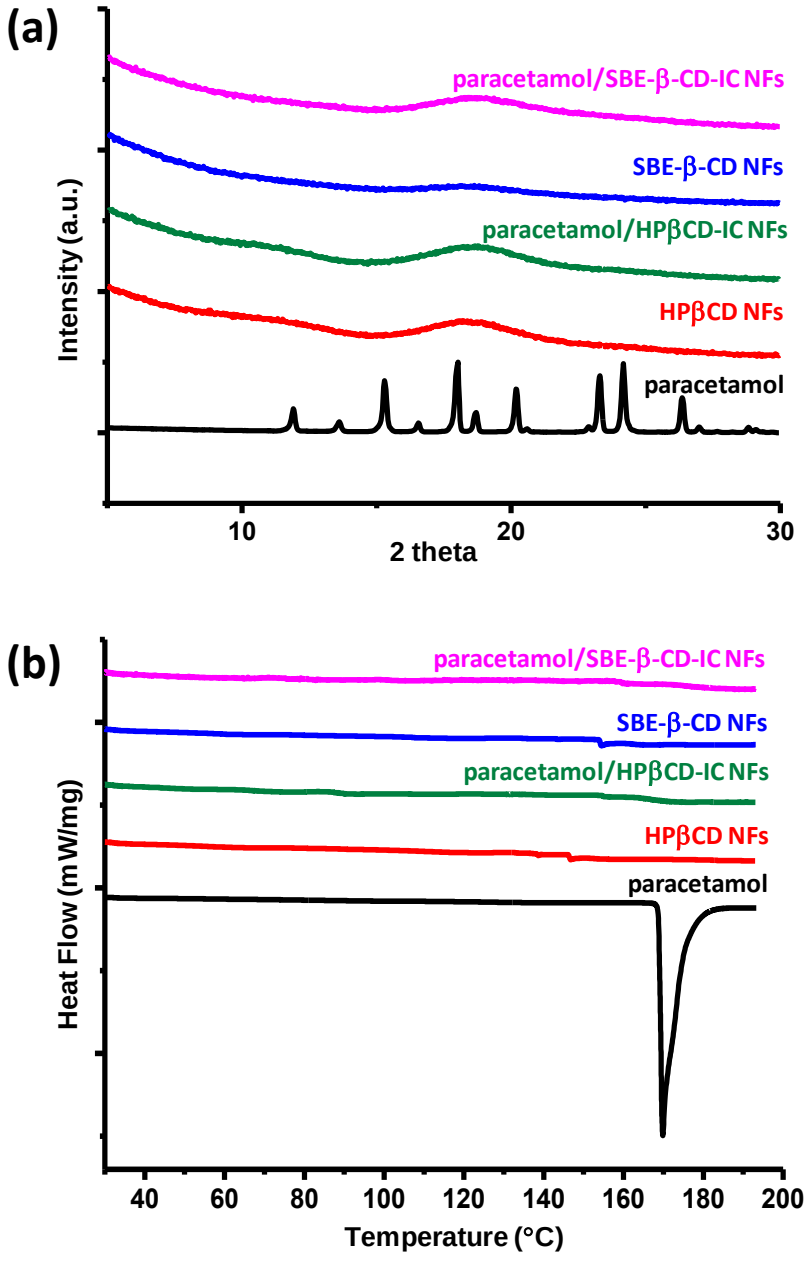

Figure 59.(a) The XRD patterns of paracetamol, pure CD NFs and paracetamol/CD-IC NFs and (b) the DSC thermogram of paracetamol, pure CD NFs and paracetamol/CD-IC NFs.

3.2.3.4 Thermal characterization

DSC technique is widely used to confirm the inclusion complexation between CD and guest molecules. When guest molecules form inclusion complexes with CDs, their melting, boiling or sublimation points disappear or shift to higher temperatures. Figure 59b shows the DSC thermogram of paracetamol, pure CD NFs and paracetamol/CD-ICs NFs. The DSC thermogram of paracetamol displayed a sharp endothermic peak at 169.8 °C, which corresponds to its melting point. For both pure CD NFs, there was no endothermic or exothermic peak observed. For the thermograms of paracetamol/CD-ICs NFs, the endothermic melting peak of paracetamol disappeared since paracetamol forms the molecular inclusion in the cavity of both CDs and become amorphous. These results confirm the formation of inclusion complexes and agree with the data of XRD.

Thermogravimetric analysis (TGA) was performed to identify the effects of inclusion complex formation on thermal decomposition of paracetamol (Figure 60). The CD samples and CD-IC samples has weight losses below 100 °C due to water loss. For pure HPβCD NFs, the degradation started at 290 °C while for the paracetamol/HPβCD-IC NFs, there is a step before 290 °C starting at 276 °C which belongs to paracetamol. For pure SBE-β-CD NFs, there is mainly two step weight lost and it started at 255 °C, while for paracetamol/SBE-β-CD-IC NFs, there is an extra step at 200 °C corresponding to paracetamol degradation. These results mean that the thermal decomposition of paracetamol which started at 172 °C shifted to higher temperature, ~275 °C for paracetamol/HPβCD-IC NFs and ~200 °C for paracetamol/SBE-β-CD-IC NFs due to inclusion complex formation with CDs.

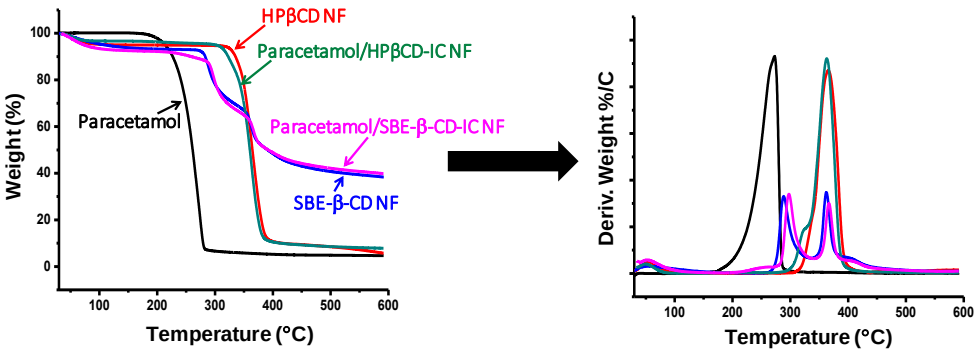

Figure 60. The TGA thermograms and derivatives of paracetamol, pure CD NFs and paracetamol/CD-IC NFs.

3.2.3.5 Dissolution behavior

Dissolution behavior of paracetamol/CD-IC NFs was examined with two different methods. In the first method, the distilled water was added to the nanofibers. In the other method, CD-IC NFs of paracetamol was exposed to distilled water soaked absorbent paper [140]. For both methods, it was seen that paracetamol/HPβCD-IC NFs and paracetamol/SBE-β-CD-IC NFs was dissolved instantly when they are in contact with water (Figure 61). This high rate is probably due to high surface area of nanofibrous structure and solubility increase mediated by CD-IC formation.

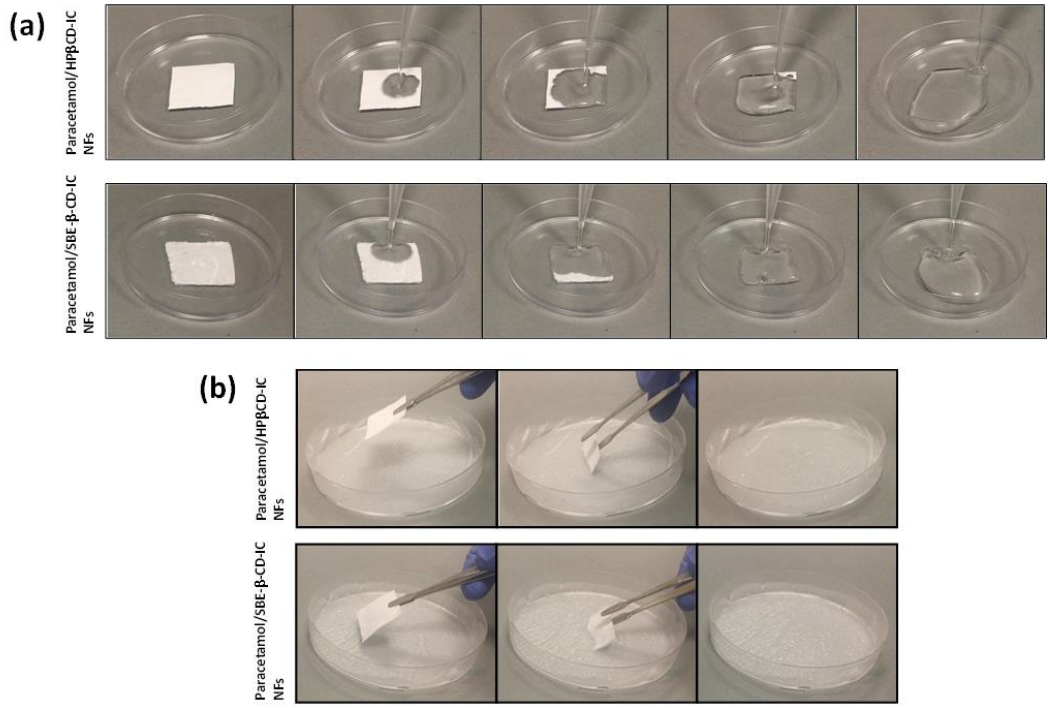

Figure 61. The dissolution behavior of paracetamol/HPβCD-IC NFs and paracetamol/SBE-β-CD-IC NFs with two different methods; (a) addition of distilled water and (b) exposure to distilled water soaked absorbent paper. The paracetamol/CD-IC NFs are dissolved in less than a second.

3.2.4 Conclusion

In this study, free-standing, easy to handle nanofibrous films of paracetamol/HPβCD-IC and paracetamol/SBE-β-CD-IC were successfully obtained by electrospinning. The obtained molar ratios from ^{1}H-NMR analysis showed that the paracetamol molecules were mostly preserved during fabrication of nanofibrous films. Presence of paracetamol in nanofibrous films and formation of inclusion complexes were confirmed by using different characterization techniques including ^{1}H-NMR, FTIR, XRD, DSC. Besides, thermal stability of paracetamol became higher after CD-IC formation. The most remarkable property

of these nanofibrous films is their ultra-fast dissolving character. Two different methods were applied to analyze the dissolution behavior of nanofibrous films and films dissolved less than even a second when they exposed to water. In the light of these results, the bioavailability of paracetamol is expected to be enhanced due to enhancement in solubility and stability. It is also expected that undesirable taste of paracetamol was masked by CD-IC formation without any necessity to additional flavoring agent. In brief, CDs are well known for their non-covalent inclusion complexes with drug molecules in which such inclusion complexation remarkably enhances the drug solubility. The use of CD-ICs is a promising approach to improve aqueous solubility and dissolution rate of the drug molecules. Here, both commercially available CD types (HPβCD and SBE-β-CD) which are already been used in drug formulations were chosen to prepare nanofibrous films of paracetamol/HPβCD-IC and paracetamol/SBE-β-CD-IC. The promising results obtained from this study regard to improved properties and fast-dissolving of paracetamol due to paracetamol/CD-IC nanofibrous structure may be quite interesting for the pharmaceutical applications.

3.3 Fast-dissolving electrospun nanofibrous films of catechin/CD-IC NFs with enhanced antioxidant activity

3.3.1 Introduction

Catechin is polyphenolic compound that is commonly found in green tea, chocolate and grapes [172]. Catechin receives great deal of attention due to its biological and pharmacological effects including antioxidant, anti-diabetic, anti-inflammatory,

anti-mutagenic, anti-carcinogenic, and antimicrobial properties [172-174]. However, low oral bioavailability, bitterness, unstability against external factors such as light, oxygen, temperature make its use difficult as a natural food additive or drug [172, 175]. Extensive research on the application of different encapsulation methods for catechin has been conducted to remove these drawbacks [173, 175-177].

The purpose of this study is to encapsulate catechin molecules by cyclodextrins in the structure of electrospun nanofibers in order to enhance properties and to remove the restrictions for its use. Catechin/HPβCD-IC in powder form, catechin/HPβCD-IC NFs and catechin/PVA NFs was produced. The samples were characterized by scanning electron microscope (SEM), Fourier transform infrared (FTIR) spectroscopy, X-Ray Diffraction (XRD) and proton nuclear magnetic resonance (^{1}H NMR). The antioxidant activity of samples was investigated by using 2,2-diphenyl-1-picrylhydrazyl (DPPH) method. Finally, water solubility of samples was analysed visually.

3.3.2 Experimental

3.3.2.1 Materials

Hydroxypropyl-β-cyclodextrin (HPβCD, CAVASOL W7 HP Pharma, degree of substitution: ~0.6, molecular weight: 1400 g/mol) was gift samples from Wacker Chemie AG (Germany). The polyvinyl alcohol (PVA, Scientific Polymer, 88% hydrolyzed, Mw 125,000) were purchased. Catechin hydrate (98%, Sigma-Aldrich), 2,2-diphenyl-1-picrylhydrazyl (Sigma-Aldrich), deuterated dimethylsulfoxide (d6-DMSO, deuteration degree of minimum 99.8%, Merck),

potassium bromide (KBr, FTIR grade, Sigma-Aldrich) and deionized water (Millipore Milli-Q ultrapure water) were used in this study.

3.3.2.2 Preparation of electrospinning solutions

The solutions of catechin/CD-IC were prepared by dissolving HPβCD (160%, w/v, 1.6 g of HPβCD in 1 mL water) in water to obtain catechin/HPβCD-IC in powder and NF forms, respectively. Then, proper amount of catechin was mixed with aqueous CD solution in order to obtain 1:1 (catechin/CD) molar ratio of catechin/CD-IC solutions. To obtain catechin/PVA solutions, the aqueous PVA solution was prepared by using 7.5% (w/v, with respect to solvent) concentration, then catechin was added to PVA solution to be in the same amount found in CD-IC NFs. These aqueous catechin/CD-IC solutions and catechin/PVA solutions were kept at room temperature under stirring overnight in order to obtain catechin/HPβCD-IC and catechin/PVA solutions. From the one of the solutions of catechin/CD-IC prepared, catechin/CD-IC powder form was obtained. For catechin/HPβCD-IC in powder form, catechin/HPβCD-IC solution was kept at -80°C for three days and then lyophilized in a freeze-dryer for 24h. Then, in addition, pure HP-β-CD solution [91] and PVA solution without catechin were also prepared in water for the electrospinning for comparative studies.

3.3.2.3 Electrospinning of nanofibers

Catechin/HPβCD-IC and catechin/PVA aqueous solutions were placed into 1 mL plastic syringes having a 27 gauge metallic needle, respectively. Then, the syringes loaded were placed on a syringe pump (NE-300, New Era Pump Systems, USA) seperately. The pumping rate of solutions was 0.5 mL/h and the electrospinning

process was performed at a voltage of ~15 kV (AU Series of HV unit, Matsusada, Japan). The collection distance of the NFs was adjusted to 15 cm, and a stationary metal plate collector covered by aluminum foil was used. In addition, pure HPβCD NFs [91] and PVA NFs were also electrospun under the same condition for comparative study.

3.3.2.4 Measurements and characterizations

Scanning electron microscope (SEM, FEI-Quanta 200 FEG) was used to investigate the samples of electrospun nanofibers morphologically. Samples were sputtered with 5nm Au/Pd layer to minimize charging by PECS-682. Average fiber diameter (AFD) for nanofibrous webs was calculated by taking average diameter of 100 fibers from different places of SEM images.

The proton magnetic resonance (^{1}H NMR, Bruker D PX-400) was used to confirm the presence of catechin in samples and to determine molar ratio of catechin in samples. d6-DMSO solvent was used to dissolve pure catechin, catechin/HPβCD-IC NFs, catechin/HPβCD-IC powder, catechin/PVA NFs, HPβCD NFs and PVA NFs in 20 g L^{-1} concentraion for the preparation of solution for ^{1}H NMR measurements.

X-Ray diffraction (XRD, PANalytical X'Pert powder diffractometer) measurements of pure catechin, catechin/HPβCD-IC NFs, catechin/HPβCD-IC powder, catechin/PVA NFs, HPβCD NFs and PVA NFs were recorded by applying Cu Kα radiation in arange of 2θ=5-30° to determine crystalline structure.

Fourier transform infrared spectrometry (FTIR, Bruker-VERTEX70) was used to obtain the infrared spectra of the samples. Samples were mixed with potassium

bromide (KBr) and pressed to get pellets.64 scans were recorded between 4000-400 cm^{-1} at a resolution of 4 cm^{-1}.

Water dissolution behaviour of pure catechin, catechin/HPβCD-IC NFs, catechin/HPβCD-IC powder, catechin/PVA NFs was investigated visually. In this experiment, the samples was positioned in a Petri dish, and then deionized water (5 mL) was poured directly on these nanofibrous mats.

The antioxidant activities of pure catechin, catechin/HPβCD-IC NFs, catechin/HPβCD-IC powder, catechin/PVA NFs were examined by 2,2-Dipheniy-1-picrylhydrazyl (DPPH) radical scavenging method. For this, DPPH solution in methanol (10^{-4} M) was prepared. The concentration of pure catechin, catechin/HPβCD-IC NFs, catechin/HPβCD-IC powder, catechin/PVA NFs in water was arranged to have catehin ranging from 5 to 40 μg mL^{-1} concentartion. Then, 500 μL of aqueous solutions of samples at different concentrations were mixed with 2.5 mL of DPPH solution, and they were stayed for 6 h. DPPH solution has maximum absorption at 517 nm, and the absorption of DPPH solution disappears along with its reduction by antioxidant compound [118]. UV–Vis spectroscopy (Varian, Cary 100) was used to examine the reduction at the absorbance intensity (517 nm) for aqueous solutions of samples at different concentrations. The experiment was carried out in triplicate, and the DPPH radical scavenging efficiency was expressed as the inhibition percentage and was calculated by the following formula:

$$\text{DPPH radical scavenging (\%)} = ((A_{blank} - A_{sample})/ A_{blank}) \times 100$$

3.3.3 Results and discussion

3.3.3.1 Morphological analyses

Optimization of parameters of electrospinning process was done to obtain bead-free and uniform nanofibers. Highly concentrated (160% CD, w/v) catechin/HPβCD-IC and catechin/PVA solutions were used for electrospinning of nanofibers. The digital photographs of nanofibers and their representative SEM images are shown in Figure 62. The catechin/HPβCD-IC NFs and catechin/PVA NFs without any beaded morphology were successfully produced. Besides, these nanofibrous webs have self-standing, easy-to-handle, lightweight and flexible features. The average fiber diameter (AFD) was calculated from SEM images of 100 fibers as 720±265 nm and 760±140 nm for catechin/HPβCD-IC NFs and catechin/PVA NFs, respectively.

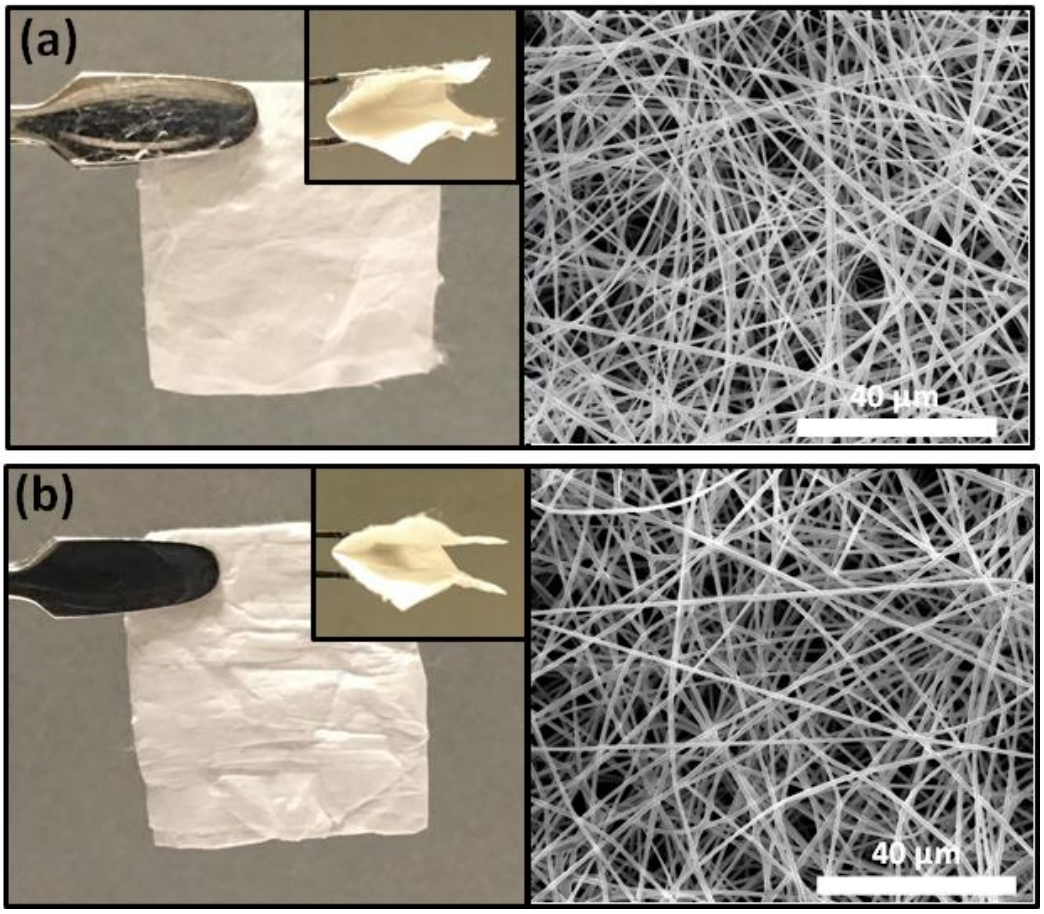

Figure 62. The photographs and SEM images of optimized (a) catechin/CD-IC NFs and (b) catechin/PVA NFs.

3.3.3.2 Structural characterization

Proton nuclear magnetic resonance (^{1}H NMR) was employed to analyze presence of catechin in nanofibers and to find the molar ratio of catechin to CDs for catechin/CD-IC powder and NFs. The presence of catechin in samples was validated by ^{1}H-NMR study since the characteristic peaks of catechin were detected in ^{1}H NMR spectra of catechin/HPβCD-IC powder, catechin/HPβCD-IC NFs and catechin/PVA NFs (Figure 63). The molar ratio was calculated by integrating peaks of catechin and CDs (Figure 63). The molar ratio was calculated as 0.84:1.00 (catechin:HPβCD) and 0.60:1.00 (catechin:HPβCD) for catechin/HPβCD-IC

powder and catechin/HPβCD-IC NFs, respectively. This results showed that catechin was mostly preserved for both samples but higher in catechin/HPβCD-IC NFs.

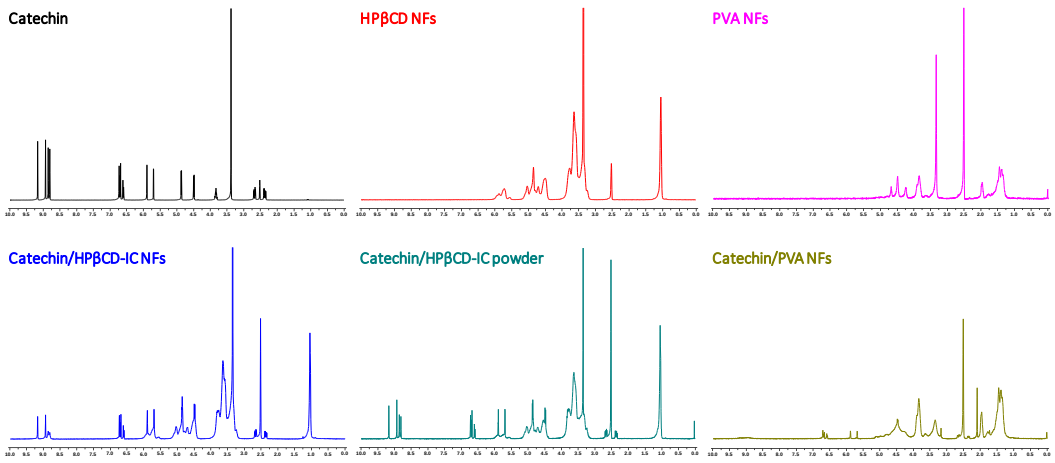

Figure 63. ^{1}H NMR spectra of catechin, CD NFs, PVA NFs, catechin/CD-IC powder, catechin/CD-IC NFs and catechin/PVA NFs.

The crystalline structure of catechin/CD-IC NFs, catechin/HPβCD-IC powder and catechin/PVA NFs were investigated and compared by catechin, CD NFs and PVA NFs by XRD (Figure 64). The XRD patterns catechin/CD-IC NFs, catechin/HPβCD-IC powder and catechin/PVA NFs were different from catechin, but they are amorphous like CD NFs and PVA NFs. The amorphous structure of catechin/HPβCD-IC NFs and catechin/HPβCD-IC powder can be explained by isolation of catechin molecules from each other by entering into CD cavities and so not forming any crystalline aggregates. On the other hand, for catechin/HPβCD-IC NFs and catechin/PVA NFs, catechin molecules were possibly spread on nanofibrous web and cannot form any crystalline aggregates. This change in crystalline structure of catechin results in increase in its solubility since compounds in crystalline forms are more stable that decreases their solubility [153].

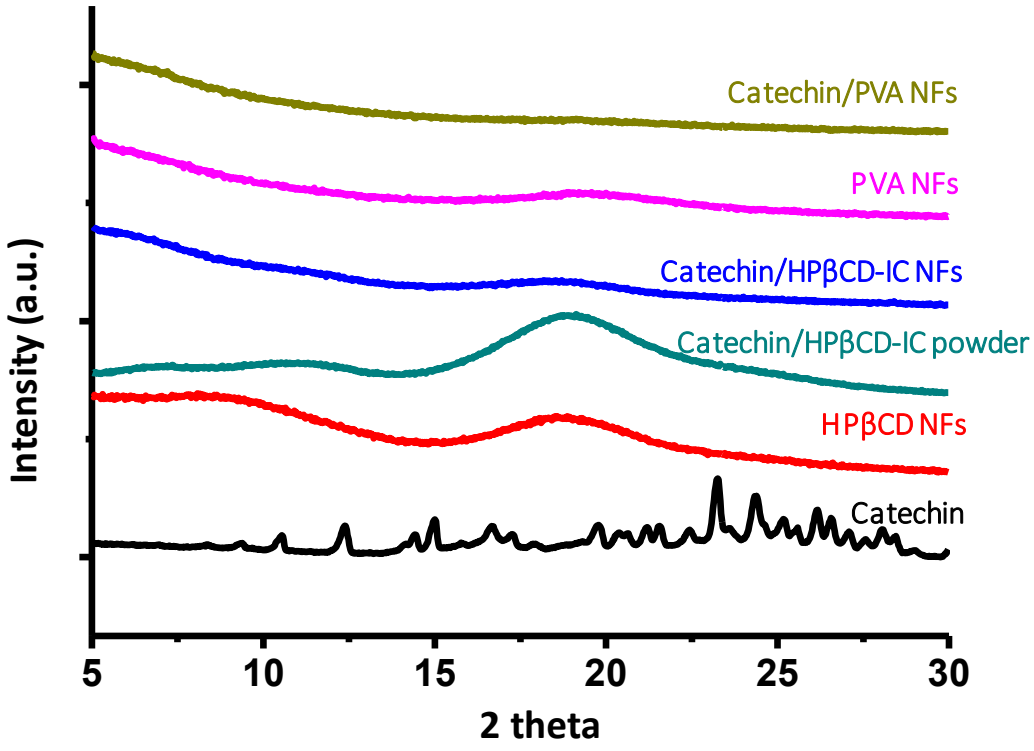

Figure 64. The XRD patterns of catechin, CD NFs, PVA NFs, catechin/CD-IC powder, catechin/CD-IC NFs and catechin/PVA NFs.

FTIR is useful characterization technique to verify cyclodextrin inclusion complexation between host and guest molecules [111]. FTIR spectroscopy can also be used to see the presence of guest molecules in the CD-IC samples. In FTIR analyses, when guest molecules are encapsulated or in the complexation state, variations for the peak position or peak intensity of guest molecules can be seen. The FTIR spectrum of catechin, CD NFs, PVA NFs, catechin/CD-IC powder, catechin/CD-IC NFs and catechin/PVA NFs are shown in Figure 65. The characteristic peaks for catechin at 1400-1600 cm^{-1} attributing to the C=C stretching vibrations of aromatic ring [178]. In the case of catechin/CD-IC powder, catechin/CD-IC NFs and catechin/PVA NFs, these characteristic peaks were present and their intensity were suppressed; besides, the peak at 1516 cm^{-1} was

shifted to 1518 cm^{-1} for catechin/CD-IC powder and catechin/CD-IC NFs, and to 1520 cm^{-1} for catechin/PVA NFs. Therefore, FTIR results suggested that the guest catechin molecules are present in catechin/CD-IC powder, catechin/CD-IC NFs and catechin/PVA NFs and inclusion complexation was formed.

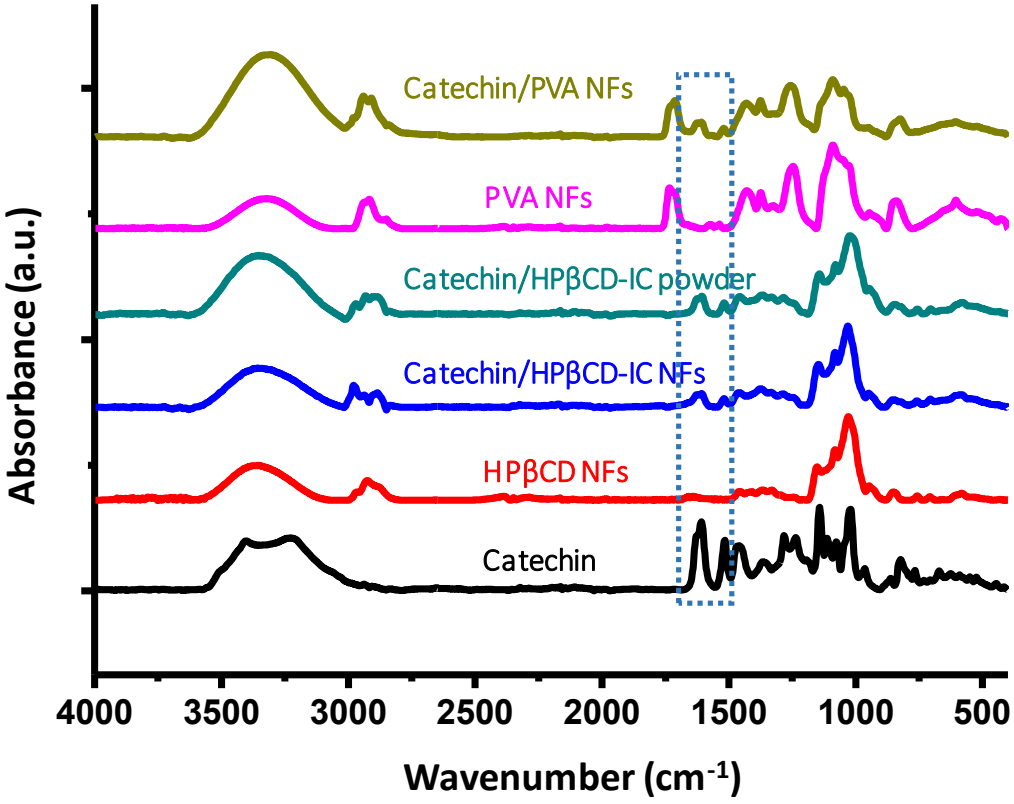

Figure 65. FTIR Spectra of catechin, CD NFs, PVA NFs, catechin/CD-IC powder, catechin/CD-IC NFs and catechin/PVA NFs.

3.3.3.3 Dissolution behavior

Dissolution behavior of samples was examined by adding distilled water to catechin powder, catechin/CD-IC powder, catechin/CD-IC NFs and catechin/PVA NFs (Figure 66). It was seen that catechin/CD-IC NFs was dissolved instantly when it is in contact with water and it showed much better dissolution than pure ctechin

powder and better dissolution rates than catechin/CD-IC powder and catechin/PVA NFs. The slowest dissolution was observed in catechin/PVA NFs after pure catechin powder. These results indicate the effect of CD-IC formation on solubility of catechin.

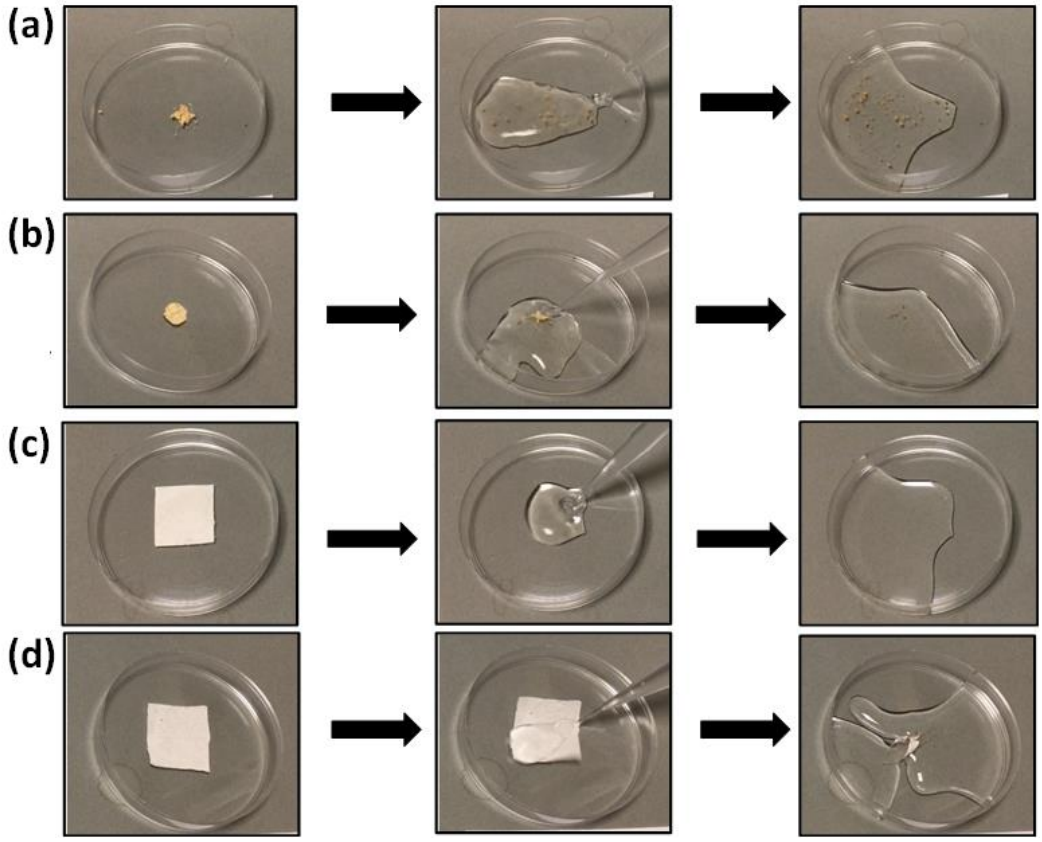

Figure 66. Dissolution behaviour of (a)catechin, (b) catechin/CD-IC powder, (c) catechin/CD-IC NFs and (d) catechin/PVA NFs.

3.3.3.4 Antioxidant activity

DPPH radical scavenging assay was used to test antioxidant property of catechin. This assay is based on reduction of DPPH molecule by a hydrogen donor. As DPPH molecule is reduced, its strongest absorption band observed in UV-Vis spectrum decreases and the purple color of the solutions turns to yellow [118]. Concentration

dependent antioxidant test was performed in which concentration of catechin/CD-IC powder, catechin/CD-IC NFs and catechin/PVA NFs was adjusted to have catechin ranging from 5 to 40 µg in 1 mL of aqueous solution of samples (Figure 67). As expected, DPPH reduction increased with increase amount of catechin in samples and DPPH was almost completely reduced (99.1 %) by the 40 µg mL^{-1} catechin having catechin/CD-IC powder after 1 hour of incubation time. Besides, the antioxidant activity was observed as 86.3 % and 78.6 % for catechin/CD-IC NFs and catechin/PVA NFs having 40 µg mL^{-1} catechin after 1 hour of incubation time, respectively. On the other hand, pure catechin system prepared by 40 µg mL^{-1} catechin in water, the antioxidant activity was observed as 76.2 % under the same condition. This result confirmed that the antioxidant activity of catechin was enhanced by the formation of nanofibrous structure and inclusion complexes with CD.

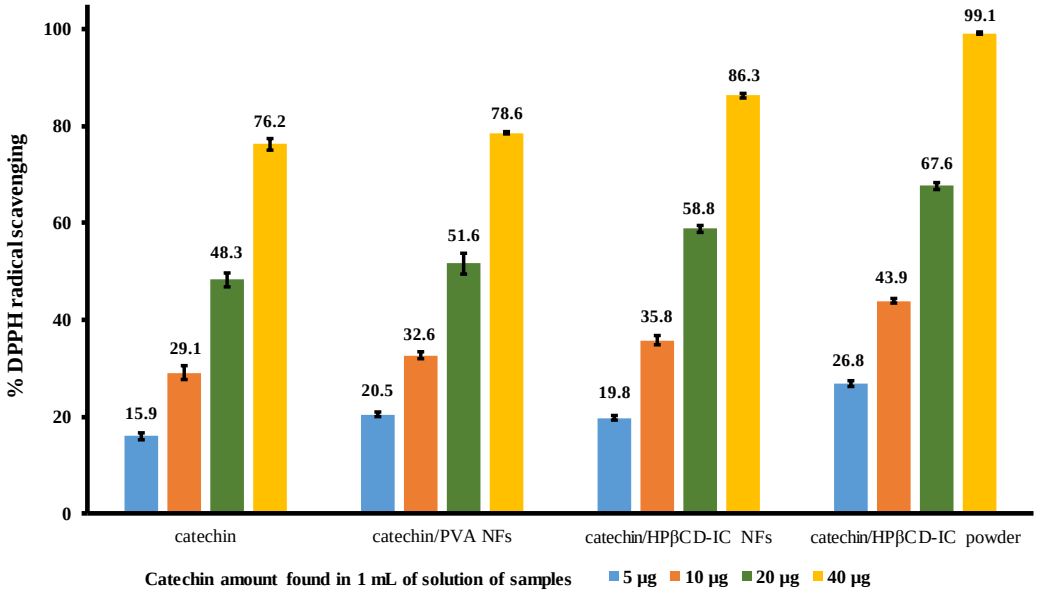

Figure 67. Concentration dependent antioxidant test graphs of catechin, catechin/PVA NFs, catechin/CD-IC NFs and catechin/CD-IC powder.

3.3.4 Conclusion

In conclusion, PVA NFs, CD-IC NFs and CD-IC powder including catechin were successfully produced. The inclusion complexation of catechin was formed with HPβCD. The electrospinning of NFs from catechin/CD-IC and catechin/PVA was successfully performed. FTIR, XRD and ^{1}H NMR studies confirmed the inclusion complex formation and the presence of catechin in catechin/CD-IC powder, catechin/CD-IC NFs and catechin/PVA NFs. Although, catechin has low water solubility, catechin/CD-IC NFs and catechin/CD-IC powder have shown fast-dissolving character in water. In addition, antioxidant activity of catechin was enhanced thanks to formation of catechin/CD-IC powder, catechin/CD-IC NFs and catechin/PVA NFs. These promising results suggest that catechin/CD-IC powder, catechin/CD-IC and catechin/PVA nanofibrous materials may be applicable in drug and food industries thanks to fast-dissolving character and enhanced antioxidant property of catechin.

CHAPTER 4

CONCLUSION AND FUTURE PROSPECTS

In this dissertation, some food additives and drug molecules were encapsulated by polymer-free electrospun CD-IC nanofibers. The first part of the thesis is composed of four studies in which encapsulation of four food additives was investigated, respectively. In the first study, CD-IC nanofibers of menthol was produced which results in enhancement for properties of menthol like increase in water solubility and thermal stability, and slow release. In the second study, fast-dissolving nanofibrous webs of carvacrol/CD-ICs were obtained with improved properties of carvacrol which are decrease in volatility, increase in solubility and stability and enhanced antioxidant activity. As a third study, cinnamaldehyde was encapsulated by CD-IC nanofibers. The nanofibrous webs show fast-dissolving character in addition to enhanced water solubility, high temperature stability and antibacterial activity of cinnamaldehyde. The final study of the first part of this thesis is about the encapsulation of β-carotene by CD-IC nanofibers. In this study, light stability of β-carotene was enhanced while its antioxidant activity was preserved.

The second part of this thesis is for the encapsulation of three different drugs by polymer-free CD-IC nanofibers. Since solubility of drugs is quite important for their bioavailability, the main aim of this part to get soluble nanofibers. The first study is based on drug named as sulfisoxazole which is known by its antimicrobial

effects. In this study, single modified CD, SBE-β-CD, was used to obtain electrospun sulfisoxazole/CD-IC nanofibers. Handy and free-standing webs of sulfisoxazole/CD-IC which shows fast-dissolving property was successfully obtained with enhanced water solubility of sulfisoxazole. In the second study, inclusion complex nanofibers of paracetamol with two modified CDs were prepared. The obtained nanofibrous webs showed fast-dissolving character in water; besides, aqueous solubility and thermal stability of paracetamol was enhanced. The final study is about encapsulation of a drug named as catechin. In this study CD-IC of catechin by a modified CD was prepared in powder and nanofibrous forms. Besides, to see differences, catechin was also encapsulated by PVA nanofibrous films without CD. Fast dissolving character and enhanced antioxidant activity of catechin was observed in all samples, catechin/CD-IC powder, catechin/CD-IC and catechin/PVA nanofibrous.

To conclude, this thesis shows that electrospun CD-IC nanofibers are promising encapsulation materials for various molecules including food additives and drugs. CDs and electrospun nanofibers are already being used in food and pharmaceutical industries. The combination of large surface area of electrospun nanofibers and unique properties of CDs provides enhancement in properties of encapsulated molecules to a great extent. In the future, due to their superior properties, we expect CD-IC nanofibrous webs of food additives to take a wide place in the field of food. We believe that this thesis will shed light on the development of other food additives by using electrospun CD nanofibers. It is known that one of the most important restrictions of the pharmaceutical industry is the low solubility of drugs in water. With the studies in this thesis we have presented an alternative that can prevent this

restriction. Therefore, we expect these studies to attract the attention of the pharmaceutical industry and to be a pioneer in the development of drugs in a similar manner.

LIST OF PUBLICATIONS

Publications from the thesis studies

1) Z. I. Yildiz, A. Celebioglu, M. E. Kilic, E. Durgun, and T. Uyar, "Fast-dissolving carvacrol/cyclodextrin inclusion complex electrospun fibers with enhanced thermal stability, water solubility, and antioxidant activity", Journal of Materials Science, 53, 15837-49, 2018.

2) Z. I. Yildiz, A. Celebioglu, M. E. Kilic, E. Durgun, and T. Uyar, "Menthol/cyclodextrin inclusion complex nanofibers: Enhanced water solubility and high-temperature stability of menthol", Journal of Food Engineering, 224, 27-36, 2018.

3) Z. I. Yildiz, A. Celebioglu, and T. Uyar, "Polymer-free electrospun nanofibers from sulfobutyl ether(7)-beta-cyclodextrin (SBE_7-β-CD) inclusion complex with sulfisoxazole: Fast-dissolving and enhanced water-solubility of sulfisoxazole", International Journal of Pharmaceutics, 531, 550-8, 2017.

4) Z. I. Yildiz, and T. Uyar, "Fast-dissolving electrospun nanofibrous films of paracetamol/cyclodextrin inclusion complexes", Applied Surface Science, 492, 626-33, 2019.

5) Z. I. Yildiz, M. E. Kilic, E. Durgun, and T. Uyar, "Molecular Encapsulation of Cinnamaldehyde within Cyclodextrin Inclusion Complex Electrospun Nanofibers: Fast-Dissolution, Enhanced Water Solubility, High Temperature Stability, and Antibacterial Activity of Cinnamaldehyde", Journal of Agricultural and Food Chemistry, 67, 11066-76, 2019.

6) Z. I. Yildiz, M. E. Kilic, E. Durgun, and T. Uyar, "β-carotene/cyclodextrin inclusion complex nanofibers: Antioxidant activity and enhanced photostability" (in preparation)

7) Z. I. Yildiz and T. Uyar, " Fast-dissolving electrospun nanofibrous films of catechin/CD-IC NFs with enhanced antioxidant activity" (in preparation)

Others

8) Z. Aytac, **Z. I. Yildiz**, F. Kayaci-Senirmak, N. O. S. Keskin, T. Tekinay, and T. Uyar, "Electrospinning of polymer-free cyclodextrin/geraniol-inclusion complex nanofibers: enhanced shelf-life of geraniol with antibacterial and antioxidant properties", Rsc Advances, 6, 46089-99, 2016.

9) Z. Aytac, **Z. I. Yildiz**, F. Kayaci-Senirmak, N. O. S. Keskin, S. I. Kusku, E. Durgun, et al., "Fast-Dissolving, Prolonged Release, and Antibacterial Cyclodextrin/Limonene-Inclusion Complex Nanofibrous Webs via Polymer-Free Electrospinning", Journal of Agricultural and Food Chemistry, 64, 7325-34, 2016

10) Z. Aytac, **Z. I. Yildiz**, F. Kayaci-Senirmak, T. Tekinay, and T. Uyar, "Electrospinning of cyclodextrin/linalool-inclusion complex nanofibers: Fast-dissolving nanofibrous web with prolonged release and antibacterial activity", Food Chemistry, 231, 192-201, 2017.

11) A. Celebioglu, **Z. I. Yildiz**, and T. Uyar, "Electrospun crosslinked poly-cyclodextrin nanofibers: Highly efficient molecular filtration thru host-guest inclusion complexation", Scientific Reports, 7, 2017

12) A. Celebioglu, **Z. I. Yildiz**, and T. Uyar, "Electrospun nanofibers from cyclodextrin inclusion complexes with cineole and p-cymene: enhanced water solubility and thermal stability", International Journal of Food Science and Technology, 53, 112-20, 2018.

13) A. Celebioglu, **Z. I. Yildiz**, and T. Uyar, "Fabrication of Electrospun Eugenol/Cyclodextrin Inclusion Complex Nanofibrous Webs for Enhanced Antioxidant Property, Water Solubility, and High Temperature Stability", Journal of Agricultural and Food Chemistry, 66, 457-66, 2018.

14) A. Celebioglu, **Z. I. Yildiz**, and T. Uyar, "Thymol/cyclodextrin inclusion complex nanofibrous webs: Enhanced water solubility, high thermal stability and antioxidant property of thymol", Food Research International, 106, 280-90, 2018.

15) Z. Aytac, A. Celebioglu, **Z. I. Yildiz**, and T. Uyar, "Efficient Encapsulation of Citral in Fast-Dissolving Polymer-Free Electrospun Nanofibers of Cyclodextrin Inclusion Complexes: High Thermal Stability, Longer Shelf-Life, and Enhanced Water Solubility of Citral", Nanomaterials, 8, 2018.

16) A. Celebioglu, F. Topuz, **Z. I. Yildiz**, and T. Uyar, "Efficient Removal of Polycyclic Aromatic Hydrocarbons and Heavy Metals from Water by Electrospun Nanofibrous Polycyclodextrin Membranes", Acs Omega, 4, 7850-60, 2019.

17) A. Celebioglu, F. Topuz, **Z. I. Yildiz**, and T. Uyar, "One-step green synthesis of antibacterial silver nanoparticles embedded in electrospun cyclodextrin nanofibers", Carbohydrate Polymers, 207, 471-9, 2019.

18) B. Patil*, **Z. I. Yildiz**, T. Uyar* "Electrospun cyclodextrin nanofibers as precursor for carbon nanofibers", Journal of Materials Science, 55(13), 5655-5666, 2020

BIBLIOGRAPHY

[1] S. Ramakrishna, K. Fujihara, W. E. Teo, T. Yong, Z. W. Ma, and R. Ramaseshan, "Electrospun nanofibers: solving global issues", *Materials Today*, 9, 40-50, 2006.

[2] J. H. Wendorff, S. Agarwal, and A. Greiner, "Electrospinning: materials, processing, and applications", Weinheim, Germany: Wiley-VCH; 2012.

[3] D. Li, Y. L. Wang, and Y. N. Xia, "Electrospinning of polymeric and ceramic nanofibers as uniaxially aligned arrays", *Nano Letters*, 3, 1167-71, 2003.

[4] A. Greiner, and J. H. Wendorff, "Electrospinning: A fascinating method for the preparation of ultrathin fibres", *Angewandte Chemie-International Edition*, 46, 5670-703, 2007.

[5] D. Li, and Y. N. Xia, "Electrospinning of nanofibers: Reinventing the wheel?", *Advanced Materials*, 16, 1151-70, 2004.

[6] S. Ramakrishna, K. Fujihara, W. E. Teo, T. C. Lim, and Z. Ma, "An introduction to electrospinning and nanofibers": World Scientific; 2005.

[7] C. Wang, C. H. Hsu, and J. H. Lin, "Scaling laws in electrospinning of polystyrene solutions", *Macromolecules*, 39, 7662-72, 2006.

[8] H. Fong, I. Chun, and D. H. Reneker, "Beaded nanofibers formed during electrospinning", *Polymer*, 40, 4585-92, 1999.

[9] K. H. Lee, H. Y. Kim, H. J. Bang, Y. H. Jung, and S. G. Lee, "The change of bead morphology formed on electrospun polystyrene fibers", *Polymer*, 44, 4029-34, 2003.

[10] C. L. Casper, J. S. Stephens, N. G. Tassi, D. B. Chase, and J. F. Rabolt, "Controlling surface morphology of electrospun polystyrene fibers: Effect of humidity and molecular weight in the electrospinning process", *Macromolecules*, 37, 573-8, 2004.

[11] P. Gupta, C. Elkins, T. E. Long, and G. L. Wilkes, "Electrospinning of linear homopolymers of poly(methyl methacrylate): exploring relationships between fiber formation, viscosity, molecular weight and concentration in a good solvent", *Polymer*, 46, 4799-810, 2005.

[12] T. Uyar, and F. Besenbacher, "Electrospinning of uniform polystyrene fibers: The effect of solvent conductivity", *Polymer*, 49, 5336-43, 2008.

[13] C. Wang, H. S. Chien, C. H. Hsu, Y. C. Wang, C. T. Wang, and H. A. Lu, "Electrospinning of polyacrylonitrile solutions at elevated temperatures", *Macromolecules*, 40, 7973-83, 2007.

[14] R. Sahay, V. Thavasi, and S. Ramakrishna, "Design Modifications in Electrospinning Setup for Advanced Applications", *Journal of Nanomaterials*, 2011.

[15] A. Celebioglu, and T. Uyar, "Electrospun porous cellulose acetate fibers from volatile solvent mixture", *Materials Letters*, 65, 2291-4, 2011.

[16] J. Wu, N. Wang, L. Wang, H. Dong, Y. Zhao, and L. Jiang, "Electrospun Porous Structure Fibrous Film with High Oil Adsorption Capacity", *Acs Applied Materials & Interfaces*, 4, 3207-12, 2012.

[17] Z. Aytac, and T. Uyar, "Applications of core-shell nanofibers: drug and biomolecules release and gene therapy", In: M. Focarete, and A. Tampieri, editors. Core-shell nanostructures for drug delivery and theranostics: Challenges, strategies

and prospects for novel carrier systems: Elsevier- Woodhead publishing; 2018. p. 375-404.

[18] D. Li, J. T. McCann, and Y. N. Xia, "Use of electrospinning to directly fabricate hollow nanofibers with functionalized inner and outer surfaces", *Small*, 1, 83-6, 2005.

[19] A. Celebioglu, Z. Aytac, O. C. O. Umu, A. Dana, T. Tekinay, and T. Uyar, "One-step synthesis of size-tunable Ag nanoparticles incorporated in electrospun PVA/cyclodextrin nanofibers", *Carbohydrate Polymers*, 99, 808-16, 2014.

[20] C. D. Saquing, J. L. Manasco, and S. A. Khan, "Electrospun Nanoparticle-Nanofiber Composites via a One-Step Synthesis", *Small*, 5, 944-51, 2009.

[21] M. A. Khalily, B. Patil, E. Yilmaz, and T. Uyar, "Atomic Layer Deposition of Pd Nanoparticles on N-Doped Electrospun Carbon Nanofibers: Optimization of ORR Activity of Pd-Based Nanocatalysts by Tuning Their Nanoparticle Size and Loading", *Chemnanomat*, 2019.

[22] A. Celebioglu, and T. Uyar, "Metronidazole/Hydroxypropyl-beta-Cyclodextrin inclusion complex nanofibrous webs as fast-dissolving oral drug delivery system", *International Journal of Pharmaceutics*, 572, 2019.

[23] Z. Aytac, H. S. Sen, E. Durgun, and T. Uyar, "Sulfisoxazole/cyclodextrin inclusion complex incorporated in electrospun hydroxypropyl cellulose nanofibers as drug delivery system", *Colloids and Surfaces B-Biointerfaces*, 128, 331-8, 2015.

[24] A. Rezaei, A. Nasirpour, H. Tavanai, and M. Fathi, "A study on the release kinetics and mechanisms of vanillin incorporated in almond gum/polyvinyl alcohol composite nanofibers in different aqueous food simulants and simulated saliva", *Flavour and Fragrance Journal*, 31, 442-7, 2016.

[25] A. Celebioglu, F. Kayaci-Senirmak, S. Ipek, E. Durgun, and T. Uyar, "Polymer-free nanofibers from vanillin/cyclodextrin inclusion complexes: high thermal stability, enhanced solubility and antioxidant property", *Food & Function*, 7, 3141-53, 2016.

[26] S. Aryal, C. K. Kim, K. W. Kim, M. S. Khil, and H. Y. Kim, "Multi-walled carbon nanotubes/TiO2 composite nanofiber by electrospinning", *Materials Science & Engineering C-Biomimetic and Supramolecular Systems*, 28, 75-9, 2008.

[27] K. S. Ranjith, B. Satilmis, and T. Uyar, "Hierarchical electrospun PIM nanofibers decorated with ZnO nanorods for effective pollutant adsorption and photocatalytic degradation", *Materials Today*, 21, 989-90, 2018.

[28] A. C. Stijnman, I. Bodnar, and R. H. Tromp, "Electrospinning of food-grade polysaccharides", *Food Hydrocolloids*, 25, 1393-8, 2011.

[29] A. C. Vega-Lugo, and L. T. Lim, "Controlled release of allyl isothiocyanate using soy protein and poly(lactic acid) electrospun fibers", *Food Research International*, 42, 933-40, 2009.

[30] F. Kayaci, and T. Uyar, "Encapsulation of vanillin/cyclodextrin inclusion complex in electrospun polyvinyl alcohol (PVA) nanowebs: Prolonged shelf-life and high temperature stability of vanillin", *Food Chemistry*, 133, 641-9, 2012.

[31] L. Ge, Y. S. Zhao, T. Mo, J. R. Li, and P. Li, "Immobilization of glucose oxidase in electrospun nanofibrous membranes for food preservation", *Food Control*, 26, 188-93, 2012.

[32] A. Celebioglu, and T. Uyar, "Antioxidant Vitamin E/Cyclodextrin Inclusion Complex Electrospun Nanofibers: Enhanced Water Solubility, Prolonged Shelf

Life, and Photostability of Vitamin E", *Journal of Agricultural and Food Chemistry*, 65, 5404-12, 2017.

[33] A. Celebioglu, Z. I. Yildiz, and T. Uyar, "Electrospun nanofibers from cyclodextrin inclusion complexes with cineole and p-cymene: enhanced water solubility and thermal stability", *International Journal of Food Science and Technology*, 53, 112-20, 2018.

[34] A. Celebioglu, Z. Aytac, M. E. Kilic, E. Durgun, and T. Uyar, "Encapsulation of camphor in cyclodextrin inclusion complex nanofibers via polymer-free electrospinning: enhanced water solubility, high temperature stability, and slow release of camphor", *Journal of Materials Science*, 53, 5436-49, 2018.

[35] A. Celebioglu, Z. I. Yildiz, and T. Uyar, "Fabrication of Electrospun Eugenol/Cyclodextrin Inclusion Complex Nanofibrous Webs for Enhanced Antioxidant Property, Water Solubility, and High Temperature Stability", *Journal of Agricultural and Food Chemistry*, 66, 457-66, 2018.

[36] A. Celebioglu, Z. I. Yildiz, and T. Uyar, "Thymol/cyclodextrin inclusion complex nanofibrous webs: Enhanced water solubility, high thermal stability and antioxidant property of thymol", *Food Research International*, 106, 280-90, 2018.

[37] Z. Aytac, S. Ipek, E. Durgun, T. Tekinay, and T. Uyar, "Antibacterial electrospun zein nanofibrous web encapsulating thymol/cyclodextrin-inclusion complex for food packaging", *Food Chemistry*, 233, 117-24, 2017.

[38] Z. Aytac, N. O. S. Keskin, T. Tekinay, and T. Uyar, "Antioxidant alpha-tocopherol/gamma-cyclodextrin-inclusion complex encapsulated poly(lactic acid) electrospun nanofibrous web for food packaging", *Journal of Applied Polymer Science*, 134, 2017.

[39] Z. Aytac, S. Ipek, E. Durgun, and T. Uyar, "Antioxidant electrospun zein nanofibrous web encapsulating quercetin/cyclodextrin inclusion complex", *Journal of Materials Science*, 53, 1527-39, 2018.

[40] Z. Aytac, Z. I. Yildiz, F. Kayaci-Senirmak, T. Tekinay, and T. Uyar, "Electrospinning of cyclodextrin/linalool-inclusion complex nanofibers: Fast-dissolving nanofibrous web with prolonged release and antibacterial activity", *Food Chemistry*, 231, 192-201, 2017.

[41] Z. Aytac, Z. I. Yildiz, F. Kayaci-Senirmak, N. O. S. Keskin, T. Tekinay, and T. Uyar, "Electrospinning of polymer-free cyclodextrin/geraniol-inclusion complex nanofibers: enhanced shelf-life of geraniol with antibacterial and antioxidant properties", *Rsc Advances*, 6, 46089-99, 2016.

[42] A. Celebioglu, Z. I. Yildiz, and T. Uyar, "Electrospun crosslinked poly-cyclodextrin nanofibers: Highly efficient molecular filtration thru host-guest inclusion complexation", *Scientific Reports*, 7, 2017.

[43] B. Satilmis, and T. Uyar, "Amine modified electrospun PIM-1 ultrafine fibers for an efficient removal of methyl orange from an aqueous system", *Applied Surface Science*, 453, 220-9, 2018.

[44] Y. E. Dogan, B. Satilmis, and T. Uyar, "Crosslinked PolyCyclodextrin/PolyBenzoxazine electrospun microfibers for selective removal of methylene blue from an aqueous system", *European Polymer Journal*, 119, 311-21, 2019.

[45] A. Celebioglu, F. Topuz, Z. I. Yildiz, and T. Uyar, "Efficient Removal of Polycyclic Aromatic Hydrocarbons and Heavy Metals from Water by Electrospun Nanofibrous Polycyclodextrin Membranes", *Acs Omega*, 4, 7850-60, 2019.

[46] A. Senthamizhan, B. Balusamy, and T. Uyar, "Glucose sensors based on electrospun nanofibers: a review", *Anal Bioanal Chem*, 408, 1285-306, 2016.

[47] B. Balusamy, A. Senthamizhan, and T. Uyar, "Functionalized Electrospun Nanofibers as Colorimetric Sensory Probe for Mercury Detection: A Review", *Sensors*, 19, 2019.

[48] P. Gomathi, D. Ragupathy, J. H. Choi, J. H. Yeum, S. C. Lee, J. C. Kim, et al., "Fabrication of novel chitosan nanofiber/gold nanoparticles composite towards improved performance for a cholesterol sensor", *Sensors and Actuators B-Chemical*, 153, 44-9, 2011.

[49] V. Thavasi, G. Singh, and S. Ramakrishna, "Electrospun nanofibers in energy and environmental applications", *Energy & Environmental Science*, 1, 205-21, 2008.

[50] H. Wu, L. B. Hu, M. W. Rowell, D. S. Kong, J. J. Cha, J. R. McDonough, et al., "Electrospun Metal Nanofiber Webs as High-Performance Transparent Electrode", *Nano Letters*, 10, 4242-8, 2010.

[51] P. Joshi, L. F. Zhang, Q. L. Chen, D. Galipeau, H. Fong, and Q. Q. Qiao, "Electrospun Carbon Nanofibers as Low-Cost Counter Electrode for Dye-Sensitized Solar Cells", *Acs Applied Materials & Interfaces*, 2, 3572-7, 2010.

[52] P. O. Rujitanaroj, N. Pimpha, and P. Supaphol, "Wound-dressing materials with antibacterial activity from electrospun gelatin fiber mats containing silver nanoparticles", *Polymer*, 49, 4723-32, 2008.

[53] Z. Aytac, S. Ipek, I. Erol, E. Durgun, and T. Uyar, "Fast-dissolving electrospun gelatin nanofibers encapsulating ciprofloxacin/cyclodextrin inclusion complex", *Colloids Surf B Biointerfaces*, 178, 129-36, 2019.

[54] G. P. Ma, D. W. Fang, Y. Liu, X. D. Zhu, and J. Nie, "Electrospun sodium alginate/poly(ethylene oxide) core-shell nanofibers scaffolds potential for tissue engineering applications", *Carbohydrate Polymers*, 87, 737-43, 2012.

[55] C. Burger, and B. Chu, "Functional nanofibrous scaffolds for bone reconstruction", *Colloids and Surfaces B-Biointerfaces*, 56, 134-41, 2007.

[56] J. Szejtli, "Introduction and general overview of cyclodextrin chemistry", *Chemical Reviews*, 98, 1743-53, 1998.

[57] K. Karakas, A. Celebioglu, M. Celebi, T. Uyar, and M. Zahmakiran, "Nickel nanoparticles decorated on electrospun polycaprolactone/chitosan nanofibers as flexible, highly active and reusable nanocatalyst in the reduction of nitrophenols under mild conditions", *Applied Catalysis B-Environmental*, 203, 549-62, 2017.

[58] B. Liu, S. X. Qu, Y. Kou, Z. Liu, X. Chen, Y. T. Wu, et al., "In Situ Electrodeposition of Cobalt Sulfide Nanosheet Arrays on Carbon Cloth as a Highly Efficient Bifunctional Electrocatalyst for Oxygen Evolution and Reduction Reactions", *Acs Applied Materials & Interfaces*, 10, 30433-40, 2018.

[59] F. Kayaci, C. Ozgit-Akgun, I. Donmez, N. Biyikli, and T. Uyar, "Polymer-Inorganic Core-Shell Nanofibers by Electrospinning and Atomic Layer Deposition: Flexible Nylon-ZnO Core-Shell Nanofiber Mats and Their Photocatalytic Activity", *Acs Applied Materials & Interfaces*, 4, 6185-94, 2012.

[60] H. F. Jia, G. Y. Zhu, B. Vugrinovich, W. Kataphinan, D. H. Reneker, and P. Wang, "Enzyme-carrying polymeric nanofibers prepared via electrospinning for use as unique biocatalysts", *Biotechnology Progress*, 18, 1027-32, 2002.

[61] W. R. Saenger, J. Jacob, K. Gessler, T. Steiner, D. Hoffmann, H. Sanbe, et al., "Structures of the common cyclodextrins and their larger analogues - Beyond the doughnut", *Chemical Reviews*, 98, 1787-802, 1998.

[62] E. M. M. Del Valle, "Cyclodextrins and their uses: a review", *Process Biochemistry*, 39, 1033-46, 2004.

[63] J. Szejtli, "Utilization of cyclodextrins in industrial products and processes", *Journal of Materials Chemistry*, 7, 575-87, 1997.

[64] A. R. Hedges, "Industrial applications of cyclodextrins", *Chemical Reviews*, 98, 2035-44, 1998.

[65] L. P. Yang, and S. J. Keam, "Sugammadex: a review of its use in anaesthetic practice", *Drugs*, 69, 919-42, 2009.

[66] B. Tian, S. Hua, and J. Liu, "Cyclodextrin-based delivery systems for chemotherapeutic anticancer drugs: A review", *Carbohydr Polym*, 232, 115805, 2020.

[67] L. Zhao, B. Tang, P. Tang, Q. Sun, Z. Suo, M. Zhang, et al., "Chitosan/Sulfobutylether-beta-Cyclodextrin Nanoparticles for Ibrutinib Delivery: A Potential Nanoformulation of Novel Kinase Inhibitor", *J Pharm Sci*, 109, 1136-44, 2020.

[68] C. S. Marques, S. G. Carvalho, L. D. Bertoli, J. C. O. Villanova, P. F. Pinheiro, D. C. M. Dos Santos, et al., "beta-Cyclodextrin inclusion complexes with essential oils: Obtention, characterization, antimicrobial activity and potential application for food preservative sachets", *Food Research International*, 119, 499-509, 2019.

[69] M. Kfoury, L. Auezova, H. Greige-Gerges, and S. Fourmentin, "Promising applications of cyclodextrins in food: Improvement of essential oils retention, controlled release and antiradical activity", *Carbohydr Polym*, 131, 264-72, 2015.

[70] H. J. Buschmann, and E. Schollmeyer, "Applications of cyclodextrins in cosmetic products: A review", *Journal of Cosmetic Science*, 53, 185-91, 2002.

[71] U. Numanoglu, T. Sen, N. Tarimci, M. Kartal, O. M. Koo, and H. Onyuksel, "Use of cyclodextrins as a cosmetic delivery system for fragrance materials: linalool and benzyl acetate", *Aaps Pharmscitech*, 8, E85, 2007.

[72] A. Lopedota, A. Cutrignelli, V. Laquintana, M. Franco, D. Donelli, L. Ragni, et al., "beta-cyclodextrin in personal care formulations: role on the complexation of malodours causing molecules", *Int J Cosmet Sci*, 37, 438-45, 2015.

[73] L. Wang, Y. Kang, C. Y. Xing, K. Guo, X. Q. Zhang, L. S. Ding, et al., "beta-Cyclodextrin based air filter for high-efficiency filtration of pollution sources", *J Hazard Mater*, 373, 197-203, 2019.

[74] C. dos Santos, P. Buera, and F. Mazzobre, "Novel trends in cyclodextrins encapsulation. Applications in food science", *Current Opinion in Food Science*, 16, 106-13, 2017.

[75] E. Fenyvesi, M. Vikmon, and L. Szente, "Cyclodextrins in Food Technology and Human Nutrition: Benefits and Limitations", *Critical Reviews in Food Science and Nutrition*, 56, 1981-2004, 2016.

[76] G. Astray, C. Gonzalez-Barreiro, J. C. Mejuto, R. Rial-Otero, and J. Simal-Gandara, "A review on the use of cyclodextrins in foods", *Food Hydrocolloids*, 23, 1631-40, 2009.

[77] R. Challa, A. Ahuja, J. Ali, and R. K. Khar, "Cyclodextrins in drug delivery: an updated review", *Aaps Pharmscitech*, 6, E329-57, 2005.

[78] A. L. Laza-Knoerr, R. Gref, and P. Couvreur, "Cyclodextrins for drug delivery", *Journal of Drug Targeting*, 18, 645-56, 2010.

[79] G. Wadhwa, S. Kumar, L. Chhabra, S. Mahant, and R. Rao, "Essential oil-cyclodextrin complexes: an updated review", *Journal of Inclusion Phenomena and Macrocyclic Chemistry*, 89, 39-58, 2017.

[80] L. Szente, and J. Szejtli, "Cyclodextrins as food ingredients", *Trends in Food Science & Technology*, 15, 137-42, 2004.

[81] T. Uyar, and E. Kny, "Electrospun Materials for Tissue Engineering and Biomedical Applications.": Woodhead Publishing; p., 2017.

[82] M. Noruzi, "Electrospun nanofibres in agriculture and the food industry: a review", *Journal of the Science of Food and Agriculture*, 96, 4663-78, 2016.

[83] F. Kayaci, O. C. O. Umu, T. Tekinay, and T. Uyar, "Antibacterial Electrospun Poly(lactic acid) (PLA) Nanofibrous Webs Incorporating Triclosan/Cyclodextrin Inclusion Complexes", *Journal of Agricultural and Food Chemistry*, 61, 3901-8, 2013.

[84] Z. Aytac, S. I. Kusku, E. Durgun, and T. Uyar, "Encapsulation of gallic acid/cyclodextrin inclusion complex in electrospun polylactic acid nanofibers: Release behavior and antioxidant activity of gallic acid", *Materials Science & Engineering C-Materials for Biological Applications*, 63, 231-9, 2016.

[85] F. Kayaci, H. S. Sen, E. Durgun, and T. Uyar, "Functional electrospun polymeric nanofibers incorporating geraniol-cyclodextrin inclusion complexes:

High thermal stability and enhanced durability of geraniol", *Food Research International*, 62, 424-31, 2014.

[86] Z. Aytac, S. I. Kusku, E. Durgun, and T. Uyar, "Quercetin/beta-cyclodextrin inclusion complex embedded nanofibres: Slow release and high solubility", *Food Chemistry*, 197, 864-71, 2016.

[87] Z. Aytac, S. Y. Dogan, T. Tekinay, and T. Uyar, "Release and antibacterial activity of allyl isothiocyanate/beta-cyclodextrin complex encapsulated in electrospun nanofibers", *Colloids and Surfaces B-Biointerfaces*, 120, 125-31, 2014.

[88] S. L. Shenoy, W. D. Bates, H. L. Frisch, and G. E. Wnek, "Role of chain entanglements on fiber formation during electrospinning of polymer solutions: good solvent, non-specific polymer-polymer interaction limit", *Polymer*, 46, 3372-84, 2005.

[89] S. A. Theron, E. Zussman, and A. L. Yarin, "Experimental investigation of the governing parameters in the electrospinning of polymer solutions", *Polymer*, 45, 2017-30, 2004.

[90] A. Celebioglu, and T. Uyar, "Electrospinning of nanofibers from non-polymeric systems: Electrospun nanofibers from native cyclodextrins", *Journal of Colloid and Interface Science*, 404, 1-7, 2013.

[91] A. Celebioglu, and T. Uyar, "Electrospinning of nanofibers from non-polymeric systems: polymer-free nanofibers from cyclodextrin derivatives", *Nanoscale*, 4, 621-31, 2012.

[92] A. Celebioglu, O. C. O. Umu, T. Tekinay, and T. Uyar, "Antibacterial electrospun nanofibers from triclosan/cyclodextrin inclusion complexes", *Colloids and Surfaces B-Biointerfaces*, 116, 612-9, 2014.

[93] A. Celebioglu, and T. Uyar, "Electrospinning of Polymer-free Nanofibers from Cyclodextrin Inclusion Complexes", *Langmuir*, 27, 6218-26, 2011.

[94] Z. Aytac, Z. I. Yildiz, F. Kayaci-Senirmak, N. O. S. Keskin, S. I. Kusku, E. Durgun, et al., "Fast-Dissolving, Prolonged Release, and Antibacterial Cyclodextrin/Limonene-Inclusion Complex Nanofibrous Webs via Polymer-Free Electrospinning", *Journal of Agricultural and Food Chemistry*, 64, 7325-34, 2016.

[95] Z. I. Yildiz, A. Celebioglu, M. E. Kilic, E. Durgun, and T. Uyar, "Menthol/cyclodextrin inclusion complex nanofibers: Enhanced water solubility and high-temperature stability of menthol", *Journal of Food Engineering*, 224, 27-36, 2018.

[96] N. Galeotti, L. D. Mannelli, G. Mazzanti, A. Bartolini, and C. Ghelardini, "Menthol: a natural analgesic compound", *Neuroscience Letters*, 322, 145-8, 2002.

[97] T. Patel, Y. Ishiuji, and G. Yosipovitch, "Menthol: A refreshing look at this ancient compound", *Journal of the American Academy of Dermatology*, 57, 873-8, 2007.

[98] H. Ades, E. Kesselman, Y. Ungar, and E. Shimoni, "Complexation with starch for encapsulation and controlled release of menthone and menthol", *Lwt-Food Science and Technology*, 45, 277-88, 2012.

[99] S. Phunpee, S. Saesoo, I. Sramala, S. Jarussophon, W. Sajomsang, S. Puttipipatkhachorn, et al., "A comparison of eugenol and menthol on encapsulation characteristics with water-soluble quaternized beta-cyclodextrin grafted chitosan (vol 84, pg 472, 2016)", *International Journal of Biological Macromolecules*, 87, 623-, 2016.

[100] X. D. Liu, T. Furuta, H. Yoshii, P. Linko, and W. J. Coumans, "Cyclodextrin encapsulation to prevent the loss of l-menthol and its retention during drying", *Bioscience Biotechnology and Biochemistry*, 64, 1608-13, 2000.

[101] G. Y. Zhu, Z. B. Xiao, G. X. Zhu, Rujunzhou, and Y. W. Niu, "Encapsulation of l-menthol in hydroxypropyl-beta-cyclodextrin and release characteristics of the inclusion complex", *Polish Journal of Chemical Technology*, 18, 110-6, 2016.

[102] T. Higuchi, and K. A. Connors, "Phase solubility techniques", *Advanced Analytical Chemistry of Instrumentation*, 4, 117-212, 1965.

[103] P. Hohenberg, and W. Kohn, "Inhomogeneous Electron Gas", *Physical Review*, 136, B864-B71, 1964.

[104] W. Kohn, and L. J. Sham, "Self-Consistent Equations Including Exchange and Correlation Effects", *Physical Review*, 140, A1133-A8, 1965.

[105] G. Kresse, and J. Furthmuller, "Efficient iterative schemes for ab initio total-energy calculations using a plane-wave basis set", *Physical Review B*, 54, 11169-86, 1996.

[106] J. P. Perdew, K. Burke, and M. Ernzerhof, "Generalized gradient approximation made simple", *Physical Review Letters*, 77, 3865-8, 1996.

[107] S. Grimme, "Semiempirical GGA-type density functional constructed with a long-range dispersion correction", *Journal of Computational Chemistry*, 27, 1787-99, 2006.

[108] P. E. Blochl, "Projector Augmented-Wave Method", *Physical Review B*, 50, 17953-79, 1994.

[109] K. Mathew, R. Sundararaman, K. Letchworth-Weaver, T. A. Arias, and R. G. Hennig, "Implicit solvation model for density-functional study of nanocrystal surfaces and reaction pathways", *Journal of Chemical Physics*, 140, 2014.

[110] Y. P. Lu, S. Y. Liu, Y. Zhao, L. Zhu, and S. Q. Yu, "Complexation of Z-ligustilide with hydroxypropyl-beta-cyclodextrin to improve stability and oral bioavailability", *Acta Pharmaceutica*, 64, 211-22, 2014.

[111] F. Kayaci, and T. Uyar, "Solid Inclusion Complexes of Vanillin with Cyclodextrins: Their Formation, Characterization, and High-Temperature Stability", *Journal of Agricultural and Food Chemistry*, 59, 11772-8, 2011.

[112] F. A. Al-Bayati, "Isolation and identification of antimicrobial compound from Mentha longifolia L. leaves grown wild in Iraq", *Annals of Clinical Microbiology and Antimicrobials*, 8, 2009.

[113] Z. J. Yang, Z. B. Xiao, and H. B. Ji, "Solid inclusion complex of terpinen-4-ol/beta-cyclodextrin: kinetic release, mechanism and its antibacterial activity", *Flavour and Fragrance Journal*, 30, 179-87, 2015.

[114] Z. I. Yildiz, A. Celebioglu, M. E. Kilic, E. Durgun, and T. Uyar, "Fast-dissolving carvacrol/cyclodextrin inclusion complex electrospun fibers with enhanced thermal stability, water solubility, and antioxidant activity", *Journal of Materials Science*, 53, 15837-49, 2018.

[115] K. H. C. Baser, "Biological and Pharmacological Activities of Carvacrol and Carvacrol Bearing Essential Oils", *Current Pharmaceutical Design*, 14, 3106-19, 2008.

[116] M. De Vincenzi, A. Stammati, A. De Vincenzi, and M. Silano, "Constituents of aromatic plants: carvacrol", *Fitoterapia*, 75, 801-4, 2004.

[117] E. H. Santos, J. A. Kamimura, L. E. Hill, and C. L. Gomes, "Characterization of carvacrol beta-cyclodextrin inclusion complexes as delivery systems for antibacterial and antioxidant applications", *Lwt-Food Science and Technology*, 60, 583-92, 2015.

[118] K. Pyrzynska, and A. Pękal, "Application of free radical diphenylpicrylhydrazyl (DPPH) to estimate the antioxidant capacity of food samples", *Analytical Methods*, 5, 4288-95, 2013.

[119] M. E. Brewster, and T. Loftsson, "Cyclodextrins as pharmaceutical solubilizers", *Advanced Drug Delivery Reviews*, 59, 645-66, 2007.

[120] A. Sá Couto, P. Salustio, and H. Cabral-Marques, "Cyclodextrins", In: K. G. Ramawat, and J. M. Merillon, editors. Polysaccharides. Switzerland: Springer International Publishing; 2015. p. 247-88.

[121] Y. Wei, J. Zhang, A. H. Memon, and H. Liang, "Molecular model and in vitro antioxidant activity of a water-soluble and stable phloretin/hydroxypropyl-b-cyclodextrin inclusion complex", *Journal of Molecular Liquids*, 236, 68-75, 2017.

[122] Z. I. Yildiz, M. E. Kilic, E. Durgun, and T. Uyar, "Molecular Encapsulation of Cinnamaldehyde within Cyclodextrin Inclusion Complex Electrospun Nanofibers: Fast-Dissolution, Enhanced Water Solubility, High Temperature Stability, and Antibacterial Activity of Cinnamaldehyde", *Journal of Agricultural and Food Chemistry*, 67, 11066-76, 2019.

[123] S. F. Nabavi, A. Di Lorenzo, M. Izadi, E. Sobarzo-Sanchez, M. Daglia, and S. M. Nabavi, "Antibacterial Effects of Cinnamon: From Farm to Food, Cosmetic and Pharmaceutical Industries", *Nutrients*, 7, 7729-48, 2015.

[124] B. J. Chen, C. S. Fu, G. H. Li, X. N. Wang, H. X. Lou, D. M. Ren, et al., "Cinnamaldehyde Analogues as Potential Therapeutic Agents", *Mini-Reviews in Medicinal Chemistry*, 17, 33-43, 2017.

[125] A. Gunia-Krzyzak, K. Sloczynska, J. Popiol, P. Koczurkiewicz, H. Marona, and E. Pekala, "Cinnamic acid derivatives in cosmetics: current use and future prospects", *International Journal of Cosmetic Science*, 40, 356-66, 2018.

[126] Y. Y. Qin, D. Liu, Y. Wu, M. L. Yuan, L. Li, and J. Y. Yang, "Effect of PLA/PCL/cinnamaldehyde antimicrobial packaging on physicochemical and microbial quality of button mushroom (Agaricus bisporus)", *Postharvest Biology and Technology*, 99, 73-9, 2015.

[127] H. Zhao, J. N. Yuan, Q. Yang, Y. H. Xie, W. Cao, and S. W. Wang, "Cinnamaldehyde in a Novel Intravenous Submicrometer Emulsion: Pharmacokinetics, Tissue Distribution, Antitumor Efficacy, and Toxicity", *Journal of Agricultural and Food Chemistry*, 63, 6386-92, 2015.

[128] F. Liu, F. T. Saricaoglu, R. J. Avena-Bustillos, D. F. Bridges, G. R. Takeoka, V. C. H. Wu, et al., "Preparation of Fish Skin Gelatin-Based Nanofibers Incorporating Cinnamaldehyde by Solution Blow Spinning", *International Journal of Molecular Sciences*, 19, 2018.

[129] K. A. Rieger, and J. D. Schiffman, "Electrospinning an essential oil: Cinnamaldehyde enhances the antimicrobial efficacy of chitosan/poly(ethylene oxide) nanofibers", *Carbohydrate Polymers*, 113, 561-8, 2014.

[130] N. Maftoonazad, M. Shahamirian, D. John, and H. Ramaswamy, "Development and evaluation of antibacterial electrospun pea protein isolate-polyvinyl alcohol nanocomposite mats incorporated with cinnamaldehyde",

Materials Science & Engineering C-Materials for Biological Applications, 94, 393-402, 2019.

[131] J. Y. Chun, Y. J. Jo, P. Bjrapha, M. J. Choi, and S. G. Min, "Antimicrobial Effect of alpha- or beta-Cyclodextrin Complexes with Trans-Cinnamaldehyde Against Staphylococcus aureus and Escherichia coli", *Drying Technology*, 33, 377-83, 2015.

[132] Y. Liu, X. Liang, R. Zhang, W. Lan, and W. Qin, "Fabrication of Electrospun Polylactic Acid/Cinnamaldehyde/β-Cyclodextrin Fibers as an Antimicrobial Wound Dressing", *Polymers*, 9, 2017.

[133] M. E. Carlotti, S. Sapino, R. Cavalli, M. Trotta, F. Trotta, and K. Martina, "Inclusion of cinnamaldehyde in modified gamma-cyclodextrins", *Journal of Inclusion Phenomena and Macrocyclic Chemistry*, 57, 445-50, 2007.

[134] M. Davaatseren, Y. J. Jo, G. P. Hong, H. J. Hur, S. Park, and M. J. Choi, "Studies on the Anti-Oxidative Function of trans-Cinnamaldehyde-Included -Cyclodextrin Complex", *Molecules*, 22, 2017.

[135] H. J. Chen, L. Li, Y. C. Ma, T. P. Mcdonald, and Y. F. Wang, "Development of active packaging film containing bioactive components encapsulated in beta-cyclodextrin and its application", *Food Hydrocolloids*, 90, 360-6, 2019.

[136] Q. M. Sun, P. X. Tang, L. D. Zhao, H. Y. Pu, Y. M. Zhai, and H. Li, "Mechanism and structure studies of cinnamaldehyde/cyclodextrins inclusions by computer simulation and NMR technology", *Carbohydrate Polymers*, 194, 294-302, 2018.

[137] P. Wen, D. H. Zhu, H. Wu, M. H. Zong, Y. R. Jing, and S. Y. Han, "Encapsulation of cinnamon essential oil in electrospun nanofibrous film for active food packaging", *Food Control*, 59, 366-76, 2016.

[138] P. Wen, D. H. Zhu, K. Feng, F. J. Liu, W. Y. Lou, N. Li, et al., "Fabrication of electrospun polylactic acid nanofilm incorporating cinnamon essential oil/beta-cyclodextrin inclusion complex for antimicrobial packaging", *Food Chemistry*, 196, 996-1004, 2016.

[139] G. Kresse, and J. Furthmuller, "Efficiency of ab-initio total energy calculations for metals and semiconductors using a plane-wave basis set", *Computational Materials Science*, 6, 15-50, 1996.

[140] X. Q. Li, M. A. Kanjwal, L. Lin, and I. S. Chronakis, "Electrospun polyvinyl-alcohol nanofibers as oral fast-dissolving delivery system of caffeine and riboflavin", *Colloids and Surfaces B-Biointerfaces*, 103, 182-8, 2013.

[141] E. Cho, and S. Jung, "Supramolecular Complexation of Carbohydrates for the Bioavailability Enhancement of Poorly Soluble Drugs", *Molecules*, 20, 19620-46, 2015.

[142] W. Q. Yuan, C. H. M. Teo, and H. G. Yuk, "Combined antibacterial activities of essential oil compounds against Escherichia coli O157:H7 and their application potential on fresh-cut lettuce", *Food Control*, 96, 112-8, 2019.

[143] X. F. Tu, F. Hu, K. Thakur, X. L. Li, Y. S. Zhang, and Z. J. Wei, "Comparison of antibacterial effects and fumigant toxicity of essential oils extracted from different plants", *Industrial Crops and Products*, 124, 192-200, 2018.

[144] M. Valero, and M. J. Giner, "Effects of antimicrobial components of essential oils on growth of Bacillus cereus INRA L2104 in and the sensory qualities of carrot broth", *International Journal of Food Microbiology*, 106, 90-4, 2006.

[145] R. S. Pei, F. Zhou, B. P. Ji, and J. Xu, "Evaluation of Combined Antibacterial Effects of Eugenol, Cinnamaldehyde, Thymol, and Carvacrol against E-coli with an Improved Method", *Journal of Food Science*, 74, M379-M83, 2009.

[146] N. Sanla-Ead, A. Jangchud, V. Chonhenchob, and P. Suppakul, "Antimicrobial Activity of Cinnamaldehyde and Eugenol and Their Activity after Incorporation into Cellulose-based Packaging Films", *Packaging Technology and Science*, 25, 7-17, 2012.

[147] S. Uzunlu, and K. Niranjan, "Laboratory antimicrobial activity of cinnamaldehyde and pomegranate-based polycaprolactone films", *Journal of Applied Polymer Science*, 134, 2017.

[148] H. Liang, Q. P. Yuan, F. Vriesekoop, and F. Lv, "Effects of cyclodextrins on the antimicrobial activity of plant-derived essential oil compounds", *Food Chemistry*, 135, 1020-7, 2012.

[149] S. H. Yalkowsky, Y. He, and P. Jain, "Handbook of aqueous solubility data", 2nd ed, Boca Raton, FL: CRC Press; 2010.

[150] X. Luo, Y. Y. Zhou, L. Bai, F. G. Liu, Y. H. Deng, and D. J. McClements, "Fabrication of beta-carotene nanoemulsion-based delivery systems using dual-channel microfluidization: Physical and chemical stability", *Journal of Colloid and Interface Science*, 490, 328-35, 2017.

[151] Z. P. Zhang, R. J. Zhang, and D. J. McClements, "Encapsulation of beta-carotene in alginate-based hydrogel beads: Impact on physicochemical stability and bioaccessibility", *Food Hydrocolloids*, 61, 1-10, 2016.

[152] Y. Kohno, Y. Kato, M. Shibata, C. Fukuhara, Y. Maeda, Y. Tomita, et al., "Fixation and stability enhancement of beta-carotene by organo-modified mesoporous silica", *Microporous and Mesoporous Materials*, 220, 1-6, 2016.

[153] N. J. Babu, and A. Nangia, "Solubility Advantage of Amorphous Drugs and Pharmaceutical Cocrystals", *Crystal Growth & Design*, 11, 2662-79, 2011.

[154] Z. I. Yildiz, A. Celebioglu, and T. Uyar, "Polymer-free electrospun nanofibers from sulfobutyl ether(7)-beta-cyclodextrin (SBE7-beta-CD) inclusion complex with sulfisoxazole: Fast-dissolving and enhanced water-solubility of sulfisoxazole", *International Journal of Pharmaceutics*, 531, 550-8, 2017.

[155] A. Tacic, I. Savic, V. Nikolic, I. Savic, S. Ilic-Stojanovic, D. Ilic, et al., "Inclusion complexes of sulfanilamide with beta-cyclodextrin and 2-hydroxypropyl-beta-cyclodextrin", *Journal of Inclusion Phenomena and Macrocyclic Chemistry*, 80, 113-24, 2014.

[156] G. Gladys, G. Claudia, and L. Marcela, "The effect of pH and triethanolamine on sulfisoxazole complexation with hydroxypropyl-beta-cyclodextrin", *European Journal of Pharmaceutical Sciences*, 20, 285-93, 2003.

[157] N. Devasari, C. P. Dora, C. Singh, S. R. Paidi, V. Kumar, M. E. Sobhia, et al., "Inclusion complex of erlotinib with sulfobutyl ether-beta-cyclodextrin: Preparation, characterization, in silico, in vitro and in vivo evaluation", *Carbohydrate Polymers*, 134, 547-56, 2015.

[158] A. D. Kulkarni, and V. S. Belgamwar, "Inclusion complex of chrysin with sulfobutyl ether-beta-cyclodextrin (Captisol (R)): Preparation, characterization, molecular modelling and in vitro anticancer activity", *Journal of Molecular Structure*, 1128, 563-71, 2017.

[159] T. Uyar, A. El-Shafei, X. Wang, J. Hacaloglu, and A. E. Tonelli, "The solid channel structure inclusion complex formed between guest styrene and host γ-cyclodextrin", *Journal of Inclusion Phenomena and Macrocyclic Chemistry*, 55, 109-21, 2006.

[160] I. Sebe, P. Szabo, B. Kallai-Szabo, and R. Zelko, "Incorporating small molecules or biologics into nanofibers for optimized drug release: A review", *International Journal of Pharmaceutics*, 494, 516-30, 2015.

[161] Z. I. Yildiz, and T. Uyar, "Fast-dissolving electrospun nanofibrous films of paracetamol/cyclodextrin inclusion complexes", *Applied Surface Science*, 492, 626-33, 2019.

[162] U. E. Illangakoon, H. Gill, G. C. Shearman, M. Parhizkar, S. Mahalingam, N. P. Chatterton, et al., "Fast dissolving paracetamol/caffeine nanofibers prepared by electrospinning", *International Journal of Pharmaceutics*, 477, 369-79, 2014.

[163] M. El-Kemary, S. Sobhy, S. El-Daly, and A. Abdel-Shafi, "Inclusion of Paracetamol into beta-cyclodextrin nanocavities in solution and in the solid state", *Spectrochimica Acta Part a-Molecular and Biomolecular Spectroscopy*, 79, 1904-8, 2011.

[164] A. S. Balte, P. K. Goyal, and S. P. Gejji, "Theoretical studies on the encapsulation of Paracetamol in the α, β and γ Cyclodextrins", *Journal of Chemical and Pharmaceutical Research*, 4, 2391-9 2012.

[165] D. G. Yu, C. Branford-White, K. White, X. L. Li, and L. M. Zhu, "Dissolution Improvement of Electrospun Nanofiber-Based Solid Dispersions for Acetaminophen", *Aaps Pharmscitech*, 11, 809-17, 2010.

[166] M. Hamori, K. Nagano, S. Kakimoto, K. Naruhashi, A. Kiriyama, A. Nishimura, et al., "Preparation and pharmaceutical evaluation of acetaminophen nano-fiber tablets: Application of a solvent-based electrospinning method for tableting", *Biomedicine & Pharmacotherapy*, 78, 14-22, 2016.

[167] H. S. Peng, S. B. Zhou, T. Guo, Y. S. Li, X. H. Li, J. X. Wang, et al., "In vitro degradation and release profiles for electrospun polymeric fibers containing paracetanol", *Colloids and Surfaces B-Biointerfaces*, 66, 206-12, 2008.

[168] W. G. Cui, X. H. Li, X. L. Zhu, G. Yu, S. B. Zhou, and J. Weng, "Investigation of drug release and matrix degradation of electrospun poly(DL-lactide) fibers with paracetanol inoculation", *Biomacromolecules*, 7, 1623-9, 2006.

[169] A. Ebrahimi, M. Saffari, F. Dehghani, and T. Langrish, "Incorporation of acetaminophen as an active pharmaceutical ingredient into porous lactose", *International Journal of Pharmaceutics*, 499, 217-27, 2016.

[170] M. K. Trivedi, S. Patil, H. Shettigar, K. Bairwa, and S. Jana, "Effect of Biofield Treatment on Spectral Properties of Paracetamol and

Piroxicam", *Chemical Sciences Journal*, 6, 2015.

[171] M. Al-Remawi, A. M. A. Ali, A. Khames, and M. Hamaidi, "Meloxicam-Paracetamol Binary Solid Dispersion Systems with Enhanced Solubility and Dissolution Rate:Preparation, Characterization, and In Vivo Evaluation", *Journal of Pharmaceutical Innovation*, 12, 206-15, 2017.

[172] H. M. Ezzat, Y. S. R. Elnaggar, and O. Y. Abdallah, "Improved oral bioavailability of the anticancer drug catechin using chitosomes: Design, in-vitro appraisal and in-vivo studies", *International Journal of Pharmaceutics*, 565, 488-98, 2019.

[173] C. Jullian, S. Miranda, G. Zapata-Torres, F. Mendizabal, and C. Olea-Azar, "Studies of inclusion complexes of natural and modified cyclodextrin with (+)catechin by NMR and molecular modeling", *Bioorganic & Medicinal Chemistry*, 15, 3217-24, 2007.

[174] K. Krishnaswamy, V. Orsat, and K. Thangavel, "Synthesis and characterization of nano-encapsulated catechin by molecular inclusion with beta-cyclodextrin", *Journal of Food Engineering*, 111, 255-64, 2012.

[175] M. Sabaghi, Y. Maghsoudlou, M. Kashiri, and A. Shakeri, "Evaluation of release mechanism of catechin from chitosan-polyvinyl alcohol film by exposure to gamma irradiation", *Carbohydr Polym*, 230, 115589, 2020.

[176] S. Z. Hoseyni, S. M. Jafari, H. S. Tabarestani, M. Ghorbani, E. Assadpour, and M. Sabaghi, "Production and characterization of catechin-loaded electrospun nanofibers from Azivash gum- polyvinyl alcohol", *Carbohydrate Polymers*, 235, 115979 (1-9), 2020.

[177] A. H. M. Yusoff, M. N. Salimi, S. C. B. Gopinath, M. M. A. Abdullah, and E. M. Samsudin, "Catechin adsorption on magnetic hydroxyapatite nanoparticles: A synergistic interaction with calcium ions", *Materials Chemistry and Physics*, 241, 122337 (1-7), 2020.

[178] J. Liu, J. F. Lu, J. Kan, X. Y. Wen, and C. H. Jin, "Synthesis, characterization and in vitro anti-diabetic activity of catechin grafted inulin", *International Journal of Biological Macromolecules*, 64, 76-83, 2014.